IMPROVEMENT OF METHODOLOGY TO STUDY ICAM-1 AND CXCL-5 EXPRESSIONS OF AMBIENT PARTICLES, IN VITRO

by

Xinzhou Hu
B.Sc., Tsinghua University, 2005

THESIS SUBMITTED IN PARTIAL FULFILLMENT OF
THE REQUIREMENTS FOR THE DEGREE OF

MASTER OF SCIENCE

In the
Department of
Chemistry

SIMON FRASER UNIVERSITY

Spring 2010

APPROVAL

Name: Xinzhou Hu

Degree: Master of Science

Title of Thesis: Improvement of Methodology to Study ICAM-1 and CXCL-5 Expressions of Ambient Particles, *in vitro*

Examining Committee:

Chair — Dr. Erika Plettner
Associate Professor, Department of Chemistry

Dr. George Agnes
Senior Supervisor
Professor, Department of Chemistry

Dr. David Vocadlo
Supervisor
Associate Professor, Department of Chemistry

Dr. Luis Sojo
Supervisor
Adjunct Professor, Department of Chemistry

Dr. Charles Walsby
Internal Examiner
Assistant Professor, Department of Chemistry

Date Defended/Approved: **January 8, 2010**

Declaration of
Partial Copyright Licence

ABSTRACT

Inhalation of ambient particulate matter is associated with adverse effects on human health. At the outset, the objective of this thesis was to identify what components of ambient particles cause more significant different responses of secreted biomolecules from human lung epithelial (A549) cells, *in vitro*, using a method a previous graduate student developed to assess ICAM-1 expression. However problems with this methodology were identified, and the majority of this work was to find solutions to these problems. Different particles (LPS-plus-carbon particles, LPS-plus-carbon-plus-$Ni(NO_3)_2$ particles, LPS-plus-carbon-plus-NaCl particles, LPS-plus-carbon-plus-$Zn(NO_3)_2$ particles, H_2SO_4-plus-carbon particles, $(NH_4)_2SO_4$-plus-carbon particles, and Na_2SO_4-plus-carbon particles) were generated in situ and were levitated using an electrodynamic trap prior to their deposition onto A549 cells. Following an incubation period, the detectable differential expression of ICAM-1 was monitored using an immunocytochemistry assay. The expression of a secreted cytokine (CXCL-5) was monitored by MALDI-TOF-MS. $Ni(NO_3)_2$ and NaCl both effected upregulation of the ICAM-1 expression when added to LPS-plus-carbon particles, but $Zn(NO_3)_2$ did not. H_2SO_4-plus-carbon particles induced ICAM-1 expression 4.6 times higher than $(NH_4)_2SO_4$-plus-carbon particles and 4.9 times higher than Na_2SO_4-plus-carbon particles, and similar results were obtained from measurement of CXCL-5 expression.

DEDICATION

For mom and dad

ACKNOWLEDGEMENTS

I would acknowledge my senior supervisor Dr. George Agnes for providing me the opportunity to work on this project and giving me guidance and support throughout the entire research.

I would also like to thank the members of my supervisory committee, the internal examiner and the chair of my defense: Dr. David Vocadlo, Dr. Luis Sojo, Dr. Charles Walsby and Dr. Erika Plettner for their advice and suggestions.

My appreciation also goes to many co-workers from over the years. Particularly, I would like to thank Allen E. Haddrell (whose work in the development of methodology truly made this thesis possible), Neil Draper (for his willingness to always help), and other lab mates who make the work environment more interesting. I sincerely thank Linda Pinto for her help on cell fixation methodology and the principle of trypan blue assay.

And of course, the support of my family and friends throughout my studies has been incredible. Through all of the unforeseen events of the past few years, without their steadfast support, I have no idea how this would have ever been finished.

TABLE OF CONTENTS

LIST OF FIGURES

LIST OF TABLES

LIST OF ABBREVIATIONS

AC	alternating current
ATCC	American Type Culture Collection
ACN	acetonitrile
B cells	bone marrow-derived lymphocytes
BSA	bovine serum albumin
CAMs	cell adhesion molecules
CMI	cell-mediated immunity
CXCL	chemokine (C-X-C motif) ligand
DC	direct current
DMSO	dimethyl sulfoxide
EDLT	electrodynamic levitation trap
eg.	for example
EU	endotoxin units
FBS	fetal bovine serum
FDA	the U.S. Food and Drug Administration
g	gram
Hz	hertz

ICAM	intercellular adhesion molecule
Ig	immunoglobulin
IHC	immunohistochemistry
IL	interleukin
IFN	interferon
L	litre
LFA	lymphocyte function-associated antigen
LPS	lipopolysaccharide
m/z	mass to charge ratio
MALDI	matrix assisted laser desorption/ionization
MCP	micro-channel plate
MEM	minimum essential medium
MS	mass spectrometry
mL	millilitre
mm	millimeter
n	nano
NF-κB	nuclear factor-κB
ng	nanogram
nm	nanometer
NOEL	no-observed-effects-levels
p	pico

PBS	phosphate buffered saline
PFA	paraformaldehyde
pg	picogram
pL	picolitre
PM	particulate matter
pmol	picomole
QIT	quadrupole ion trap
rcf	relative centrifugal force
SA	sinapic acid
SFM	serum-free medium
TBS	tris(hydroxymethyl)aminomethane buffered saline
T cell	thymus-derived lymphocyte
TFA	trifluoroacetic acid
Th	T helper cells
TLF	time lag focusing
TNF-α	tumour necrosis factor-α
TOF	time of flight
V	volts
v/v	volume to volume ratio
VCAM	vascular cell adhesion molecule
VLA	very late antigen

w/v	weight to volume ratio
ºC	degree celsius
µg	microgram
µL	microlitre
µm	micrometre

Chapter 1 Introduction

1.1 Particulate matter

Epidemiological studies have shown air pollution is associated with adverse health effects [1-16]. Particulate matter (PM) is a mixture of solid and liquid particles suspended in the air with various sizes ranging from a few nm to tens of μm [12, 16]. There are numerous sources of PM from natural processes (such as windblown soil dusts, volcanic emissions, sea spray, pollens) and human activities (such as motor vehicle emissions, construction dusts, road dusts, industrial and agricultural debris, residential combustion) [12]. Although thousands of chemicals have been detected in PM [12], the most common chemical components are geological materials (a variety of metal oxides), sulfates, nitrates, ammonium, sodium chloride, elemental and organic carbon, organic compounds (such as polycyclic aromatic hydrocarbons), biological compounds (such as endotoxin and cell fragments), and liquid water [12, 17, 18].

PM can be categorized by their sources. Primary particles are released directly into the atmosphere by combustion processes, or wind, or other human activities, whereas secondary particles are formed through physicochemical transformation of gaseous compounds, such as nitrogen oxides, sulfur dioxide (SO_2) and ammonia (NH_3) [12], via homogeneous, heterogeneous, and multiphase processes [19].

Aerodynamic diameter is a physical property which is used to describe a particle in the air. If the particle's aerodynamic behavior is the same as a perfect sphere with uniform density, the diameter of the sphere is defined as the aerodynamic diameter of the particle. PM_{10} (with a median aerodynamic diameter of <10 μm), is one measurement of

PM monitored in most locations worldwide because these particles deposit in all regions of the respiratory tract or even deeper [12, 16]. $PM_{2.5}$ (particles having a median aerodynamic diameter of <2.5 μm), also referred to as the "fine particle fraction", is able to penetrate deep into the lungs, settling into the alveolar region of the lung [12, 16]. In general, $PM_{10\text{-}2.5}$, also referred to as the "coarse fraction", is predominated by particles of geological dusts, industrial grinding activities and biological compounds, such as construction dusts, road dusts, soil dusts, and endotoxin. In contrast, fine particles are composed of primary particles (eg. from combustion sources) and secondary gaseous emissions followed by atmospheric oxidation (eg. $SO_2 \rightarrow SO_4^{2-}$) [12, 17]. $PM_{0.1}$ (with a median aerodynamic diameter of <0.1 μm), also referred to as the "ultrafine particle", shows high deposition in human alveoli and has been measured to readily cross the lung-circulatory system barrier [12]. In the atmosphere, $PM_{0.1}$ readily coagulates with larger particles [12, 16, 17].

1.2 Inflammation

Inflammation is the body's response that can occur in any tissue that is traumatized by noxious stimuli and tissue injury [20, 21]. Inflammation is a complex process involving many soluble factors, cells, tissues, and systems. The process initiates with tissue based responses, followed by the recruitment and dispatch of leukocytes (white blood cells), and then the killing of microbes and infected host cells, liquefaction of surrounding tissue to prevent microbial spread, and finally the healing of tissues damaged by the microbes or by the host response [20, 22].

The inducers of inflammation can be classified into two groups: exogenous or endogenous. Exogenous inducers include microbial and non-microbial inducers.

Endogenous inducers of inflammation include signals produced by stressed or damaged tissues [21]. Several air pollution components in PM, such as bio-available transition metals (eg. iron, cobalt, nickel, copper and zinc), organic compounds (eg. polycyclic aromatic hydrocarbons) and biological compounds (eg. endotoxins), have been observed to induce inflammation in the respiratory tract [15]. Studies have revealed airway inflammation, initiated with uptake of PM into lung epithelial cells and alveolar macrophages, followed by the secretion of the downstream mediators, resulting in neutrophil migration and thymus-derived lymphocyte (T cell) recruitment [16, 23].

Leukocyte recruitment and migration from the blood to the site of injury, which was previously mentioned as the second step of inflammation, is an important step. This step is initiated by downstream effects of regulation of pro-inflammatory mediators, such as chemokines, cytokines, components of the complement cascade, plasma mediators and lipid inflammatory mediators[22]. These mediators, mainly cytokines, which are small proteins that released by cells and have effects on the communications between cells, migrate into the circulation system and stimulate the bone marrow to release leukocytes [23]. The newly released leukocytes randomly contact endothelial cells located proximal to the injury site, followed by rolling on the endothelial cells caused by interactions with selectins, and then adhesion to endothelial cells via binding with cell adhesion molecules (CAMs), that belong to the immunoglobulin (Ig) gene superfamily, and their ligands (integrins), and finally migration from the blood to injury site with help of integrins (Figure 1.1) [24, 25].

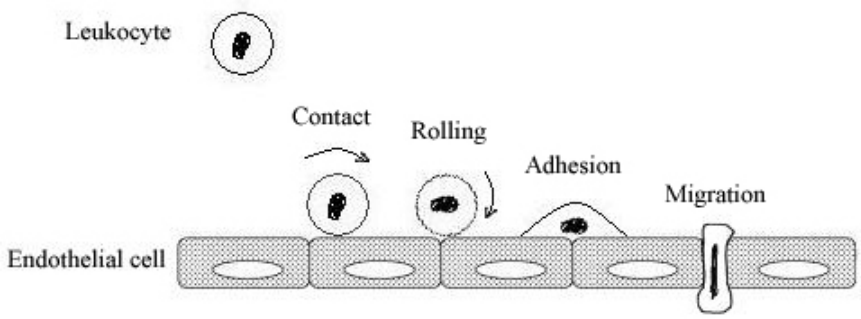

Figure 1.1 Schematic diagram of the step of leukocyte recruitment and migration.

1.3 Epithelial cell-derived neutrophil-activating peptide-78 (ENA-78 or CXCL-5)

Chemokines are a superfamily of pro-inflammatory mediators that can recruit and activate leukocytes [26]. Epithelial cell-derived neutrophil-activating peptide-78 (ENA-78 or CXCL-5) is a chemokine that belongs to the member of CXC motif ligand subfamily, in which the two N-terminal cysteines "CC" are separated by one amino acid "X" [26]. This subfamily consists of several structurally related peptides, such as interleukin-8 (IL-8/CXCL-8) and CXCL-5 [27]. Both CXCL-8 and CXCL-5 are potent neutrophil-activating peptides [26, 28]. They induce chemotaxis and mediate neutrophil adhesion molecule expression [26]. They both can be up-regulated by transcription factor nuclear factor κB (NF-κB), which can be activated by many stress signals [27], such as oxidative stress [29, 30], hypoxia [31], tumour development [32], cytokines, bacterial cell wall products, viral infection, vasopressors and DNA damage [29]. They both can bind to neutrophils via CXC receptor 2 (CXCR-2), and thus they cross compete with each other [26, 27, 33], however, CXCL-8 also binds to CXC receptor 1 (CXCR-1) [26], resulting in different responses of the target cells and the binding affinities [26, 33].

CXCL-5 was first identified in alveolar epithelial cells although it is expressed by various types of cells [28]. Expression of CXCL-5 has been reported upregulated in inflamed lungs [28] and its secretion can be induced with exposure to interleukin-1 (IL-1) and tumor necrosis factor alpha (TNF-α) [33].

1.4 Intercellular adhesion molecule-1 (ICAM-1)

As mentioned previously, the CAMs that belong to Ig gene superfamily are important molecules responsible for the firm adhesion of leukocytes to endothelial cells [24, 34]. Intercellular adhesion molecule-1 (ICAM-1) [24, 25, 34, 35], intercellular adhesion molecule-2 (ICAM-2), intercellular adhesion molecule-3 (ICAM-3) and vascular cell adhesion molecule-1 (VCAM-1) are examples of transmembrane glycoproteins that are CAM members of the Ig gene superfamily [24]. They have similar functions however they are produced and expressed by different types of cells. ICAM-1 can be expressed by endothelial cells, macrophages, lymphocytes, fibroblasts and epithelial cells [24, 25, 34, 36]. ICAM-2 can be expressed by endothelial cells, platelets and some leukocytes but is down-regulated by pro-inflammatory mediators [24]. ICAM-3 can be expressed by endothelial cells and leukocytes and is the only ICAM that can present on neutrophils [24]. VCAM-1 can be expressed by endothelial cells, macrophages, myoblasts and dendritic cells [24]. It binds monocytes and lymphocytes that express integrin very late antigen-4 (VLA-4), which is a ligand of VCAM-1 [24, 34]. Whereas ICAMs bind several leukocytes (such as T cells, bone marrow-derived lymphocytes (B cells), macrophages and neutrophils) that express integrin lymphocyte function-associated antigen-1 (LFA-1), which is a ligand of all ICAMs [24, 34].

Lung ICAM-1, expressed by lung epithelial cells, plays an important role in lung inflammatory diseases. It is constitutively expressed on alveolar type I cells but not constitutively expressed on alveolar type II cells. However, in alveolar type II cells, ICAM-1 expression can be induced with exposure to, for example, tumor necrosis factor alpha (TNF-α), interleukin-1 beta (IL-1β), or lipopolysaccharide (LPS) [25].

Since the pulmonary epithelium is the first site of contact with different agents that trigger airway inflammation [37, 38], ICAM-1 expression on alveolar type II cells can be considered and studied as an important step in lung inflammation.

1.5 A549 cell line

There are two major alveolar cell types in the alveolar wall as epithelial cells: alveolar type I cells and alveolar type II cells. Alveolar type I cells are large cells covering a majority of the alveolar surface area, while alveolar type II cells are smaller cells with approximately twice as numerous as alveolar type I cells. Since alveolar type I cells constitutively express ICAM-1 but alveolar type II cells express ICAM-1 only by triggering [25], ICAM-1 expression is appropriate to be used as a readout on alveolar type II cells in the study of lung inflammation.

The A549 cell line was initiated in 1972 through an explant culture of lung carcinomatous tissue from a 58 years old male. Since A549 cells are transformed cells, they are different from primary cells, which are polarized cells directly taken from biopsy. A549 cells can divide infinitely without mutation, yet A549 cells retain similar characteristics to human lung alveolar type II cells [39]. Thus, as a starting point, A549 cells are appropriate to be used in replacement of primary alveolar type II cells in the study of lung inflammation.

1.6 Immunocytochemistry

ICAM-1 expression on A549 cells was measured using immunocytochemistry. Immunocytochemistry is a technique that uses specific antibodies, which have been tagged with visible labels that bind to protein antigens in cells, allowing measurement of the antibodies [40].

Immunocytochemistry includes several steps: cells fixation, antibody staining and observation. The purpose of cell fixation is to immediately stop the life processes within the cells and therefore the cells are killed with the relative locations of the proteins and their abundance within the cells fixed. Antibody staining, in this thesis, includes primary antibody, which is specific to human ICAM-1 produced by mouse, and the secondary antibody, which is specific to the primary antibody produced by goat, is tagged with a fluorophore. The fluorophore can be detected by fluorescence spectroscopy and therefore whether the individual cell expresses ICAM-1 or not can be evaluated.

1.7 Mass Spectrometry and proteomics

Matrix-assisted laser desorption/ionization time-of-flight mass spectrometry (MALDI-TOF-MS) with high sensitivity, high mass accuracy, efficient ionization of peptides, and rapid analysis time, has been widely used to investigate complex protein mixtures [41-43].

Proteomics is a term used to describe studies that focus on a large number of different proteins produced by cells [44, 45]. Since cellular proteins have a high degree of complexity and are present at varied abundance, soft ionization mass spectrometry, which has high sensitivity, has been increasingly used to analyze complex protein samples [44].

1.8 Thesis objectives

Ambient PM is a mixture of particles having different sizes and different chemicals, from inorganic to organic, from water soluble to water insoluble. Inhalation of PM is associated with adverse effects on human health, however few studies have systematically characterized the compounds in a specific particle type with respect to their being a factor in this relationship. This thesis is based on a hypothesis that different chemicals in a particle cause measurably different ICAM-1 and CXCL-5 responses. Allen Haddrell, a previous graduate student, developed a methodology to assess the inflammation potential of ambient PM_{10}, *in vitro*, where the term inflammation potential was used by the former graduate student to reflect the differential expression of ICAM-1 and other mediators such as cytokines and chemokines. However my work identified problems with this methodology, and the majority of my work was focused on finding solutions to these problems. The objective of this thesis was to dose A549 cells with different particle types and monitor downstream biomolecules secreted by the cells using immunocytochemistry and MALDI-TOF-MS. The contribution of this thesis is to understand more about how A549 cells respond to the different particle compositions.

Chapter 2 Apparatus Used in This Study

2.1 Electrodynamic levitation trap (EDLT)

Electrodynamic levitation traps (EDLT) have been used in the Agnes group to generate particles [46, 47] for the purpose of investigating the effect of ambient particle mimics on lung cells [48-50]. The apparatus consists of a droplet dispenser, an induction electrode with a 5 mm in diameter hole cut in the centre, a pair of parallel ring electrodes and a bottom electrode (Figure 2.1).

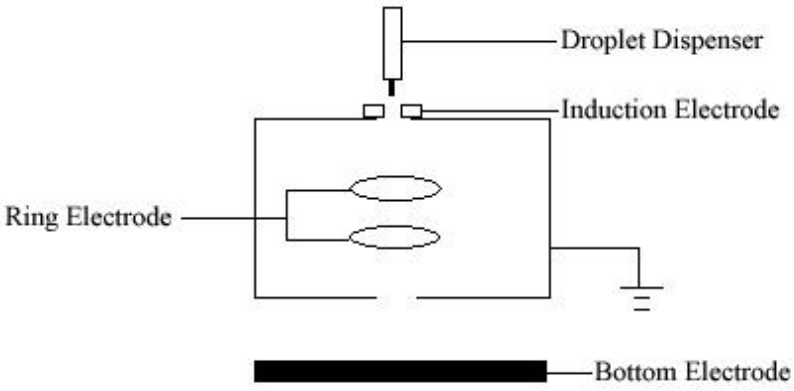

Figure 2.1 Schematic diagram of EDLT.

A commercially available droplet dispenser (MJ-AB-01-60, MicroFab Technologies Inc., Plano, TX, USA) with a nozzle having a 60 μm internal diameter was used to dispense monodisperse droplets. A cylinder piezoelectric actuator was bonded to the droplet dispenser reservoir. The droplet dispenser reservoir was loaded with ~10 μL aliquot of a starting solution consisting of both volatile and non-volatile components. A 120 Hz pulsed waveform with amplitude of 50 V was applied to the cylinder piezoelectric actuator. Thus, with each activation of the piezoceramic, the dispenser reservoir, which bonded to the cylinder piezoelectric actuator, produced a pressure

change, resulting in an acoustic wave within the solution in the dispenser tube. The pressure wave propagated towards the nozzle and caused a jet of liquid to separate from the nozzle and then collapse into a droplet. The nozzle of the droplet dispenser was positioned 1 mm above the induction electrode and centred over the hole that had been cut into it.

A +120 V direct current (DC) potential was applied to the induction electrode. The electric field between the nozzle and the induction electrode induced different ion mobility in the jet of liquid emerging from the nozzle, resulting in a droplet with net charge when the jet separated from the nozzle and collapsed to a single droplet (under normal conditions).

A pair of parallel ring electrodes were used to levitate the droplets. The pair of ring electrodes was similar to the ring electrode in a quadrupole ion trap (QIT) [51]. Although there are differences between an EDLT and a QIT, the relationships between the voltage of the waveform, the frequency of the waveform applied to the ring electrode and the particle mass-to-charge ratio that could stably levitate and object having net charge remain applicable [51]. A solution to the particle motion can be described as: $\frac{4ezV_{ac}}{m(r_0\omega)^2} < 0.908$, where $\frac{z}{m}$ was the charge-to-mass ratio of the particle with net charge, e was the elementary electron charge, z was the number of elementary charges, V_{ac} was the amplitude of the alternating current (AC) sinusoidal waveform, $\omega=2\pi f$, in which f was the AC frequency, r_0 was radius of the ring electrode [51, 52]. To levitate the droplets in an EDLT, an AC sinusoidal waveform with an amplitude of 4.5 kV_{p-p} was applied to the ring electrodes. The frequency of the waveform was ramped from 60 Hz while the

droplets were generated to 460 Hz within 2 seconds because the volatile components within the droplet evaporated within a short time, and the mass of the droplets decreased. Following a 30 second levitation period, the droplet residue, the materials comprised of low volatility, were either solid, liquid, or a mixture of solid and liquid states depending on the materials added to the starting solution. These residues are referred to as particles. The mass of each component in the particle was estimated based on the initial known concentration of low volatility materials in each starting solution and the average volume of the dispensed droplets, which was 330 ± 190 pL [53].

The levitated particles were removed from the EDLT by applying an attractive 4000 V DC potential to the bottom electrode while reducing the frequency of the AC field back to 60 Hz. The particles could be deposited onto a culture of A549 cells by putting a cell culture plate on the bottom electrode prior to extraction of the particles from the EDLT. 4000 V was a high voltage that could extract the particles from the EDLT to the bottom electrode and demonstrated no harm to the cell cultures [53].

2.2 Matrix-assisted laser desorption/ionization time-of-flight mass spectrometry (MALDI-TOF-MS)

Matrix-assisted laser desorption/ionization (MALDI), as a soft ionization technique, has become a widely used method to ionize and detect intact, thermally fragile, and low volatility compounds, such as proteins. The process of MALDI was described in 1988 during the 11th International MS Conference in Bordeaux [42]. The compound used as the “matrix” is usually an acidic aromatic molecule that is mixed in aqueous solutions with analyte molecules, and that mixture aliquoted onto a target plate and allowed to dry forming matrix-analyte co-crystals [43]. It has been reported that molar ratios from 100 :

1 to 50,000 : 1 of matrix to analyte is optimal for ion production [54]. A pulsed laser (usually a N_2 laser) is used for desorption and ionization of the analyte molecule [43, 55]. The light energy is mostly absorbed by matrix molecules and they are heated in a short period (p ~ n second) causing those molecules to sublimate from solid phase to gas phase in vacuum, carrying with them the analyte molecules into the gas phase [42]. In gas phase, electronically exited matrix molecules transfer a proton to an analyte molecule in favorable collisions to ionize the analyte molecule [43, 55]. Though fragmentation of analyte does occur, MALDI tends to generate predominately $[M+H]^+$ or $[M-H]^-$ ions [42].

MALDI is typically interfaced with a time-of-flight (TOF) mass analyzer [42, 43]. In a TOF analyzer, ions are accelerated to the same kinetic energy by an electric potential and then allowed to pass through a field-free region (drift tube) [54] and therefore the time that each ion flies through the drift tube is proportional to the square root of the mass-to-charge ratio (m/z) of the ion, so that following calibration of drift times using standard molecules, the m/z of unknowns can be determined. The equation is described as followed: $KE = \frac{1}{2}mv^2 = zeV$, where KE is the kinetic energy of ion, m is mass of ion, v is velocity of ion, z is number of net charges on the ion, eV is the kinetic energy gained by a single electron when it accelerates through an electrostatic potential. $v = \frac{L}{t}$, where v is velocity of ion, L is drift length, t is drift time. Thus $\frac{m}{z} = \frac{2eVt^2}{L^2}$.

2.3 Fluorescence microscope

An inverted fluorescence microscope (Figure 2.2) is used for detecting the substances using the phenomena of fluorescence. Fluorescence is luminescence by a

substance that absorbed a photon and emitted a UV-vis photon, usually of a longer wavelength. An electron in an atom can be promoted from a lower energy state to a higher energy state by absorbing a photon. The electron releases energy in the form of light (eg. luminescence) or heat when it returns back to the original energy state. Some of the energy is lost in molecular rotations, vibrations or heat before emission of the light, thus, the emission wavelength is typically longer than the excitation wavelength.

In a fluorescence microscope, light is first passed through a dichroic filter cube containing a fluorescence bandpass excitation filter. The frequency of light that passes through the filter is a specific small range of frequency, and the filter is selected so that the transmitted light can be absorbed by the sample. The light passes through the objective lens, and reaches the sample. The sample absorbs the light and then, in the case of molecule non-resonant fluorescence, emits a longer wavelength of light. An emission filter is selected so that only light emitted from the sample can pass through and go to the detector and eyepiece of the microscope to provide the fluorescence image.

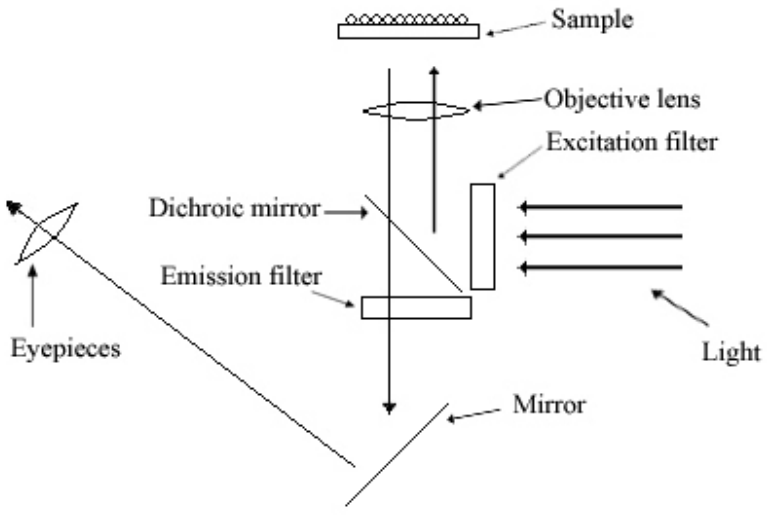

Figure 2.2 Schematic diagram of an inverted fluorescence microscope.

Chapter 3 Improvement of Methodology to Measure Differential Expression of ICAM-1, *in vitro*, in Response to Incubation with Particles Prepared by EDLT

3.1 Introduction

Many studies conclude that there is a link between exposure to ambient air particulate matter (PM) and adverse health effects [1-12]. To study the effect of PM on human lung tissue, a common methodology is to collect atmospheric dusts from air filters, followed by resuspension of these dusts in liquid [56, 57], or they are re-dispersed using a powder disperser [58], prior to being injected or instilled [57] or inhaled [56, 58] respectively into animal models, or suspended in cell growth medium prior to incubation with cell cultures [59, 60]. Conversely, standard solutions of compositions that have been identified in PM have been instilled in animal models [61] or incubated with cell cultures [60, 62].

In this chapter, I first introduce Allen Haddrell's methodology of assessing the inflammation potential of ambient PM_{10}, point out the problems encountered in using his methodology, and then I describe solutions to these problems, with subsequently collected data and data processing strategies. Lastly, I describe the entire procedure of the modified methodology.

3.2 Compositions of particles used in this chapter

3.2.1 Lipopolysaccharide (LPS)

Endotoxin is a toxic compound detected as a component of the outer membrane of Gram-negative bacteria [63-72]. However the word "Lipopolysaccharide" (LPS) has different definitions in the literature. Many authors consider endotoxin and LPS as being synonymous [63-67], while some reports consider LPS as the chemically pure form of endotoxin [68, 73], others define LPS as a part of endotoxin [69, 74], and one literature report indicates that endotoxin is biologically active LPS [70].

LPS comprises three segments: lipid A, core domain and O-specific chain [75]. All the three segments have various structures from different LPS [75]. Lipid A, which is a family of (phospho)glycolipid molecules, is responsible for the toxicity of the LPS [75]. Core domain, which is a branched heteropolysaccharide without repeating glycosyl structures, attaches directly to the lipid A [75]. The function of the core domain is to modulate biological activity of lipid A [75]. O-specific chain, which is a repetitive glycan polymer, attaches to the core domain [75]. O-specific chain can downregulate the endotoxic activity of the LPS [75].

The rationale to incorporate LPS into particles used in this work was because previous studies have shown that LPS is ubiquitous in the environment [68, 70-72, 76-78]. LPS, alone or as a component of ambient particles, is able to induce strong lung innate immune response characterized by cytokine production and immune system activation [66, 67, 70, 73, 74, 77, 79]. No-observed-effects-levels (NOEL) are used to define tolerable exposure concentrations. From field studies, guidelines have been proposed by Rylander in 1997 for the NOEL concentration of endotoxin in dust for airway

inflammation at 10 ng/m^3; for systemic effects at 100 ng/m^3, and for toxic pneumonitis at 200 ng/m^3 [80]. Another study reported that endotoxin exposure above 4 ng/m^3 is associated with a decline in lung function [78].

Environmental reports of endotoxin are expressed either as ng, a measurement of chemical activity, or as endotoxin units (EU), a measurement of biological activity [81]. Depending on the source of the endotoxin and its purification, the conversion from weight to EU varies [82]. The U.S. Food and Drug Administration (FDA) initially defined 1 ng endotoxin equals to 5 EU as Reference Endotoxin Standard (EC-2) [83]. However, the current Reference Endotoxin Standard (EC-6) defines 1 ng endotoxin as equal to 10 EU [84].

Various endotoxin measurements in PM have been reported around the world. A study in the USA reported that the average endotoxin concentration in Southern California was 13.6 EU/mg dust [65] while another study in the USA showed that the average endotoxin concentration inside Denver houses was 178.2 EU/mg dust, with a range from 20.8 – 2000 EU/mg dust [77]. A study in a USA fiberglass wool manufacturing plant reported that the 8 hour time-weighted average personal exposure endotoxin could be up to 759 ng/m^3 [78]. A study in Brazil showed that a medium of endotoxin concentration was 10.8 EU/mg dust, with the range being 0.03 – 1100 EU/mg dust [66]. A study in Germany reported that the average concentration of endotoxin in living rooms is 2.27 ng/mg dust [71]. A study in New Zealand showed that the average endotoxin levels in a whole home is 28.4 EU/mg dust [72]. A study in Holland reported that the average endotoxin concentration in ambient particles collected at agricultural site

is 105 ng/m^3 [73]. A study in UK reported that the endotoxin levels in agricultural environments, such as grain handling, could be up to as high as 770,000 ng/m^3 [81].

One literature reported that the receptor for LPS, Toll-like receptor 4 (TLR-4), is not expressed on the surface of A549 cells, but it exists intracellularly [85], while some literatures reported low level of surface expression of TLR-4 in A549 cells [86, 87]. One literature reported that TLR-4 exists intracellularly in A549 cells, but it translocates into membrane when induced with LPS [88]. Despite of the discrepancy in the literatures regarding of the surface expression of TLR-4 in A549 cells, all literatures agreed that LPS do affect ICAM-1 expression in these cells.

In this study, up to 250 particles containing up to 1570 pg LPS from Escherichia coli O111:B4 (Sigma-Aldrich, L2630-10MG, Oakvillle, ON, Canada) per particle were deposited onto a culture of A549 cells. Since the culture contained ~7.5×10^4 cells [89], the total LPS added per cell was ~5 pg, which equaled ~0.05 EU. Since LPS is heterogeneous and tends to form aggregates of different sizes [90, 91], according to instructions provided by the supplier, the molecular weight can vary from 10 kDa to 4,000 kDa. Therefore, it was meaningless to calculate the number of moles of LPS per cell.

3.2.2 Carbon

Carbonaceous PM, soots, are mainly composed of the products in the combustion of heavy petroleum distillates, including residual oils, coal-tar products, natural gas, acetylene and octane [92-94]. Carbon was used in this study as a mimic because soots in ambient samples have been found to be carcinogenic in animal and human studies [94-96]. In this study, a particle residue of India Ink was considered as elemental carbon,

because in the India Ink, the carbon is present as nanoparticles ~20 nm in dimension, and the quantity of solids in India Ink, assumed to be predominantly carbon, was measured as 227 ± 5 mg residue per mL ink using gravimetric analysis.

3.3 Agnes laboratory existing methodology

Allen Haddrell, a previous graduate student, developed a methodology to assess the pro-inflammatory potential of ambient PM_{10}, *in vitro*, using a particle levitation trap apparatus, as the tool by which ambient particle mimics were prepared and then delivered to a human lung cell culture [97]. This methodology included cell culturing, particle generation and deposition, and incubation followed by assays of soluble biomolecules in supernatant using soft ionization mass spectrometry and immunocytochemistry.

The Haddrell methodology

3.3.1 Cell culture

A549 cell lines (American Type Culture Collection [ATCC], CCL 185, Manassas, VA, USA) were grown to ~95% confluence on an 18 mm × 18 mm glass coverslip in a 6-well plate (Corning, 3516, Lowell, MA, USA) in minimum essential medium (MEM) (Sigma-Aldrich, M0769-10X1L, Oakvillle, ON, Canada) supplemented with 10% heat-inactivated fetal bovine serum (FBS) (Invitrogen Canada Inc., 26140-079, Burlington, ON, Canada) in 5% CO_2 at 37 ºC and 100% humidity [97].

3.3.2 Particle generation and deposition onto lung cells *in vitro*

With a population of particles generated and levitated using an EDLT (described in chapter 2), a cell culture grown on a coverslip was drained by touching onto a kimwipe

tissue, leaving behind 15.9 ± 2.5 μL [97] of the growth medium. The coverslip was immediately placed under the EDLT. The particles were then deposited from the AC trap directly onto the cell culture. The coverslip was then placed into a sterile (35 mm × 10 mm) tissue culture dish and then incubated in an atmosphere of 5% CO_2 at 37 ºC and 100% humidity for 24 hours. No additional medium was added to the cell culture during the incubation period.

The negative controls were cell cultures grown to ~95% confluence on an 18 mm × 18 mm glass coverslip that followed all steps of the procedure described above except deposition of the particles. The positive controls were cell cultures grown to ~95% confluence on an 18 mm × 18 mm glass coverslip bathed in 50 ng/mL tumor necrosis factor alpha (TNF-α) (Sigma-Aldrich, T6674-10UG, Oakvillle, ON, Canada) in 2 mL of growth medium and incubated for 24 hours. TNF-α is known to induce ICAM-1 expression on A549 cells [98-100].

3.3.3 Collection of the Supernatant for MALDI-TOF-MS analysis

Following an incubation period, the supernatant was collected by washing with a 50 μL aliquot of Phosphate Buffered Saline (PBS) solution over two entire cell cultures to harvest sufficient biomolecules to be detected using MALDI-TOF-MS. The harvested supernatant samples were stored in a micro-centrifuge tube at -20 ºC until analysis.

To remove the PBS in the supernatant, a C_{18} ZipTip (Millipore, ZTC18S096, Etobicoke, ON, Canada), which is a pipette tip with a bed of chromatography media fixed at its end, was used to purify and concentrate the biomolecules in the supernatant. A MALDI-TOF-MS (Waters Corp., model MALDI-LR, Manchester, UK) was used to characterize supernatant samples. The mass range that monitored was from 3 to 24 kDa.

To compare data, the relative abundance of every ion in a spectrum was normalized to the abundance of the ion having the highest signal intensity per spectrum.

3.3.4 Immunocytochemistry assay

The cells were fixed with 1% acetone water solution for 10 minutes after the 24-hour incubation period. The primary antibody was mouse monoclonal antibody directed to the human CD54 (ICAM-1) antigen (Invitrogen Canada Inc., MHCD54F, Burlington, ON, Canada). The secondary antibody was fluorescently labeled goat anti-mouse IgG antibody (Invitrogen Canada Inc., A-11003, Burlington, ON, Canada). Both the primary and secondary antibody dilution buffers were Tris(hydroxymethyl)aminomethane buffered saline (TBS)/Bovine serum albumin (BSA) (Sigma-Aldrich, A9647-50G, Oakville, ON, Canada) solution. 0.01 M TBS solution was prepared by adding 8.7 g TBS powder and 6.05 g sodium chloride (NaCl) powder to 950 mL Milli-Q water. The pH was adjusted to 7.6 with 1N hydrochloric acid (HCl) or 1N sodium hydroxide (NaOH) and the volume was brought up to 1 L by adding Milli-Q water. 0.001% (w/v) BSA solution was prepared by adding 0.01 g BSA powder to 1 L Milli-Q water. 500 mL 0.01 M TBS solution and 500 mL 0.001% (w/v) BSA solution were mixed to make the TBS/BSA antibody dilution buffer. 2 μL of 0.1 mg/mL primary antibody was added to 100 μL of antibody dilution buffer for staining the cells on one coverslip. 1 μL of 2 mg/mL secondary antibody was added to 100 μL of antibody dilution buffer for staining the cells on one coverslip.

3.3.5 Image from fluorescence microscopy and data analysis

The coverslip supporting the cell cultures was mounted upside down onto a 75 mm × 25 mm microscope glass slide with a drop of glycerol in between. Nail polish was used to make the coverslip adhere to the glass slide. An inverted fluorescence microscope (Motic Instrument Inc., AE31, ON, Canada) with an Epi-FI filter block (Motic Instrument Inc., Green MG-1, ON, Canada) was used for observing and capturing images of the fluorescently labeled cell cultures from the site of particle deposition. The intensity of the fluorescence emission in each image was processed using Image J software (Research Services Branch, National Institute of Mental Health, Bethesda, MD, USA) and those pixel intensity values integrated using Excel (Microsoft, Seattle, Washington). The total fluorescence signal relative to positive control was expressed as a percentage and plotted as a function of the numbers of particles deposited.

3.4 Problems with the existing methodology and problem solving

3.4.1 Culture wide cell-death due to drying out and particles not adhering to the cells

3.4.1.1 Trypan blue staining assay

Trypan blue is a high molecular weight acid blue dye which has been widely used in cell-death experiments because it is inexpensive and the methodology for its use in such assays is well developed and simple [101, 102]. Trypan blue can be used for both adherent and suspended cells to distinguish their viability [101]. This dye stains cells having damaged plasma membranes based on the principle of "dye exclusion" [101, 102]. Intact cell membranes are selective in compounds that can cross the barrier. The two

chromophores in trypan blue are negatively charged and they belong to the compounds that are not allowed to cross intact cell membranes [102]. Viable cells having an intact membrane exclude trypan blue and thus appear transparent, while non-viable cells with compromised membrane integrity allow entry of trypan blue and thus appear blue. Trypan blue can be taken up by viable cells if it is exposed to cells for a long period of time. Trypan blue binds more strongly with serum proteins than cellular proteins [102], therefore PBS should be used to wash the cell culture before and 5 minutes after a trypan blue solution is added [102].

3.4.1.2 Culture wide cell-death after 30 minutes incubation period due to cell culture drying out

All of the photomicrographs including bright field and fluorescence images in this thesis were taken using inverted microscopes with an eyepiece magnification ×10 and objective lenses having different magnification power. Cell cultures prepared as described and incubated for 30 minutes were then bathed by a 0.4% (w/v) trypan blue solution (Sigma-Aldrich, T8154, Oakvillle, ON, Canada) to ascertain the viability of the cell culture after a brief rinse with PBS solution (Figure 3.1). According to Trypan blue staining assay results, the cells were non-viable after 30 minutes incubation period using Haddrell's methodology.

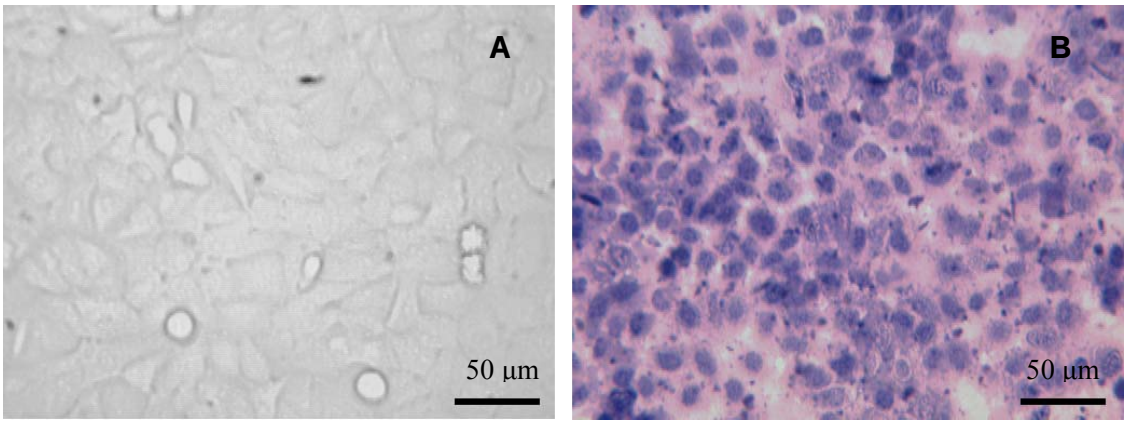

Figure 3.1 Trypan blue cell viability assays. Cell cultures were grown in 2 mL of growth medium on coverslip (A) or drained with a piece of kimwipe tissue (B) were put into an incubator for a 30-minute incubation period. 50 µL of 0.4% (w/v) trypan blue solution was added onto the coverslip supporting the cell cultures after a brief rinse with PBS solution. Cells from (A) were viable; cells prepared using the Haddrell's methodology (intended for receipt of a particle population from an AC trap) (B) were non-viable. Images were taken using an objective magnification of 20X.

3.4.1.3 Use of a 6-well plate to address cell death and particles not adhering

In an effort to prevent the cells from drying out, causing their death, a 6-well plate was used in replacement of the coverslip because a uniform, thin layer of medium bathing the cells could be realized. A study to determine the minimum volume of growth medium necessary to keep the cells viable for a 2-hour period was performed. Trypan blue solution was used to test the viability of the cell culture after a 2-hour incubation period following a brief rinse with PBS solution (Figure 3.2). All the cells were viable after a 2-hour incubation period according to a trypan blue staining assay when 200 µL of growth medium was used to incubate with the cells.

Although cells remained viable, carbon particles did not adhere to the cells, because of the additional growth medium added (Figure 3.3). While viewing the culture plate using the optical microscope, most of the particles (in region B) were observed to be floating and moving in the same direction, likely because of convective flow of the

growth medium. Increases in the incubation period did not improve particle adherence to the cells, and it increased the number of cells that were not viable (Figure 3.4).

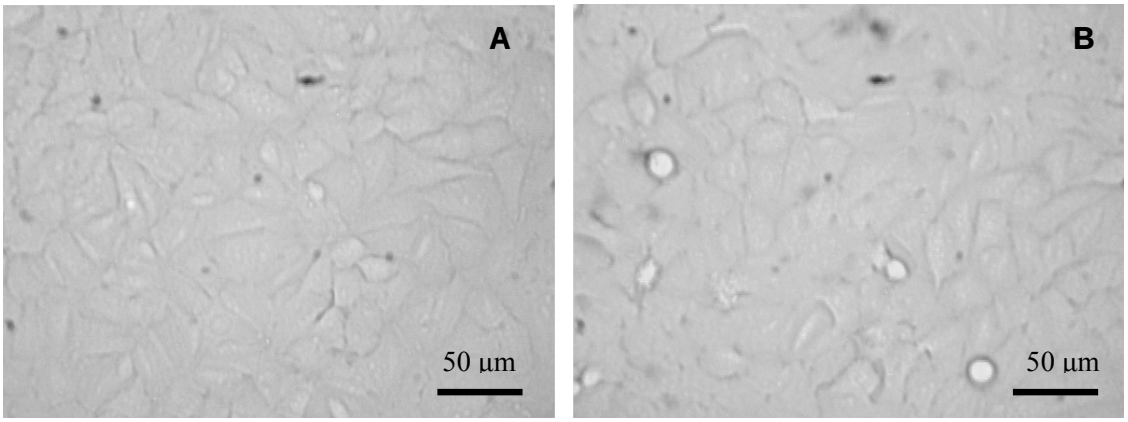

Figure 3.2 Trypan blue cell viability assays. Cell cultures were grown in 6-well plate in 2 mL of growth medium (A), or with medium aspirated by a water faucet driven vacuum aspirator followed by immediate introduction of 200 µL of additional growth medium (B), were put into an incubator for a 2-hour incubation period. 50 µL of 0.4% (w/v) trypan blue solution was added onto the cell cultures after a brief rinse with PBS solution. Cells from (A) and (B) were both viable. Images were taken using an objective magnification of 20X.

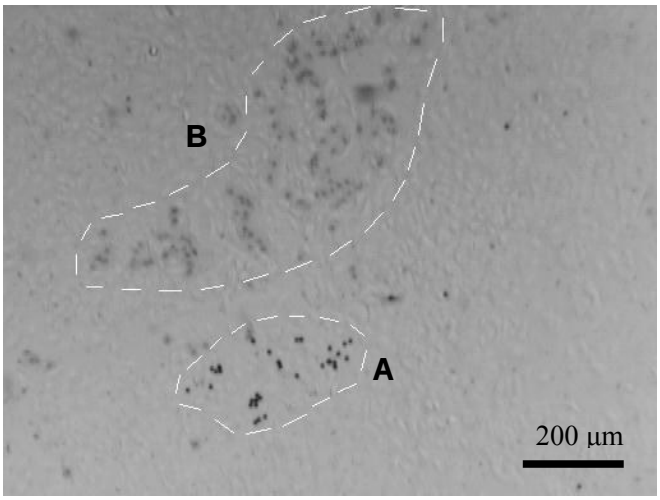

Figure 3.3 Photomicrographs of A549 cells with carbon particles. Cell culture in 6-well plate having 200 µL growth medium and ~100 8µm diameter carbon particles were deposited following a 2.5-hour incubation period. After a gentle shake of the cell culture, the focal plane of the image was positioned on the cells, and a few particles (the black dots highlighted in Region A) remained stationary and in focus with cells while particles (the grey dots highlighted in Region B) were observed to be not stationary and not in focus. Image was taken using an objective magnification of 5X.

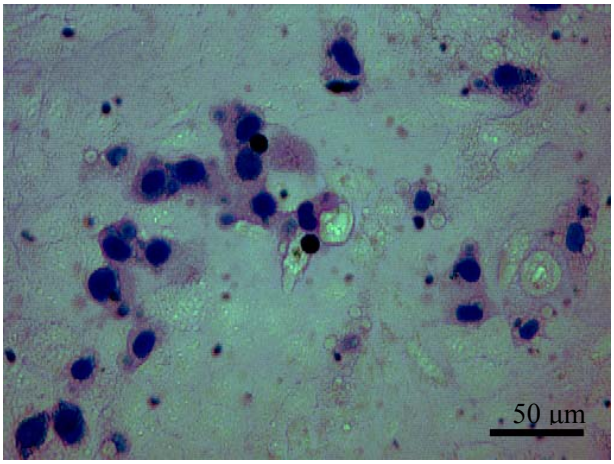

Figure 3.4 Trypan blue cell viability assay. Cell culture in 6-well plate having 200 µL growth medium and ~100 8µm diameter carbon particles were deposited and then incubated for 4-hour. Then 50 µL of 0.4% (w/v) trypan blue solution was added into the 6-well plate after a brief rinse with PBS solution. Approximately 30% of the cells were non-viable. Image was taken using an objective magnification of 20X.

3.4.1.4 Cell viability and observed particle cell adhesion

Cell cultures were grown on coverslips and drained of growth medium by gently dabbing for no more than 1 second once onto a glass slide by tilting the coverslip to ~45°. The coverslip was immediately placed into a sterile well of a 6-well plate after depositing the particles from the AC trap. If multiple populations of particle depositions were needed, the total time from removing medium to all particle depositions was no more than 2 minutes. After 10-15 minutes incubation period, 1 mL of medium was added to the 6-well plate by slowly delivering the aliquot to the side wall of the well. After 24 hours incubation period, most of the cells were viable and most of the particles were adhering to the cells (Figure 3.5).

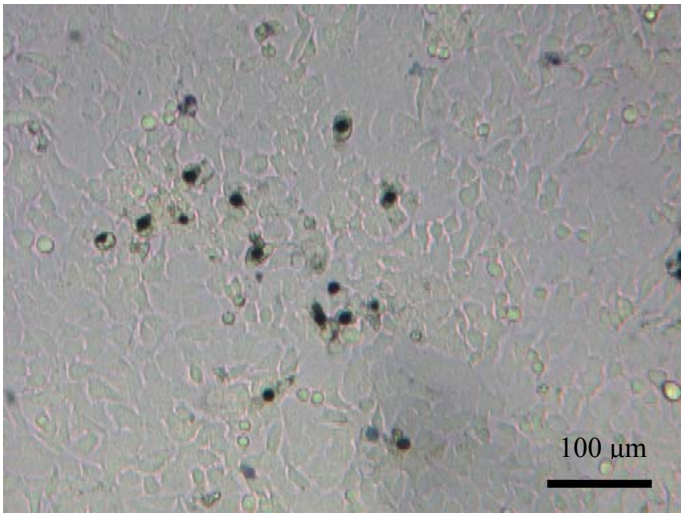

Figure 3.5 Trypan blue cell viability assay. Cell cultures were grown on a coverslip and drained by gently dabbing once onto a glass slide. The coverslip was immediately placed into a well of 6-well plate after depositing the particles. After 10-15 minutes incubation period, 1 mL of medium was added to the 6-well plate by slowly adding against the side wall of the well. After 24 hours incubation period, 50 μL of 0.4% (w/v) trypan blue solution was added onto the coverslip after a brief rinse with PBS solution. Most of the cells were viable. Image was taken using an objective magnification of 10X.

3.4.2 Acetone fixation causing cells to detach from the surface of the supporting material

3.4.2.1 Acetone fixation causing cells detaching from the surface of the supporting material

In Haddrell's methodology, the cells were fixed with 1% acetone water solution for 10 minutes after a 24-hour incubation period. Since additional medium had been added to the cell culture, the cells were moister than in Haddrell's methodology, and the 1% acetone solution caused cells to detach from the surface of the supporting material (Figure 3.6).

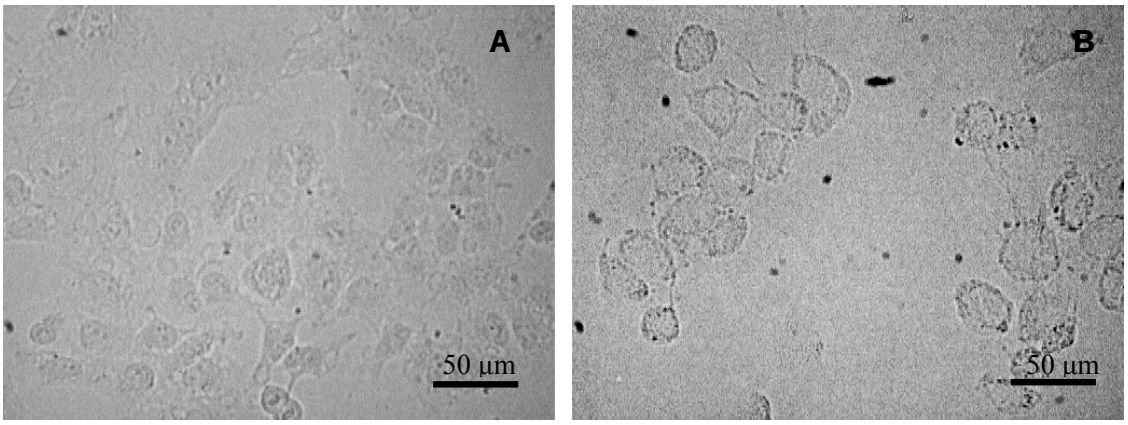

Figure 3.6 Photomicrographs of A549 cells cultured on coverslip and incubated for 24-hour incubation period. The pictures were the cells before (A) and after (B) fixation with 1% acetone solution for 10 minutes. Image was taken using an objective magnification of 20X.

3.4.2.2 Alternative methods of cell fixation

Warm (37 ºC) 1% acetone water or PBS solution was used to fix cell cultures for 10 minutes at room temperature. In all instances, cells were observed to detach from the surface of the supporting material.

Ice cold 1% acetone water or PBS solution was used to fix cell cultures for 10 to 30 minutes at 37 ºC, room temperature or -4 ºC. Cells were observed to either be not all fixed or to detach from the surface of the supporting material.

Ice cold 2% acetone water solution was used to fix cell cultures for 10 minutes at room temperature. Cells were observed to not be all fixed, and many of them were observed to detach from the surface of the supporting material.

4% (w/v) paraformaldehyde (PFA)/PBS (pH 7.4) solution was used to fix the cell cultures [103, 104]. Cell cultures were washed with PBS solution twice before warm (37 ºC) 4% PFA/PBS solution added to them for 20 minutes at room temperature. Cells were

fixed and kept the same shape as they were alive, and they remained fixed to the supporting material.

3.4.3 Biomolecule ion signal intensity suppression in MALDI-TOF-MS characterization of supernatants

3.4.3.1 Growth medium was observed to cause biomolecule ion signal intensity suppression in MALDI-TOF-MS characterization of supernatants

Both growth medium itself and supernatant from A549 cell cultures were characterized by MALDI-TOF-MS (Figure 3.7). Spectra from growth medium itself and cell supernatant were observed to be similar though small differences were noted. Since more medium was added to the cell cultures in an effort to keep them viable, biomolecules from serum in the growth medium could be observed in cell supernatant in the MALDI-TOF-MS spectra. The similarity in the spectra shown in figure 3.7 are presumably attributed to compounds in serum, and the ion signal intensities of the biomolecules in serum were so strong, because of their relatively higher abundance than cell-secreted biomolecules, that they suppressed the ion signal intensities of the cell-secreted biomolecules making those ion signal intensities undetectable from the background. Therefore, it was concluded that most ion signals observed in figure 3.7 (B) were from serum as the same ions were observed in figure 3.7 (A).

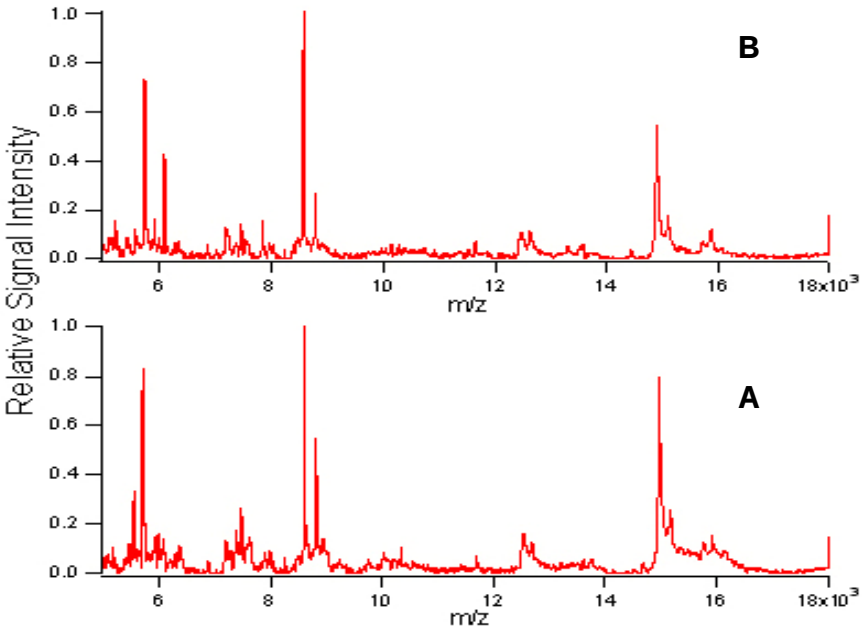

Figure 3.7 MALDI-TOF mass spectra of growth medium (A) or supernatants of A549 cell cultures incubated in incubator for a 22-hour incubation period after confluence (B). The growth medium and supernatant were each processed using a C_{18} ZipTip prior to co-crystallization with SA matrix on a MALDI target plate.

3.4.3.2 Biomolecules in serum in growth medium interact with $Al(NO_3)_3$ and NaOH mixture

To prepare the growth medium with $Al(NO_3)_3$ and NaOH mixture, 0.12 g $Al(NO_3)_3 \cdot 9H_2O$ and 730 µL of 1N NaOH were added to 10 mL growth medium. Both growth medium itself, and growth medium with $Al(NO_3)_3$ and NaOH, were characterized by MALDI-TOF-MS (Figure 3.8). From figure 3.8, the ion signals at 6.20 kDa, 6.97 kDa and 13.74kDa were observed in growth medium with $Al(NO_3)_3$ and NaOH mixture, but not in growth medium itself. The ion signals at 5.71 kDa, 7.47 kDa and 12.49 kDa were observed in growth medium itself, but not in growth medium with $Al(NO_3)_3$ and NaOH. The ion signals at 8.58 kDa and 8.79 kDa were observed in both growth medium itself, and growth medium with $Al(NO_3)_3$ and NaOH. By comparison of ion signals in these two

mass spectra, it was proposed that ion signals at 5.71 kDa and 12.49 kDa in figure 3.8 (A) shifted to a higher mass range of 6.20 kDa and 13.74 kDa in figure 3.8 (B) while the ion signal at 7.47 kDa in figure 3.8 (A) shifted to a lower mass range of 6.97 kDa in figure 3.8 (B). The two mass spectra indicated that the biomolecules in serum interacted with $Al(NO_3)_3$ and NaOH, causing their ion signals detected to change to different m/z. However the specific compounds with respect to it being a factor in this interaction were not identified, because this experiment was only designed for further study of serum interfering with the results. This phenomenon suggested that those mass-to-charge changes in ion signal intensities observed previously in the old methodology may not all have been caused by cells secreting new proteins triggered by particles [105]. There is also a probability that they may have been caused by serum in the growth medium interacting with compounds in particles.

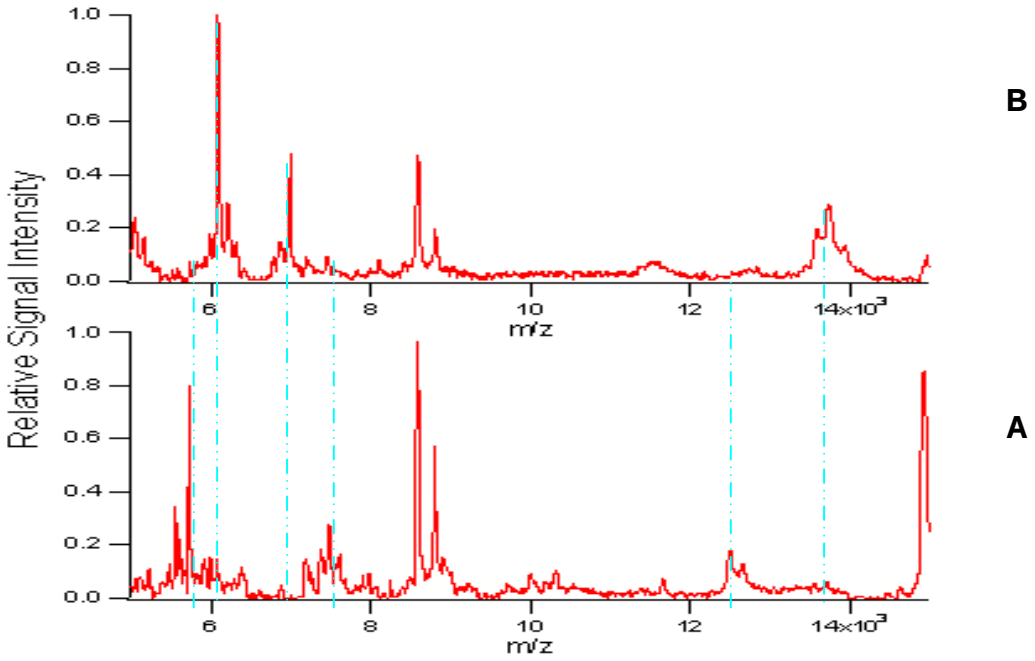

Figure 3.8 MALDI-TOF mass spectra of growth medium (A) or growth medium containing $Al(NO_3)_3$ and NaOH (B). The growth medium with and without chemicals were each proceesed using a C_{18} ZipTip prior to co-crystallization with SA matrix on a MALDI target plate.

3.4.3.3 Diminishing of ion signal intensity suppression from serum in growth medium

A549 cell cultures were incubated in serum-free medium (SFM) in replacement of growth medium during the incubation period prior to the collection of the supernatant. Both cell supernatants with growth medium or with SFM were characterized by MALDI-TOF-MS (Figure 3.9). New and greater ion signal intensities were observed in SFM relative to those observed from samples incubated in growth medium, presumably due to alleviation of ion suppression in the ion source in supernatant samples incubated with SFM. SFM was therefore used to alleviate the suppression of ion signal intensities observed when present in a serum medium.

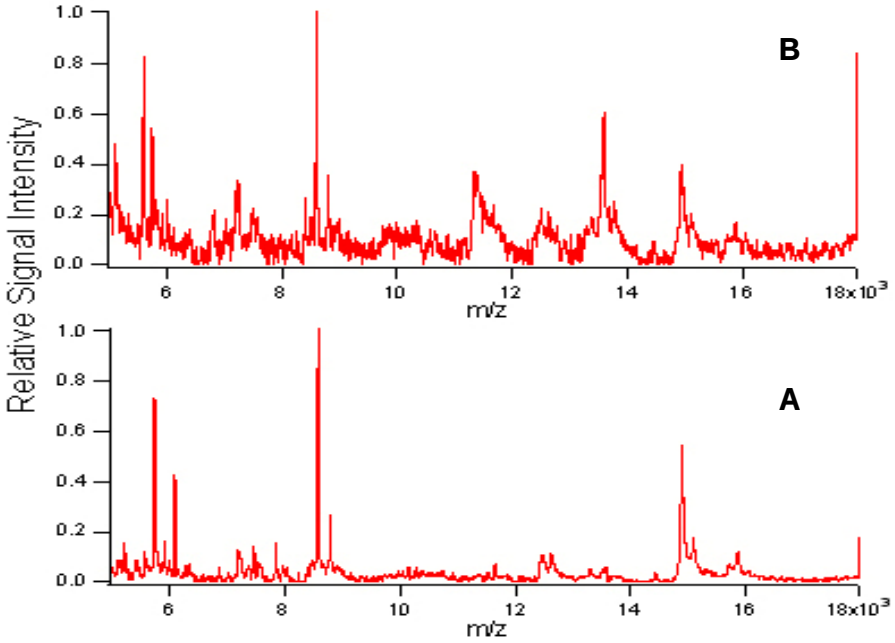

Figure 3.9 MALDI-TOF mass spectra of the supernatants of A549 cell cultures incubated for a 22-hour incubation period after confluence in growth medium (A) or in SFM (B). The supernatants were each processed using a C_{18} ZipTip prior to co-crystallization with SA matrix on a MALDI target plate.

3.5 Methodology improvements

3.5.1 F-12K medium used as cell growth medium

In Haddrell's methodology, MEM was used as cell culture medium although MEM was not the medium that ATCC recommends for culturing of the A549 cell line. The medium recommended for this cell line was Kaighn's Modification of Ham's F-12 Medium (F-12K medium) with FBS added to a final concentration of 10%.

Although there was no obvious difference on cell morphology as observed with a microscope, F-12K was used in replacement of MEM since MEM did not contain enough compounds that A549 cells need such as vitamins, L-Glutamine, sodium pyruvate.

3.5.2 Internal standard for MALDI-TOF-MS analysis

In Haddrell's methodology, to compare the data, the relative abundance of every ion in a mass spectrum was normalized to the abundance of the ion having the highest signal intensity which was not a proper way to normalize the data since the ion having the highest signal intensity could change from spectrum to spectrum and sample to sample. However an internal standard was required, and there was no ion signal at m/z 14.4 kDa from the MALDI-TOF-MS spectra, and therefore lysozyme from chicken egg white (Sigma-Aldrich, L7651-1G, Oakvillle, ON, Canada) was selected based on mass as an internal standard to further investigate. To determine the concentration of lysozyme to be added into the supernatant, several aliquots of a lysozyme stock solution were added to the supernatants and characterized by MALDI-TOF-MS (Figure 3.10). 6.3×10^{-8} M proved to be an optimal quantity of lysozyme, for supernatants harvested at 30 minutes

incubation period since the lysozyme could be detected by MALDI-TOF-MS while not suppressing other ion signal intensities.

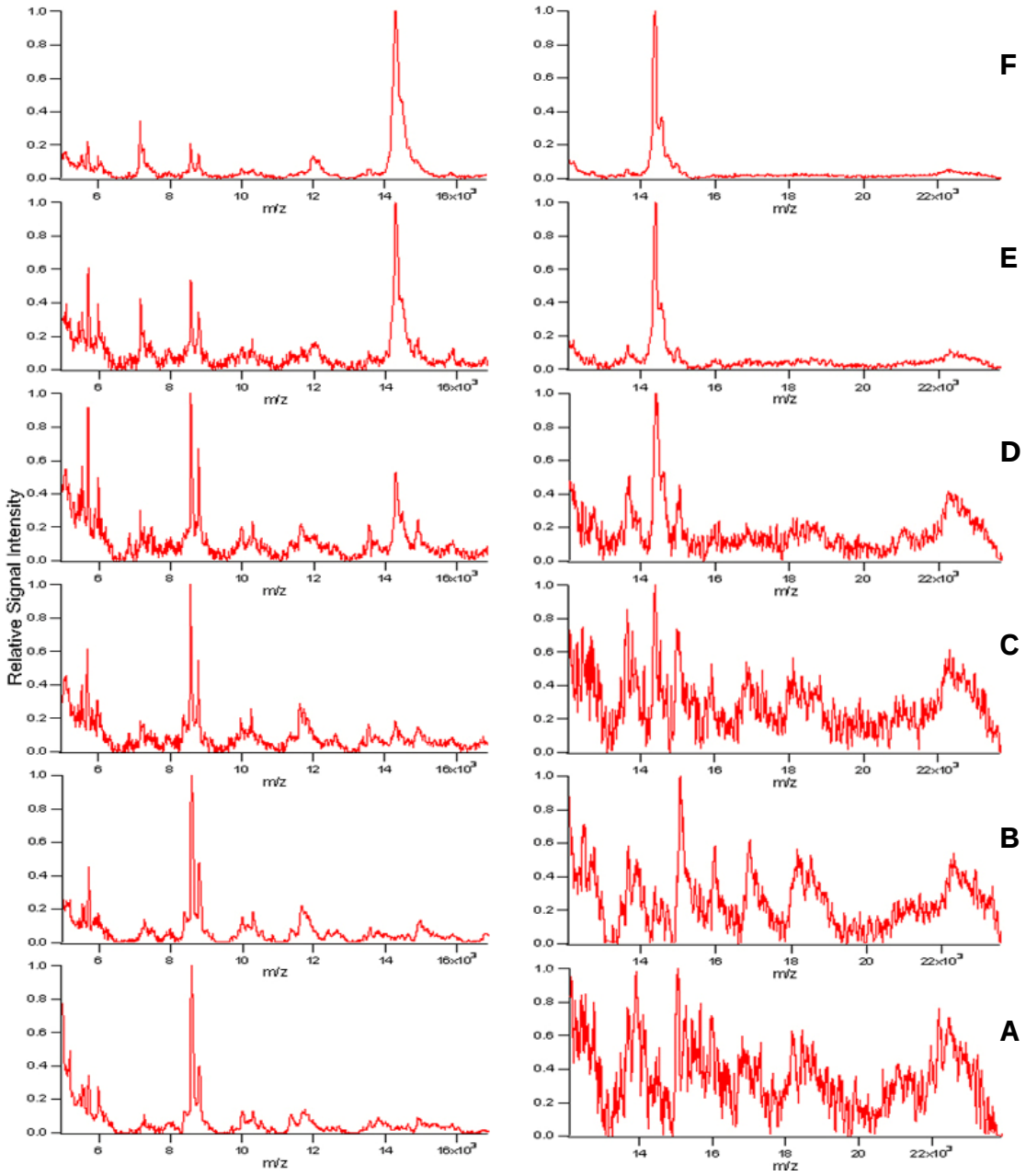

Figure 3.10 MALDI-TOF mass spectra of the supernatant of A549 cell cultures incubated in incubator for 30 minutes with SFM. The supernatant from one cell culture was split into 6 equal volume portions. Final concentrations of 0.0 M (A), 1.3×10^{-8} M (B), 3.2×10^{-8} M (C), 6.3×10^{-8} M (D), 1.6×10^{-7} M (E) and 3.2×10^{-7} M (F) lysozyme were prepared respectively. The supernatants were then purified using a C_{18} ZipTip prior to co-crystallization with SA matrix on a MALDI target plate. Spectra on both left and right sides were different mass ranges with 5 kDa overlapping.

3.5.3 PBS solution used in replacement of TBS solution in immunocytochemistry

In Haddrell's methodology, the antibody dilution buffer for both the primary and secondary antibody was TBS/BSA solution. However, from immunohistochemistry (IHC) World Life Science Information Network's antibody dilution buffer protocols, it claimed that TBS pH 7.6 used in either primary or secondary antibody dilution buffer produces weaker staining. It also suggested that BSA or other reagents not be used with serum to dilute secondary antibodies, since secondary antibodies can interact with BSA or serum that would reduce antibody affinity. With knowledge of these considerations, the primary antibody dilution buffer was changed to 1% (w/v) BSA/PBS solution, and the secondary dilution buffer was changed to PBS solution.

3.5.4 Step-gradient elution experiment

To ensure that Haddrell's methodology's ZipTip elution solution was optimized, step-gradient elution was performed. One supernatant sample was split into two equal volume portions. One portion was ZipTiped and eluted with the Haddrell's methodology's elution solution which was sinapic acid (SA) saturated in an acetonitrile (ACN)/trifluoroacetic acid (TFA) solution. The elution solution was prepared by adding excess SA (Sigma-Aldrich, 85429, Oakvillle, ON, Canada) powder into 50 μL ACN with 50 μL 0.1% (v/v) TFA mixture solution to make SA saturate. Followed a centrifugation at a relative centrifugal force (rcf) of 2000 g for 5 minutes, the supernatant without solid SA was used for elution. The eluted sample was directly spotted to the MALDI target plate. The other portion was eluted with different concentrations of ACN in 0.1% TFA with saturated SA solutions:

(1) 50 μL ACN with 1 μL TFA in 949 μL Milli-Q water (5% ACN/0.1% TFA),

(2) 100 μL ACN with 1 μL TFA in 899 μL Milli-Q water (10% ACN/0.1% TFA),

(3) 200 μL ACN with 1 μL TFA in 799 μL Milli-Q water (20% ACN/0.1% TFA),

(4) 300 μL ACN with 1 μL TFA in 699 μL Milli-Q water (30% ACN/0.1% TFA),

(5) 500 μL ACN with 1 μL TFA in 499 μL Milli-Q water (50% ACN/0.1% TFA),

(6) 700 μL ACN with 1 μL TFA in 299 μL Milli-Q water (70% ACN/0.1% TFA).

Solutes retained on the ZipTip were first eluted by 4 μL 5% ACN/0.1% TFA by aspirating and dispensing the solution through the ZipTip using 5 cycles without introducing air followed by transferring the solution directly onto a sample well of stainless steel MALDI plate. The same ZipTip was then washed with 5% ACN using 3 cycles without introducing air into the tip prior to next elution with 4 μL 10% ACN/0.1% TFA. The concentration of ACN was increased each time and the steps were repeated until step-gradient was completed (Figure 3.11). All the ion signals from figure 3.11 B to G could be observed in figure 3.11 A, which suggested that Haddrell's methodology's elution solution was optimal.

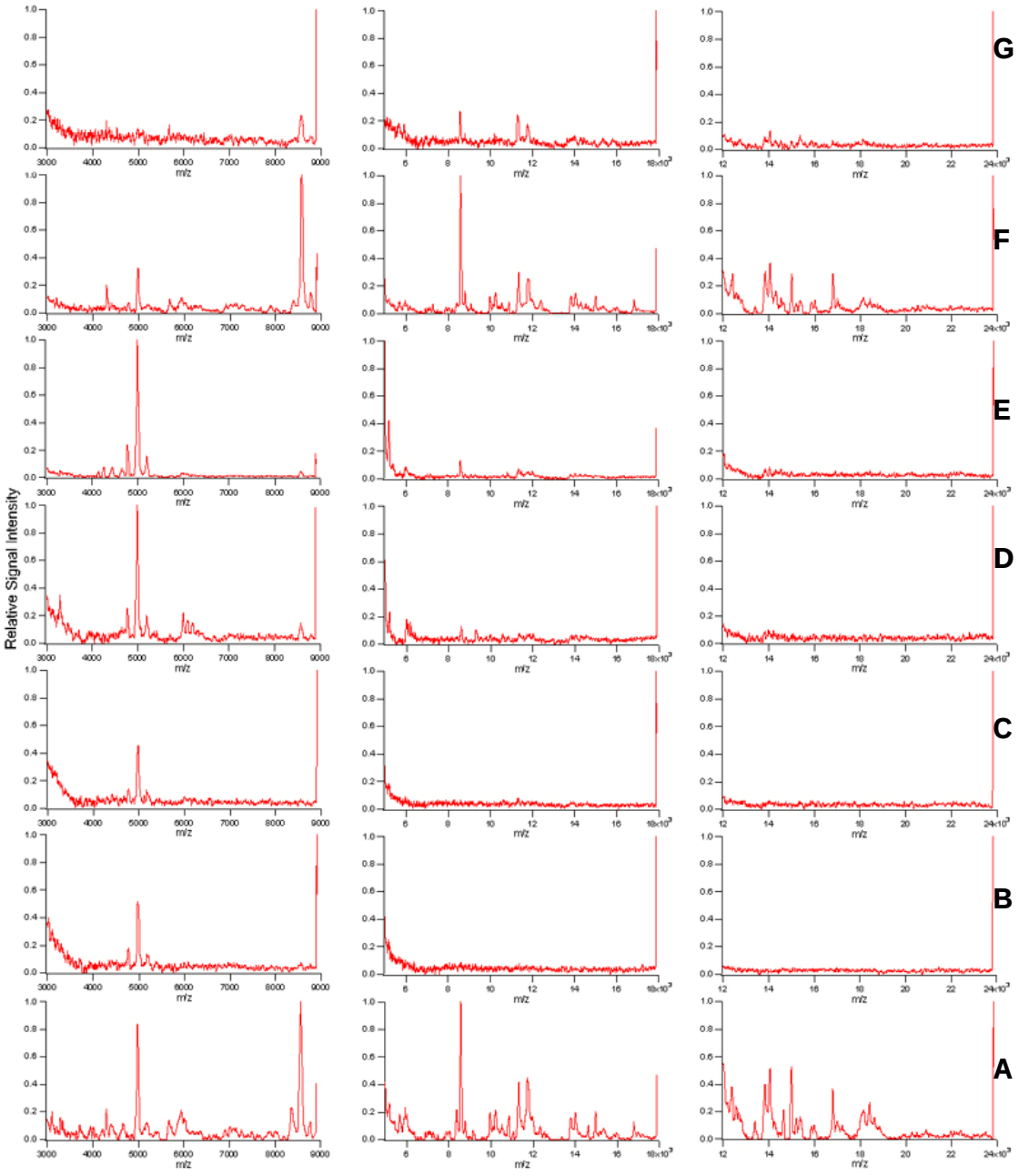

Figure 3.11 MALDI-TOF mass spectra of the supernatants of A549 cell cultures incubated in incubator for 30 minutes with SFM using Haddrell's elution methodology (A) and step-gradient elution: 5% ACN/0.1% TFA (B), 10% ACN/0.1% TFA (C), 20% ACN/0.1% TFA (D), 30% ACN/0.1% TFA (E), 50% ACN/0.1% TFA (F), 70% ACN/0.1% TFA (G). Spectra on left, middle and right sides were different mass ranges with 4-6 kDa overlapping.

3.5.5 Minor changes in the methodology

My study focused on 6-8 μm diameter particles. After all of the changes described, the methodology was used for my studies. Alice Kardjaputri, another graduate student, tried to use this modified methodology in 2.4 μm diameter particles study but found it did not work very well. For example, smaller particles did not adhere to the cells themselves. Kardjaputri made some changes to this modified methodology again. In an effort to make the whole group have one uniform methodology, I made additional changes in my methodology to be consistent with that being used by Kardjaputri.

3.5.5.1 Cells cultured in centre-well organ culture dish

Since cells cultured on coverslips had greater risk of contamination than cells cultured in a centre-well organ culture dish. The latter was used in replacement of coverslip since it had a similar surface area as the coverslip used in previous experiments. Moreover, water was added into the moat of the dish to assist keeping the cells moist while only a small volume of SFM was added to the cells to facilitate particle contact and adherence to the cells, and the cells did not dry out.

3.5.5.2 FluoSpheres added into the particles

Particles < 6 μm were difficult to locate with a bright field microscope, whereas by comparison 6-8 μm diameter particles were easy to find. FluoSpheres beads (Invitrogen Inc., F-8787, Burlington, ON, Canada), 0.02 μm polystyrene microspheres with dyes, were added to particles in the ~2 μm size range by Kardjaputri to aid in locating the particles through a fluorescence microscope. Since these dye containing microspheres

had been used in cells and showed no harm to cell cultures [106, 107], I added them into my types of particles to keep methodology uniform with other group members.

3.5.5.3 Centrifugation after deposition of particles

Particles in the ~2 μm size range required assistance (eg. an extra force) beyond gravitational settling alone to enable them to make contact with the cells, whereas 6-8 μm diameter particles made contact and adhered to the cells themselves. Trypan blue assay was used to assess cell viability after centrifugation and the cells were viable. Therefore centrifugation (at rcf of 1200 g for 1 minute) was added to my methodology to maintain method uniformity with other group members.

3.6 MALDI-TOF-MS data processing

3.6.1 Ion signals monitored by MALDI-TOF-MS

A549 cells were cultured in centre-well organ dishes and bathed in 250 μL SFM in an incubator with 500 ng/mL TNF-α, as positive control, or without TNF-α as negative control. Cell supernatants were collected after 24 or 48 hours and characterized by MALDI-TOF-MS (Figure 3.12). The ion signal at 14.4 kDa in Figure 3.12 was the internal standard of lysozyme which was described in section 3.5.2. The relative ion signal intensity of lysozyme was set to 1. From figure 3.12, it was observed that the biomolecules secreted by cells increased when the incubation period increased. However, it may also have been caused by simply one MALDI-TOF-MS data to the next MALDI-TOF-MS data, eg. routine variability in MALDI-TOF-MS. The ion signal intensity at 8.37 kDa was much higher in positive controls than in negative controls in both 24 and 48 hours incubation period. To learn if there is a dose response relationship between

number of particles and the ion signal intensity at 8.37 kDa secreted by A549 cells, A549 cells were cultured in centre-well organ dishes and dosed with different numbers of particles containing 320 pg LPS and 1110 pg carbon per particle and incubated in an incubator with 250 µL SFM. Cell supernatants were collected after 72 hours and characterized by MALDI-TOF-MS (Figure 3.13).

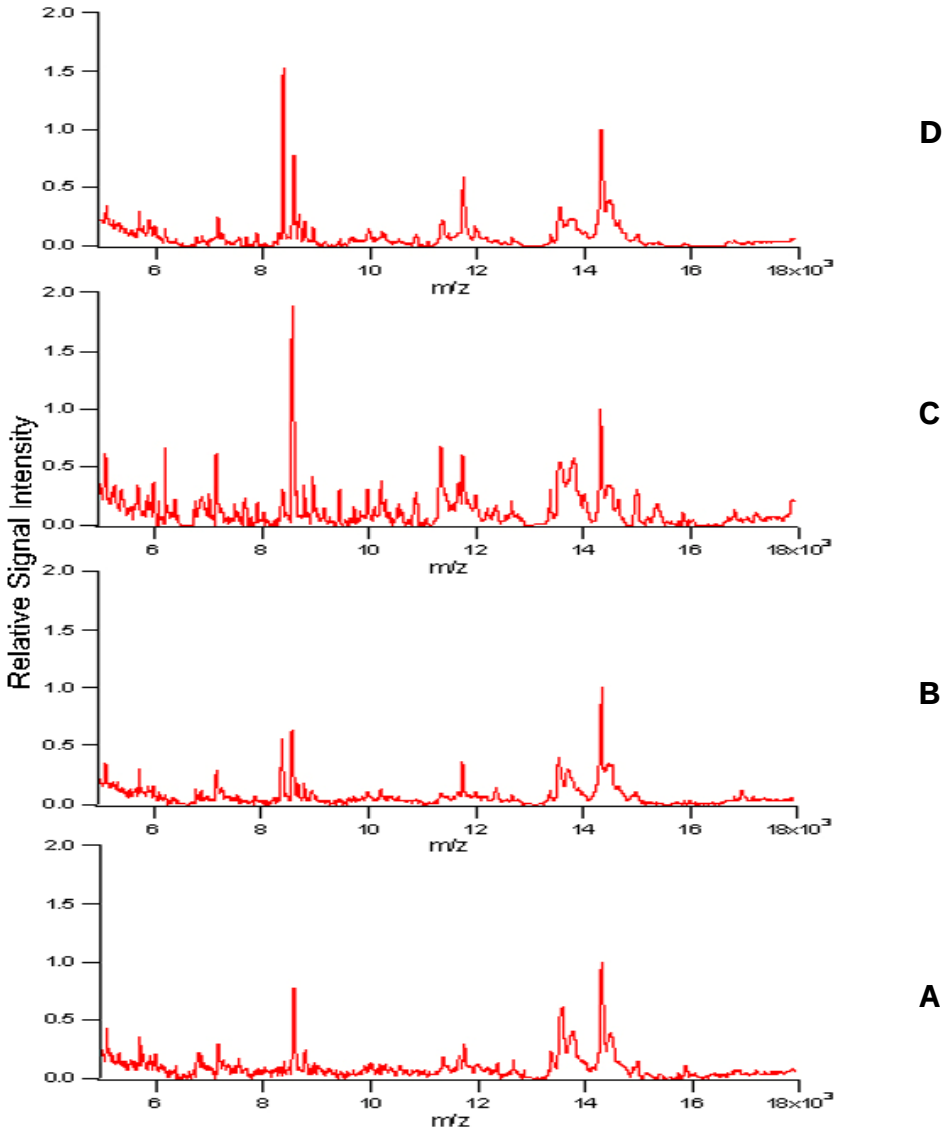

Figure 3.12 MALDI-TOF mass spectra of the supernatants of A549 cell cultures incubated in 250 µL SFM with 500 ng/mL TNF-α (B) (D) or without TNF-α(A) (C) in incubator for 24 hours (A) (B) or 48 hours (C) (D) incubation period. Lysozyme as an internal standard was added to the supernatants with a final concentration of 1.3×10^{-7} M. The supernatants were each processed using a C_{18} ZipTip prior to co-crystallization with SA matrix on a MALDI target plate.

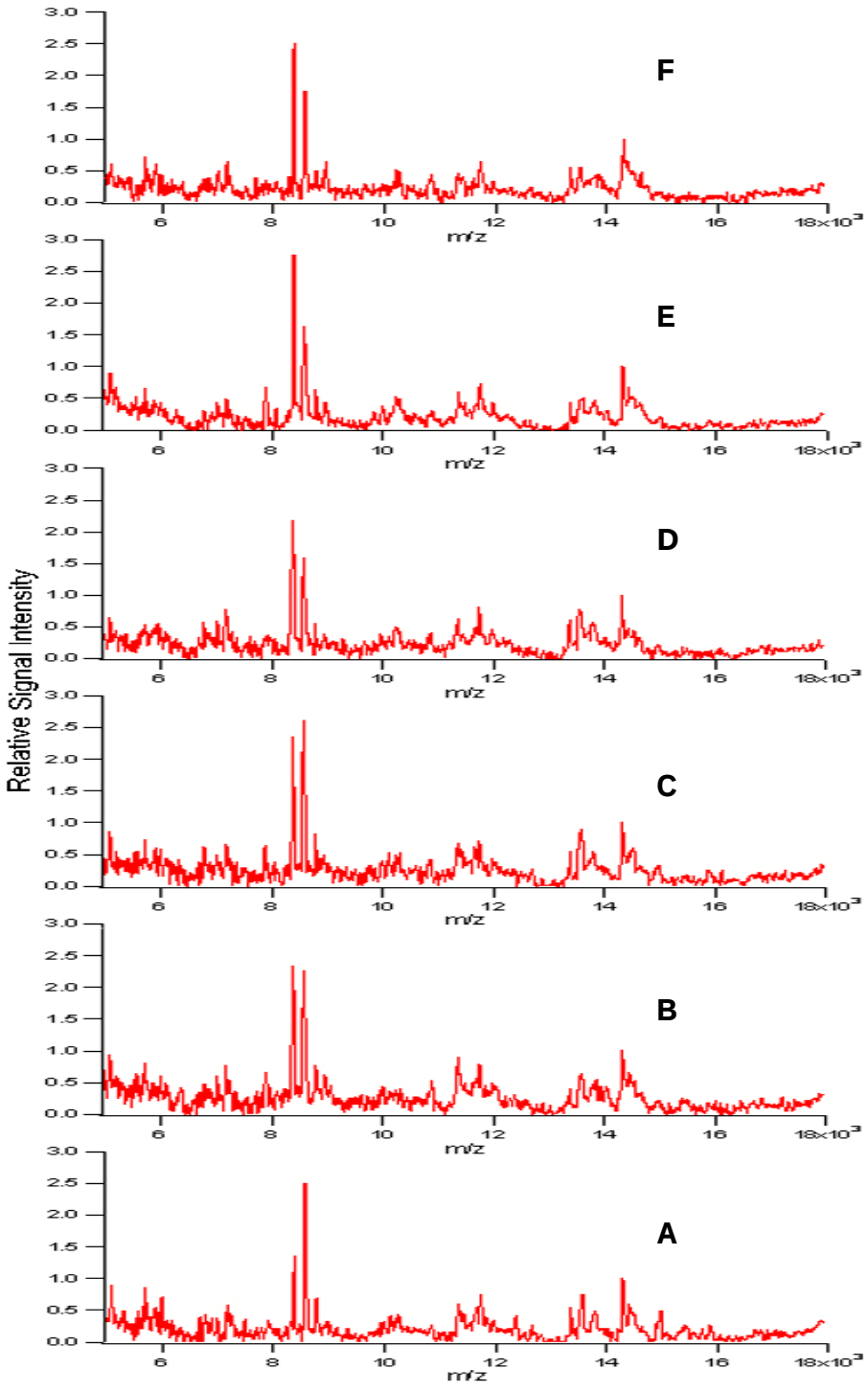

Figure 3.13 MALDI-TOF mass spectra of the supernatants of A549 cell cultures incubated in 250 µL SFM in incubator for 72 hours incubation period after deposition of 0 (A), 24 (B), 35 (C), 51 (D), 65 (E), 90 (F) particles containing 320 pg LPS and 1110 pg carbon per particle. Lysozyme as an internal standard was added to the supernatants with a final concentration of 1.3×10^{-7} M. The supernatants were each processed using a C_{18} ZipTip prior to co-crystallization with SA matrix on a MALDI target plate.

Ratios of ion signal intensities at 8.37 kDa to internal standard, the ratio of ion signal intensities at 8.58 kDa to internal standard, and the ratio of ion signal intensities at 8.37 kDa to 8.58 kDa from figure 3.13 were plotted as functions of number of particles (Figure 3.14). Ion signal intensities at 8.37 kDa were observed increasing while ion signal intensities at 8.58 kDa were observed decreasing when the number of particles increased and therefore the ratios of the ion signal intensity at 8.37 kDa to 8.58 kDa were observed increasing. All of the three plots could be fitted by least squares linear fits.

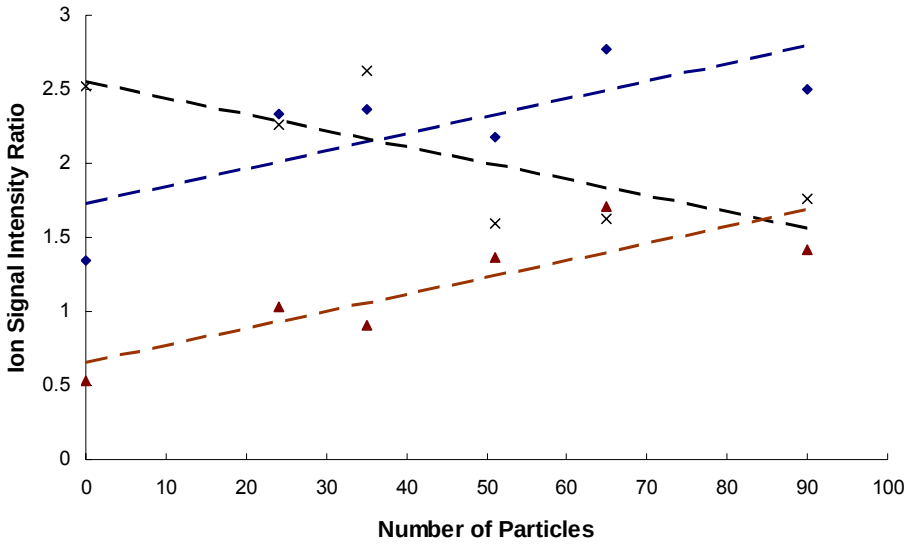

Figure 3.14 ratios of ion signal intensities at 8.37 kDa to internal standard (◆), ratios of ion signal intensities at 8.58 kDa to internal standard (x), ratios of ion signal intensities at 8.37 kDa to 8.58 kDa (▲) were plotted as functions of number of particles. The equations of the least squares linear fits were y = 0.0117x + 1.7313 for ratios of ion signal intensities at 8.37 kDa to internal standard, y = -0.0110x + 2.5496 for ratios of ion signal intensities at 8.58 kDa to internal standard, and y = 0.0114x + 0.6572 for ratios of ion signal intensities at 8.37 kDa to 8.58 kDa.

Next, A549 cells were cultured in centre-well organ dishes and dosed with different numbers of particles containing different compositions (50 pg LPS and 290 pg carbon per particle or 320 pg LPS and 1110 pg carbon per particle) and incubated with 250 μL SFM. Cell supernatants were collected after 24 hours or 72 hours and characterized by MALDI-TOF-MS. The ion signal intensity ratios of 8.37 kDa to 8.58 kDa were plotted as

functions of number of particles (Figure 3.15). For each particle composition, 72 hours incubation period experiment was replicated. In figure 3.15, the plots with the same composition of particles deposited could be fitted with the same least squares linear regression line although the incubation periods were different. My conclusion was that the different slopes indicated different cellular responses to the two particle types.

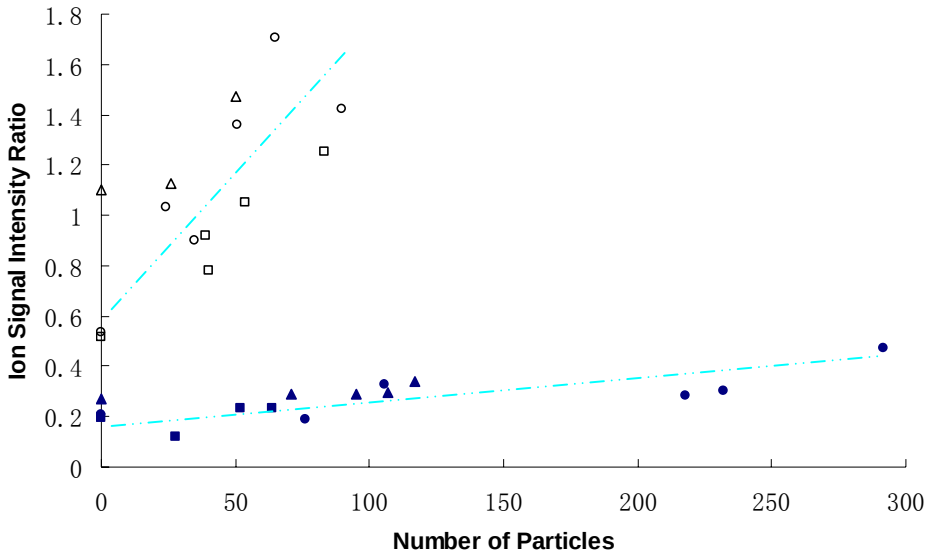

Figure 3.15 Ratios of ion signal intensities at 8.37 kDa to 8.58 kDa were plotted as functions of number of particles. A549 cells were cultured in centre-well organ dishes and dosed with different numbers of particles containing 50 pg LPS and 290 pg carbon (■) (●) (▲) or 320 pg LPS and 1110 pg carbon (□) (○) (Δ) per particle and incubated in incubator with 250 µL SFM. Cell supernatants were collected after 24 (■) (□) or 72 (●) (▲) (○) (Δ) hours. The supernatants were each processed using a C_{18} ZipTip prior to co-crystallization with SA matrix on a MALDI target plate and characterized by MALDI-TOF-MS. Different symbols represent different experimental runs.

The ratio of ion signals at 8.37 kDa to 8.58 kDa was found to be a useful cellular readout to indicate relative response to incubation with different compositions of particles. MALDI-TOF-MS could be an easier and faster way to monitor cellular response in a dose-response lung cell stimulation study, especially if more mediators can be detected and identified. The ion signal at 8.37 kDa has been assigned to chemokine CXCL-5 and

the ion signal at 8.58 kDa has been assigned to ubiquitin, which were both identified through a sequencing experiment by another graduate student Edward Lau who used an LC-MS/MS procedure.

3.7 Immunocytochemistry data processing

3.7.1 Patterns of ICAM-1 expression

3.7.1.1 Every single cell expressing ICAM-1

A549 cells were cultured in centre-well organ dishes and bathed in 250 μL SFM in an incubator with 500 ng/mL TNF-α. Cells were fixed after 24 hours incubation period and stained with ICAM-1 fluorescence antibodies. Both bright field and fluorescence images were taken from the cell culture at random spots (Figure 3.16). Figure 3.16 C was a combination of figure 3.16 A and B. Red colour indicated the ICAM-1 expression, and from figure 3.16 C, it showed each single cell was red, but to differing degrees. It suggested that ICAM-1 was upregulated and expression was effected by every single cell although some of the cells expressed more ICAM-1 than the others, assuming all ICAM-1 expressed was labelled with equal efficiency.

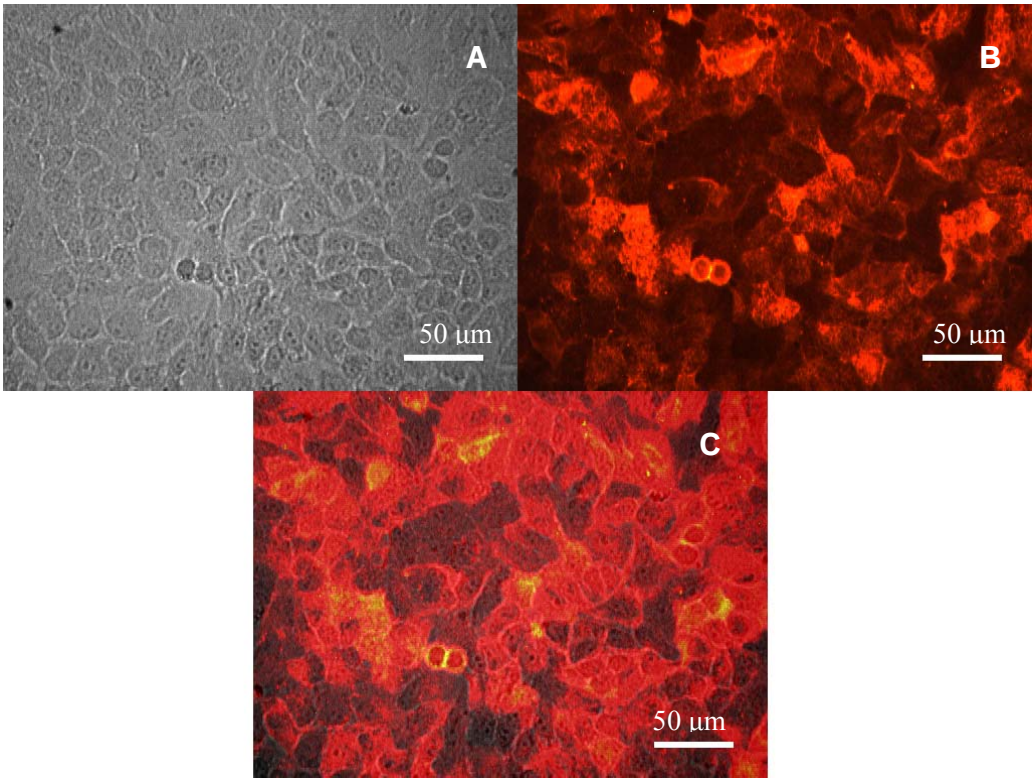

Figure 3.16 A549 cells were cultured in centre-well organ dishes and bathed in 250 µL SFM in an incubator with 500 ng/mL TNF-α. Cells were fixed after 24 hours incubation period and stained with ICAM-1 fluorescence antibodies. Bright field (A) and fluorescence images (B) of A549 cells were taken at the same spot. (C) was a combination of (A) and (B) using imaging software (Photoshop, Adobe) with the bright field image indicating the boundaries of cells and the fluorescence image indicating the locations of ICAM-1 expression. Images were taken using an objective magnification of 20X.

3.7.1.2 Non-uniform ICAM-1 expression

A549 cells were cultured in centre-well organ dishes and dosed with 115 particles containing 1550 pg LPS, 2180 pg carbon, 1 pg $Ni(NO_3)_2$ and 6 pg FluoSpheres per particle and incubated with 250 µL SFM. Cells were fixed after 24 hours incubation period and stained with ICAM-1 fluorescence antibodies. Both bright field and fluorescence images were taken from the cell culture at one spot in which particles were found (Figure 3.17). Again, figure 3.17 C was a combination of figure 3.17 A and B. ICAM-1 expression was not uniform with only a few cells expressing ICAM-1.

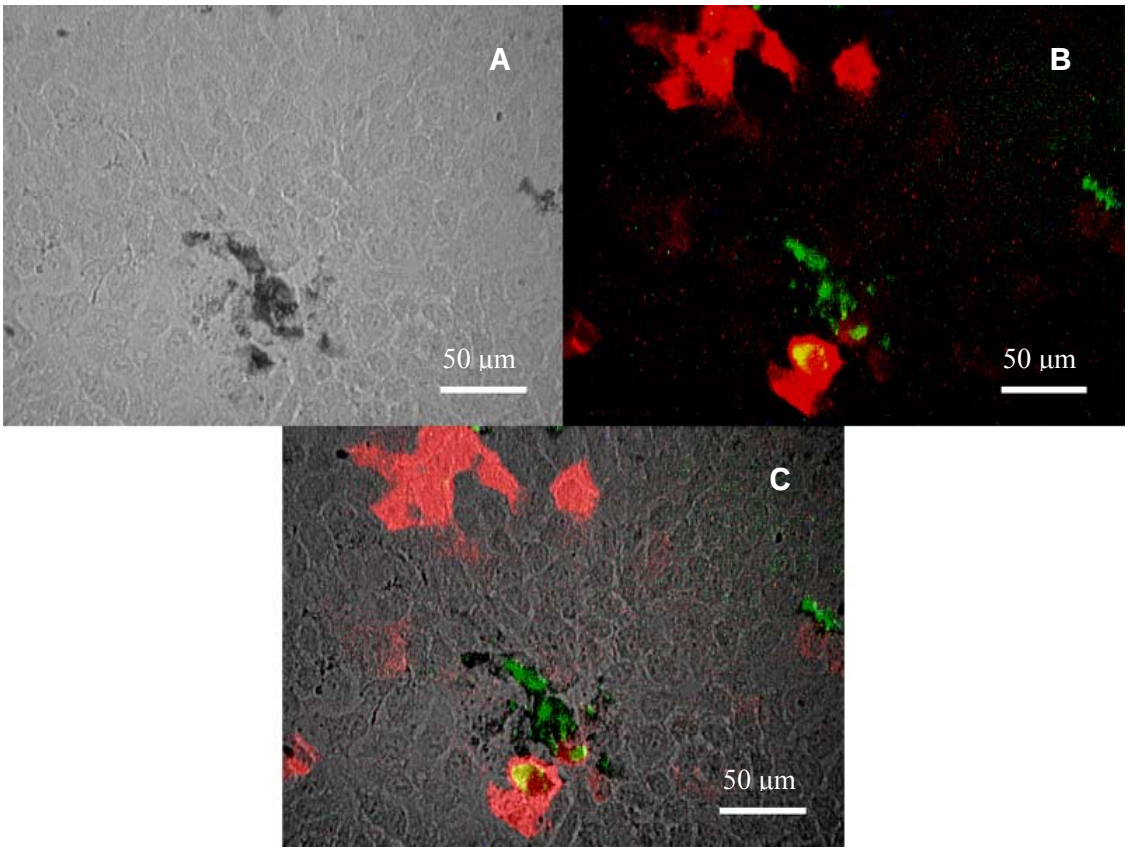

Figure 3.17 A549 cells were cultured in centre-well organ dishes and dosed with 115 particles containing 1550 pg LPS, 2180 pg carbon, 1 pg $Ni(NO_3)_2$ and 6 pg FluoSpheres per particle and incubated with 250 µL SFM. Cells were fixed after 24 hours incubation period and stained with ICAM-1 fluorescence antibodies. Bright field (A) and fluorescence images (B) of A549 cells were taken at the same spot. Fluorescence image of ICAM-1 (red colour) and fluorescence image of FluoSpheres (green colour) were taken respectively and combined into one image (B) using photoshop software. (C) was a combination of (A) and (B). Images were taken using an objective magnification of 20X.

Another observation from figure 3.17 was that a majority of the cells in contact with particles did not express ICAM-1, however the neighbouring cells expressed ICAM-1. Similar observations can be found on the higher magnification fluorescence image (Figure 3.18). Figure 3.18 was the same cells' image taken at the particle deposition site, defined as an approximately 2 mm diameter circular region at the centre of the centre-well organ dish where most of the particles were observed to have settled after their deposition there.

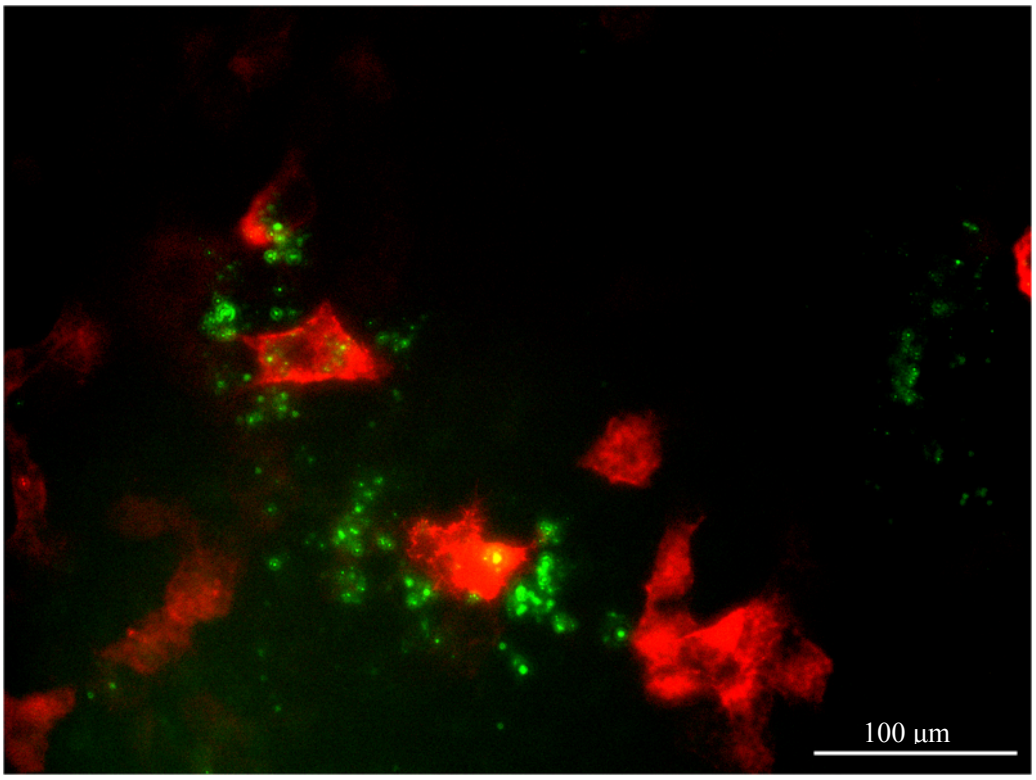

Figure 3.18 Fluorescence image of A549 cells was taken at the particle deposition site. A549 cells were cultured in centre-well organ dishes and dosed with particles containing 1550 pg LPS, 2180 pg carbon, 1 pg $Ni(NO_3)_2$ and 6 pg FluoSpheres per particle and incubated with 250 µL SFM. Cells were fixed after 24 hours incubation period and stained with ICAM-1 fluorescence antibodies. Fluorescence image of ICAM-1 (red colour) and fluorescence image of FluoSpheres (green colour) were taken respectively and combined into one image using photoshop software. Images were taken using an objective magnification of 40X.

A series of fluorescence images were taken from the same cell culture. Images were taken along one direction from the edge of particle deposition site of the cell culture. Each two images acquired contained about 10% overlap region, which was cropped when combing images into a single image of a new 2.8 mm by 0.2 mm using photoshop software (Figure 3.19). Not only the cells around particle deposition site expressed ICAM-1, but the cells as far as 3 mm away expressed ICAM-1 and the fluorescence intensity of ICAM-1 antibody was not decreasing with the distance from particle deposition site. Although the particles were deposited in the centre of the culture dish, they stimulated the whole culture to form ICAM-1 expression.

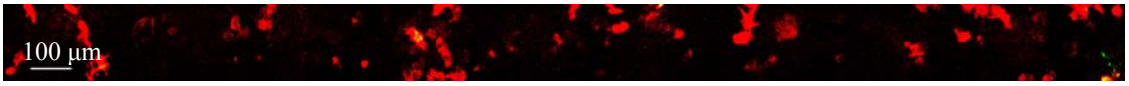

Figure 3.19 Fluorescence image of A549 cells. A549 cells were cultured in centre-well organ dishes and dosed with 115 particles containing 1550 pg LPS, 2180 pg carbon, 1 pg $Ni(NO_3)_2$ and 6 pg FluoSpheres per particle and incubated with 250 µL SFM. Cells were fixed after 24 hours incubation period and stained with ICAM-1 fluorescence antibodies. A series of fluorescence images were taken along one direction from the edge of particle deposition site of the cell culture. Each two images acquired contained about 10% overlap region, which was cropped when combing images into a single image of a new 2.8 mm by 0.2 mm using photoshop software. Fluorescence image of ICAM-1 (red colour) and fluorescence image of FluoSpheres (green colour) were taken respectively and combined into one image using photoshop software. Images were taken using an objective magnification of 20X.

3.7.1.3 ICAM-1 expression patterns

To study if the pattern of ICAM-1 expression related to the concentration of the materials incubated with cells, A549 cells were cultured in centre-well organ dishes and bathed in 250 µL SFM in an incubator with different concentrations of TNF-α. Cells were fixed after 24 hours incubation period and stained with ICAM-1 fluorescence antibodies. A series of fluorescence images were taken along one direction from a random spot at the centre of the cell culture. Each two images acquired contained about 10% overlap region, which was cropped when combing images into a single image of a new 2.8 mm by 0.2 mm area using photoshop software (Figure 3.20). As the concentration of TNF-α increased, the number of cells expressing ICAM-1 increased and the pattern of ICAM-1 expression changed from random to every cell expressing ICAM-1. Therefore, for whatever reasons the pattern of ICAM-1 expression was a function of the concentration of the soluble TNF-α incubated with cells. Therefore, the upregulation of ICAM-1 by random cells across the cell culture at low doses of either particles or TNF-α solution, yielded similar looking images.

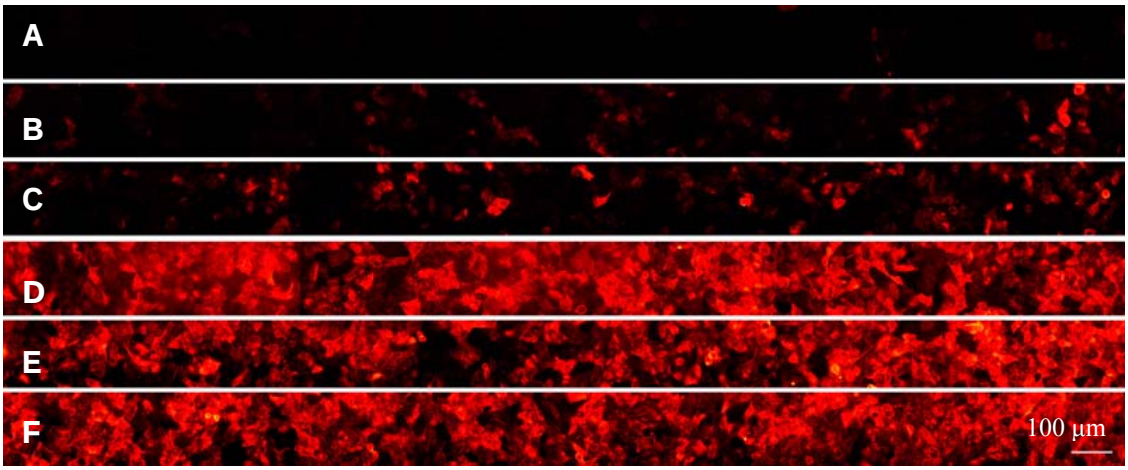

Figure 3.20 Fluorescence image of A549 cells. A549 cells were cultured in centre-well organ dishes and bathed in 250 μL SFM in incubator with final concentrations of 0 ng/mL (A), 50 ng/mL (B), 100 ng/mL (C), 250 ng/mL (D), 500 ng/mL (E), 1000 ng/mL (F) of TNF-α. Cells were fixed after 24 hours incubation period and stained with ICAM-1 fluorescence antibodies. A series of fluorescence images were taken along one direction from a random spot near the centre of the cell culture. Each two sequential images acquired contained about 10% overlap region, which was cropped when combing images into a single image of a new 2.8 mm by 0.2 mm using photoshop software. Images were taken using an objective magnification of 20X.

3.7.2 Fluorescence Image capture

In Haddrell's methodology, 3 pictures from particle deposition site were taken and the intensity of the fluorescence emission in the image was calculated by Image J software. Since ICAM-1 was not only expressed at the deposition site in my study, 9 pictures were taken in an array (Figure 3.21) and the average of the 9 fluorescence intensities was used for data analysis.

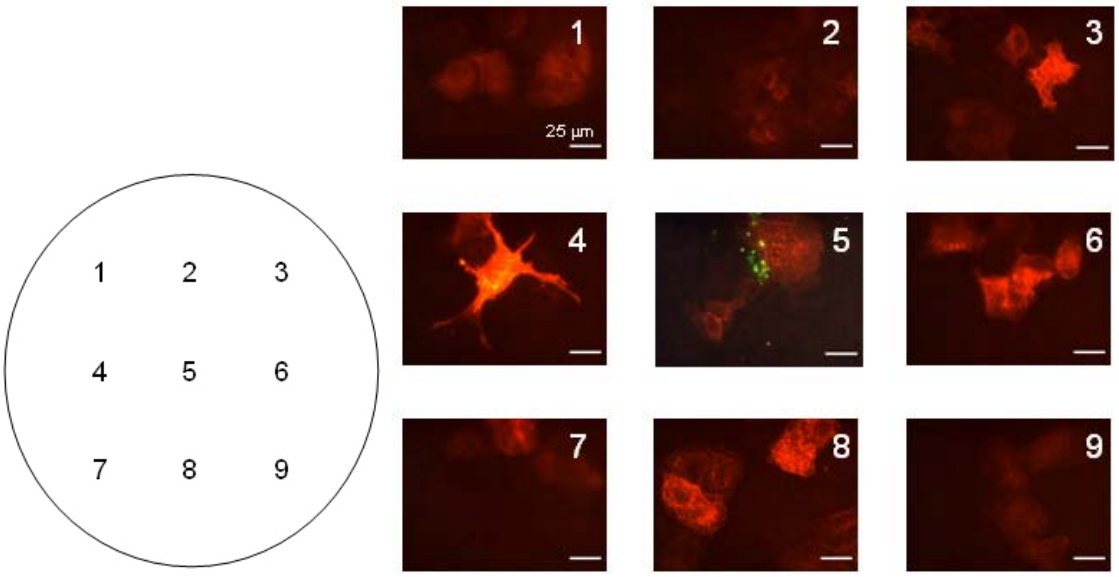

Figure 3.21 An example of 9 pictures taken from one cell culture. 71 particles containing 1570 pg LPS, 2200 pg carbon and 6 pg FluoSpheres per particle were dosed onto this cell culture. The array of images corresponded to the numbers as the scheme showed. The fluorescence image of number 5 was a combination of fluorescence image of ICAM-1 (red colour) and fluorescence image of FluoSpheres (green colour) using photoshop software. Images were taken using an objective magnification of 40X.

3.7.3 Comparison of several different image processing methodologies

Since particles deposited in the centre of the centre-well organ dish were able to effect culture-wide, yet random, ICAM-1 expression, my suggestion of this phenomenon was that the soluble components of particles could desorb from the particle and dissolve in SFM and diffuse to stimulate the whole cell culture. The hypothesis of my thesis was that different (soluble / insoluble) compositions of particles cause different cellular responses, as suggested by the data plotted in figure 3.15. But there were only two different compositions of particles and therefore it was difficult to distinguish what was more important to influence the cellular responses. In addition, MALDI-TOF-MS was known to provide semi-quantitative analysis. Based on the above reasons, immunocytochemistry was used to complete this study.

Compound of LPS (soluble) plus nanoparticles of carbon were used as particles in this study. Three possibilities that could influence the cellular responses were proposed here:

1. Mass ratio between LPS and carbon per particle.
2. Mass of LPS per particle.
3. Total mass of LPS plus carbon per particle

To study which factor was the most important in affecting cellular response, several types of particles containing different mass ratios of LPS to carbon were used. The particles from all types of compositions were 6.6 ± 1.3 μm diameter. The images of two types of particles with lowest mass and highest mass are shown in figure 3.22 as examples. The reason why these different particles (in terms of mass) have similar size was not fully understood. Further investigation related to particle mass and size was performed by Edward Lau.

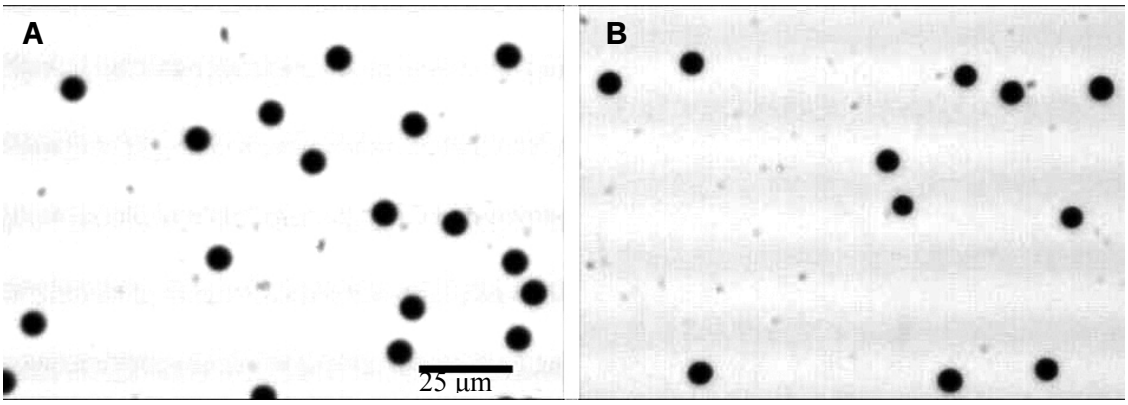

Figure 3.22 Photomicrographs of particles containing 50 pg LPS, 290 pg carbon and 6 pg FluoSpheres (A) or 1570 pg LPS, 2200 pg carbon and 6 pg FluoSpheres (B) per particle on glass slide. Image was taken using an objective magnification of 40X.

ICAM-1 antibody fluorescence images were captured for data processing. In an effort to compare different image processing methodologies, three replicates of cells dosed with different numbers of particles containing 1570 pg LPS, 2200 pg carbon and 6

pg FluoSpheres per particle and incubated for 24 hours were performed. After immunocytochemistry, the data from those experiments were processed in 5 different ways (Figure 3.23, Figure 3.31, Figure 3.39, Figure 3.48 and Figure 3.55) as discussed below. To address the 3 possibilities as stated above, ICAM-1 expressions induced by all types of particles were processed following the 5 different methodologies and plotted in terms of mass ratio between LPS and carbon per particle, mass of LPS per particle and total mass of LPS plus carbon per particle respectively.

3.7.3.1 Total fluorescence signal relative to positive control methodology

Total fluorescence signal relative to positive control (cells incubated with 500 ng/mL TNF-α) was expressed as a percentage. The relative fluorescence intensity was plotted as a function of number of particles deposited onto the cells (Figure 3.23). This data suggested that the ICAM-1 expression was dose dependent when the cells were dosed with low number of particles. With the number of particles increasing, the ICAM-1 expression reached its maximum under the condition of this specific particle type, and then was no longer dose dependent. A trypan blue assay was used to confirm that with the number of particles increasing, the ICAM-1 expression having a region of data fitted to a line having a slope approaching 0 was not because of cell death (Figure 3.24).

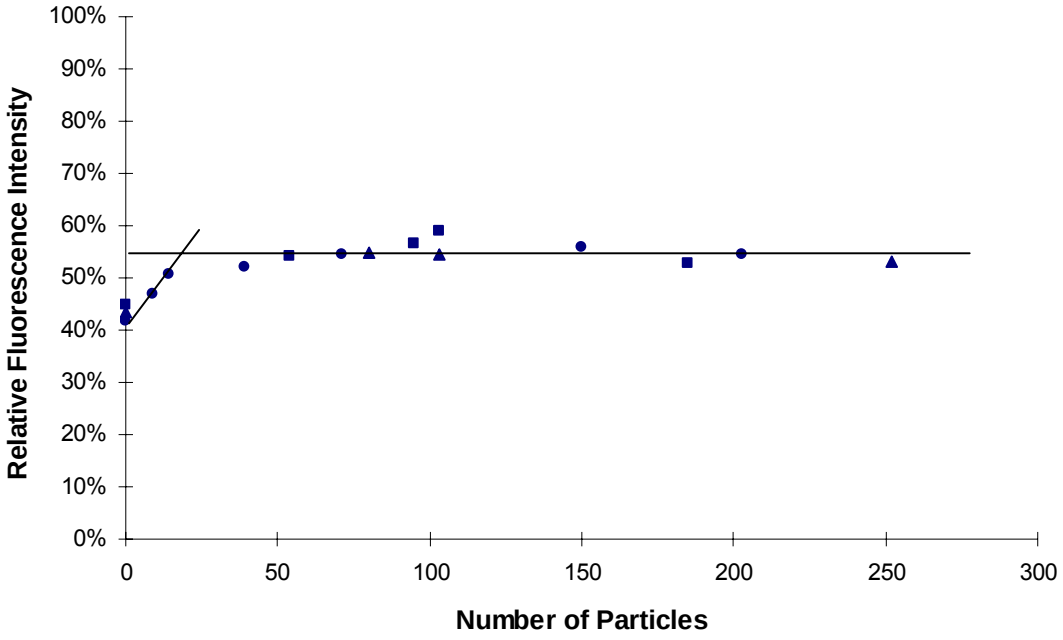

Figure 3.23 Plot of the relative ICAM-1 antibody fluorescence intensity as a function of number of particles. Different numbers of particles containing 1570 pg LPS, 2200 pg carbon and 6 pg FluoSpheres per particle were deposited onto the cells. (■) (●) (▲) indicate replicates.

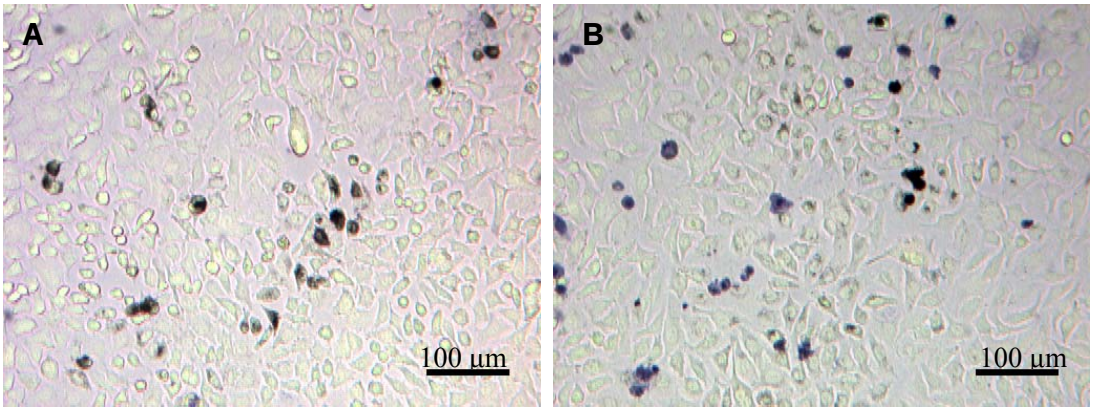

Figure 3.24 Trypan blue cell viability assay. A549 cells were cultured in centre-well organ dishes and dosed with ~100 particles (two populations) containing 1570 pg LPS, 2200 pg carbon and 6 pg FluoSpheres per particle and incubated in incubator with 250 µL SFM. After 24 hours incubation period, 50 µL of 0.4% (w/v) trypan blue solution was added into the centre-well organ dish after a brief rinse with PBS solution. A and B were pictures taken from two different spots of the cell culture. It was observed that more than 90% of the cells were viable. Images were taken using an objective magnification of 10X.

Since there were two distinct regions from the plot that were able to be fitted with least squares linear regression lines: a region of positive slope, and a region of data points

able to be fitted to a line which had a slope approaching 0 (plateau region), two numbers were used to present ICAM-1 expressions: the magnitude of the slope of the least squares linear fit to the region of data fitted to a positive slope and the magnitude of the intercept of the least squares linear fit to the region of data fitted to a line having a slope approaching 0.

3.7.3.1.1 Results from the region of positive slope of a least squares linear fit

A549 cells were cultured in centre-well organ dishes and dosed with different compositions of particles containing LPS and carbon and incubated for 24 hours before being fixed and stained with ICAM-1 fluorescence antibodies. The relative fluorescence intensities, which were the total fluorescence signals from test sample relative to positive control expressed as percentages, were plotted as a function of the number of particles for each individual experiment. The magnitude of the slope of the least squares linear fit to the region of data fitted to a positive slope from each type of particles were plotted as functions of mass ratio between LPS and carbon per particle, mass of LPS per particle and total mass of LPS plus carbon per particle respectively (Figure 3.25, Figure 3.26, Figure 3.27).

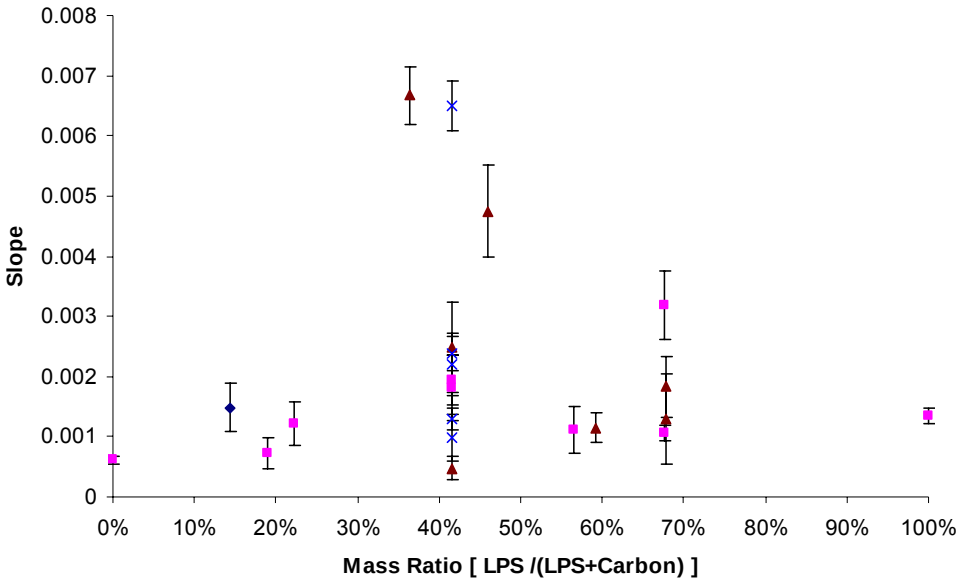

Figure 3.25 The magnitude of the slope of the least squares linear fit to the region of data fitted to a positive slope as a function of mass ratio between LPS and carbon per particle. Particles with ~340 pg (♦), ~1200 pg (■), ~2400 pg (▲) and ~3700 pg (x) total mass of LPS plus carbon per particle were generated and deposited onto the cells. Error bars represent the error of slopes.

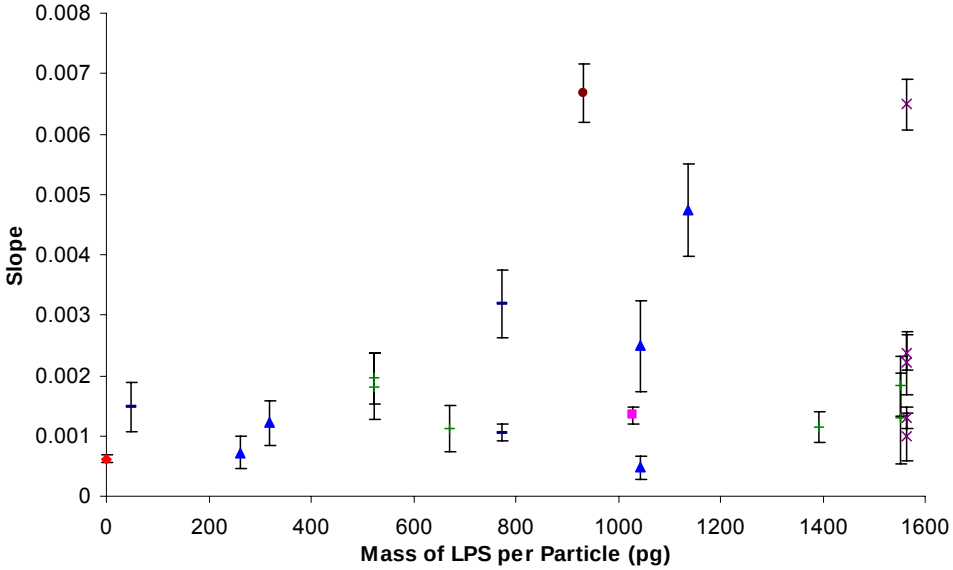

Figure 3.26 The magnitude of the slope of the least squares linear fit to the region of data fitted to a positive slope as a function of mass of LPS per particle. Particles with 0 pg LPS but ~1200 pg carbon (♦), 0 pg carbon but ~1200 pg LPS (■), < 500 pg carbon (—), 500 pg to 1000 pg carbon (+), 1000 pg to 1500 pg carbon (▲), 1500 pg to 2000 pg carbon (●) and ~2200 pg carbon (x) per particle were generated and deposited onto the cells. Error bars represent the error of slopes.

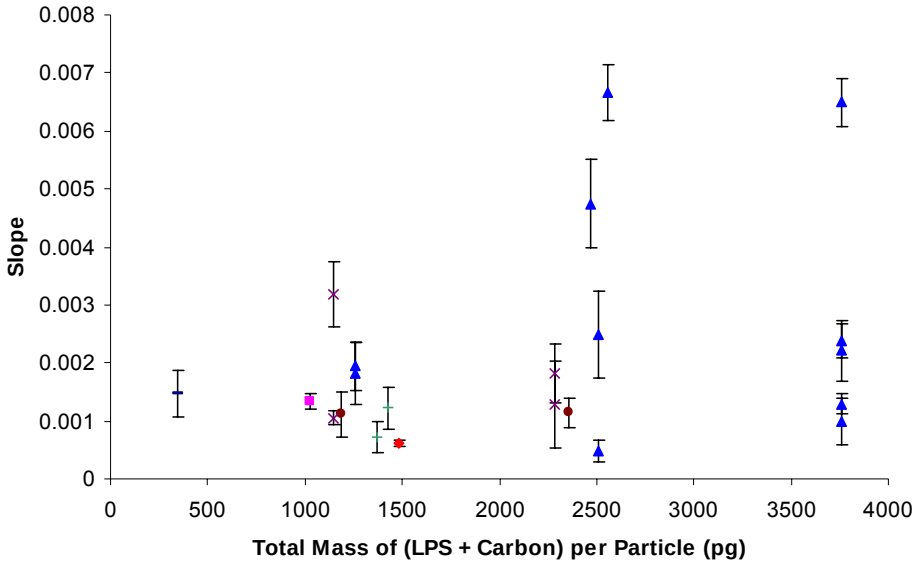

Figure 3.27 The magnitude of the slope of the least squares linear fit to the region of data fitted to a positive slope as a function of total mass of LPS plus carbon per particle. Particles with 0% of LPS to total mass (♦), 100% of LPS to total mass (■), ~15% of LPS to total mass (—), ~20% of LPS to total mass (+), ~40% of LPS to total mass (▲), ~60% of LPS to total mass (●) and ~70% of LPS to total mass (X) per particle were generated and deposited onto the cells. Error bars represent the error of slopes.

3.7.3.1.2 Results from the region of data that was fitted to a least squares linear fit to data that yielded a line having a slope approaching 0

A549 cells were cultured in centre-well organ dishes and dosed with different compositions of particles containing LPS and carbon and incubated for 24 hours before being fixed and stained with ICAM-1 fluorescence antibodies. The relative fluorescence intensities were plotted as a function of the number of particles for each individual experiment. The intercept of the least squares linear fits, that all had slopes approaching 0, were plotted for each type of particle. The intercept of negative control from each individual experiment was subtracted from the data points respectively. The differences between the magnitudes of intercepts of the least squares linear fit to the region of data fitted to a line having a slope approaching 0 and the negative controls were plotted as

functions of mass ratio between LPS and carbon per particle, mass of LPS per particle and total mass of LPS plus carbon per particle respectively (Figure 3.28, Figure 3.29, Figure 3.30).

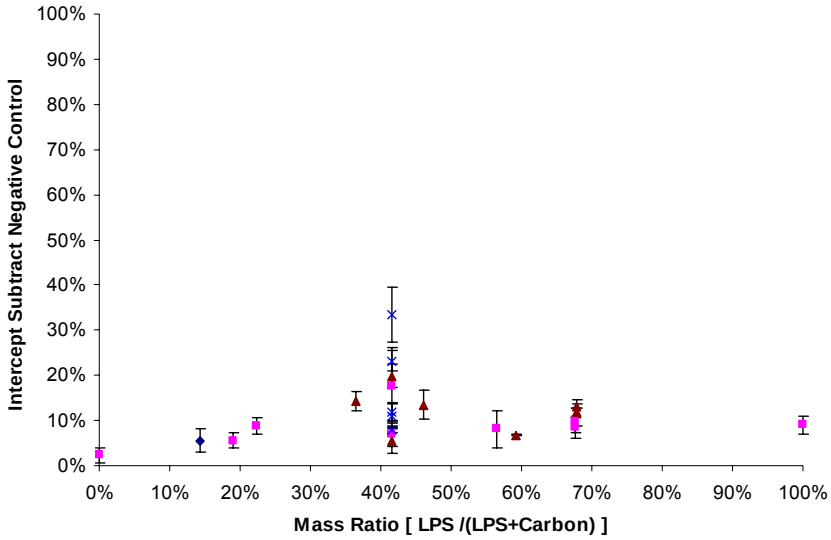

Figure 3.28 Plot of differences between the magnitude of intercept of the least squares linear fit to the region of data fitted to a line having a slope approaching 0 and the negative control as a function of mass ratio between LPS and carbon per particle. Particles with ~340 pg (♦), ~1200 pg (■), ~2400 pg (▲) and ~3700 pg (x) total mass of LPS plus carbon per particle were generated and deposited onto the cells. Error bars represent the standard deviation of the intercept.

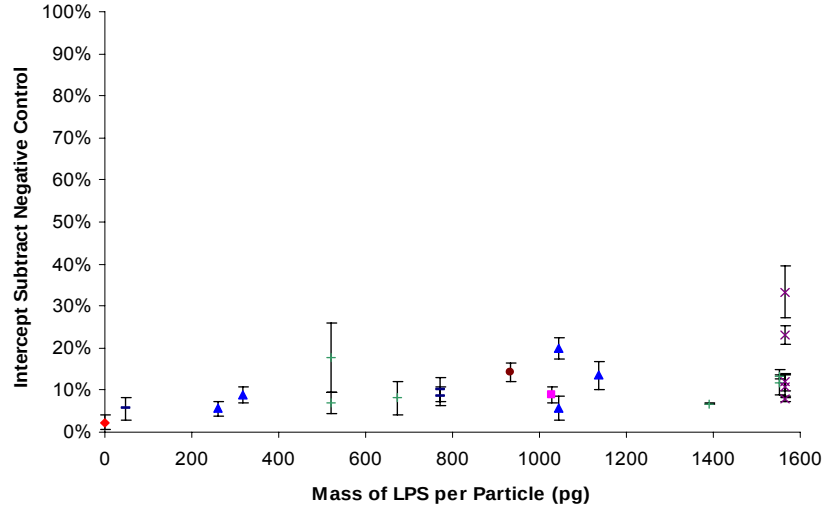

Figure 3.29 Plot of differences between the magnitude of intercept of the least squares linear fit to the region of data fitted to a line having a slope approaching 0 and the negative control as a function of mass of LPS per particle. Particles with 0 pg LPS but ~1200 pg carbon (♦), 0 pg carbon but ~1200 pg LPS (■), < 500 pg carbon (—), 500 pg to 1000 pg carbon (+), 1000 pg to 1500 pg carbon (▲), 1500 pg to 2000 pg carbon (●) and ~2200 pg carbon (x) per particle were generated and deposited onto the cells. Error bars represent the standard deviation of the intercept.

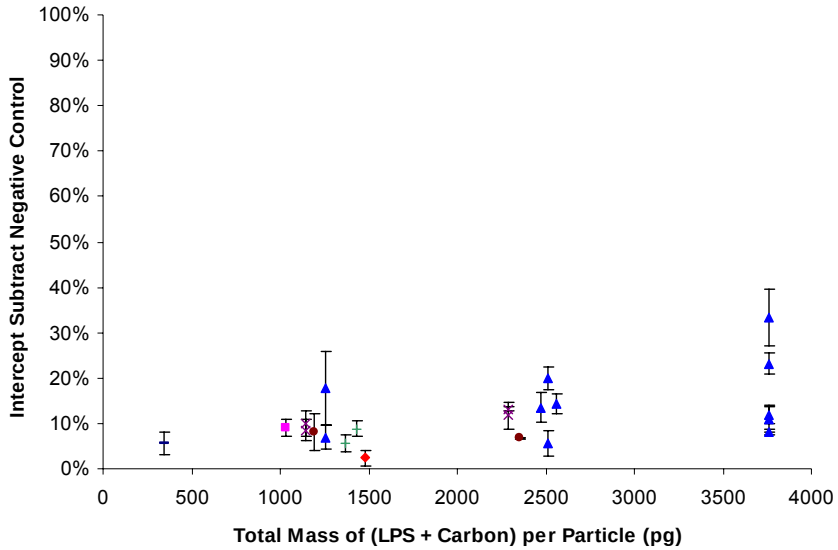

Figure 3.30 Plot of differences between the magnitude of intercept of the least squares linear fit to the region of data fitted to a line having a slope approaching 0 and the negative control as a function of total mass of LPS plus carbon per particle. Particles with 0% of LPS to total mass (♦), 100% of LPS to total mass (■), ~15% of LPS to total mass (—), ~20% of LPS to total mass (+), ~40% of LPS to total mass (▲), ~60% of LPS to total mass (●) and ~70% of LPS to total mass (x) per particle were generated and deposited onto the cells. Error bars represent the standard deviation of the intercept.

3.7.3.2 Background subtraction before fluorescence signal relative to positive control

Fluorescence signals from negative control were calculated by Image J and subtracted from fluorescence signals from both positive control and test samples. The difference of fluorescence signals between sample and negative control relative to the difference of fluorescence signals between positive control and negative control was expressed as a percentage. The relative fluorescence intensity was plotted as a function of the number of particles deposited onto the cells (Figure 3.31). It was observed that there were also two distinct regions able to be fitted with least squares linear regression lines: a region of positive slope, and a region of data points able to be fitted to a line which had a slope approaching 0. Because it was plotted in a different way, the magnitude of Y axis in

figure 3.31 (~20%) was more extended than in figure 3.23 (~10%), yet the data trend was similar to that in figure 3.23.

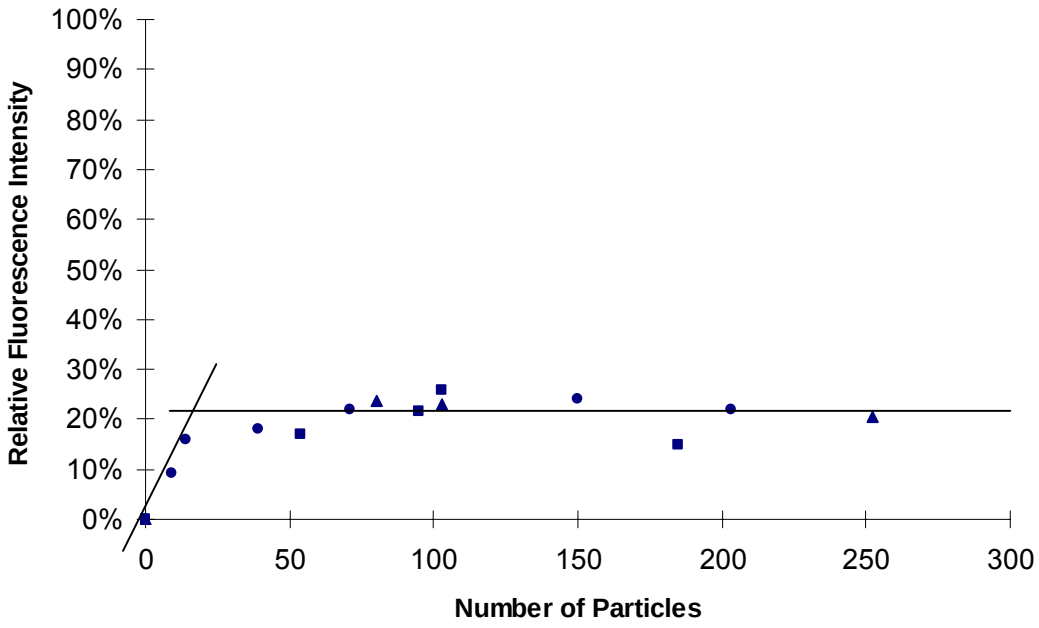

Figure 3.31 Plot of the relative ICAM-1 antibody fluorescence intensity (after background subtraction) as a function of number of particles. Different numbers of particles containing 1570 pg LPS, 2200 pg carbon and 6 pg FluoSpheres per particle were deposited onto the cells. (■) (●) (▲) indicate replicates.

Again, two numbers were used to present ICAM-1 expressions: the magnitude of the slope of the least squares linear fit to the region of data fitted to a positive slope and the magnitude of the intercept of the least squares linear fit to the region of data also fitted to another line having a slope approaching 0.

3.7.3.2.1 Results from the region of positive slope of a least squares linear fit

A549 cells were cultured in centre-well organ dishes and dosed with different compositions of particles containing LPS and carbon and incubated for 24 hours before being fixed and stained with ICAM-1 fluorescence antibodies. After background subtraction, the relative fluorescence intensities were plotted as a function of the number

of particles for each individual experiment. The magnitude of the slope of the least squares linear fit to the region of data fitted to a positive slope from each type of particles were plotted as functions of mass ratio between LPS and carbon per particle, mass of LPS per particle and total mass of LPS plus carbon per particle respectively (Figure 3.32, Figure 3.33, Figure 3.34).

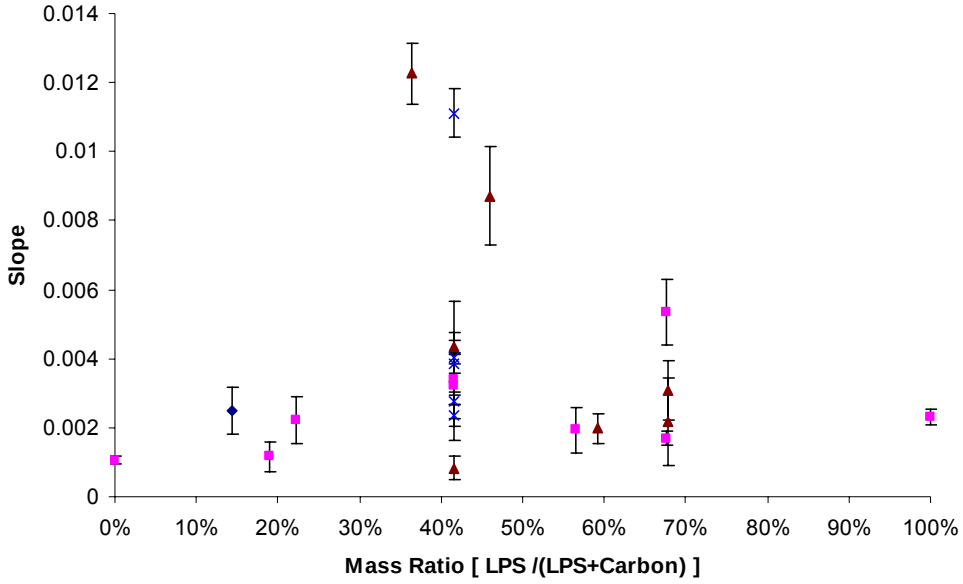

Figure 3.32 The magnitude of the slope of the least squares linear fit to the region of data fitted to a positive slope as a function of mass ratio between LPS and carbon per particle. Particles with ~340 pg (♦), ~1200 pg (■), ~2400 pg (▲) and ~3700 pg (x) total mass of LPS plus carbon per particle were generated and deposited onto the cells. Error bars represent the error of slopes.

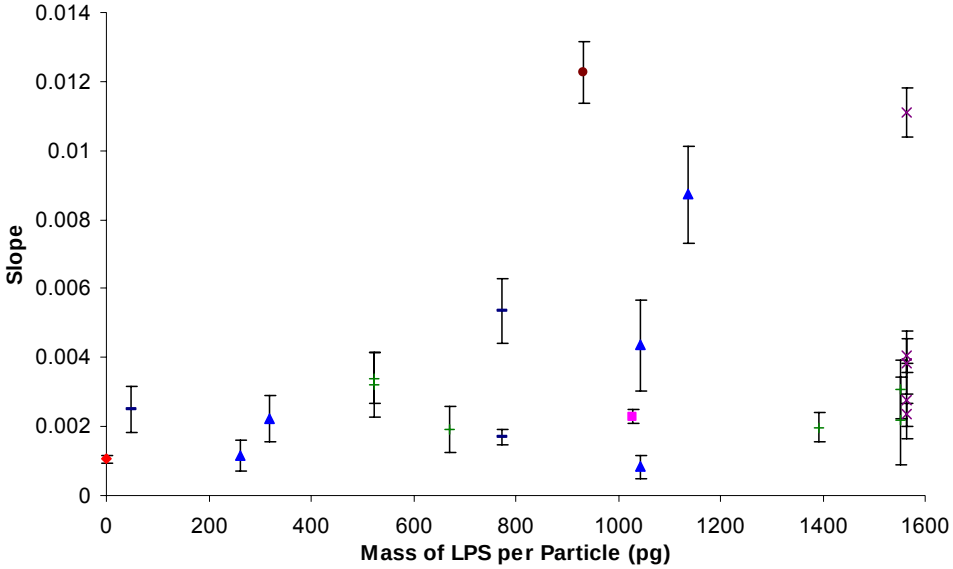

Figure 3.33 The magnitude of the slope of the least squares linear fit to the region of data fitted to a positive slope as a function of mass of LPS per particle. Particles with 0 pg LPS but ~1200 pg carbon (♦), 0 pg carbon but ~1200 pg LPS (■), < 500 pg carbon (—), 500 pg to 1000 pg carbon (+), 1000 pg to 1500 pg carbon (▲), 1500 pg to 2000 pg carbon (●) and ~2200 pg carbon (x) per particle were generated and deposited onto the cells. Error bars represent the error of slopes.

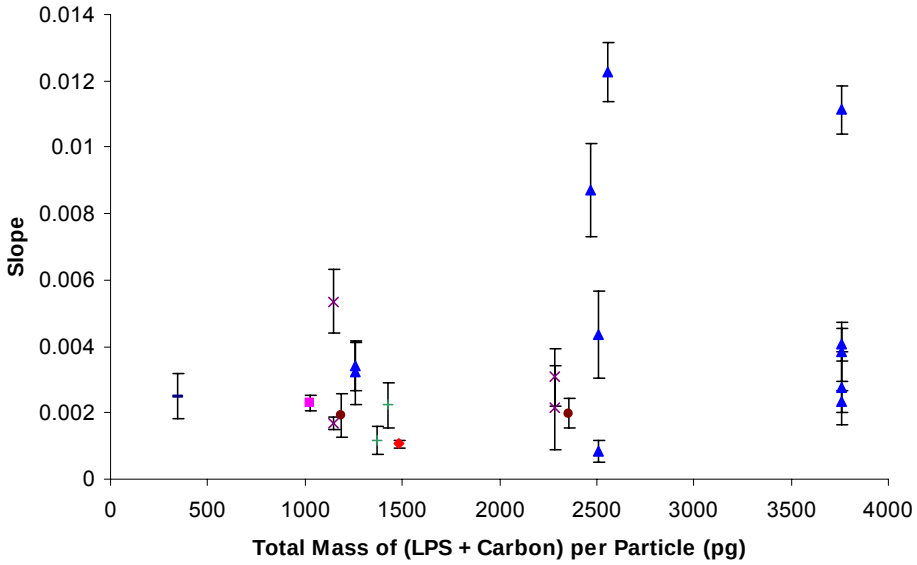

Figure 3.34 The magnitude of the slope of the least squares linear fit to the region of data fitted to a positive slope as a function of total mass of LPS plus carbon per particle. Particles with 0% of LPS to total mass (♦), 100% of LPS to total mass (■), ~15% of LPS to total mass (—), ~20% of LPS to total mass (+), ~40% of LPS to total mass (▲), ~60% of LPS to total mass (●) and ~70% of LPS to total mass (x) per particle were generated and deposited onto the cells. Error bars represent the error of slopes.

3.7.3.2.2 Results from the region of data that was fitted to a least squares linear fit to data that yielded a line having a slope approaching 0

A549 cells were cultured in centre-well organ dishes and dosed with different compositions of particles containing LPS and carbon and incubated for 24 hours before being fixed and stained with ICAM-1 fluorescence antibodies. After background subtraction, the relative fluorescence intensities were plotted as a function of the number of particles for each individual experiment. The intercept of the least squares linear fits, that all had slopes approaching 0, were plotted for each type of particle. The intercept of negative control was 0 because of background subtraction. The relative magnitudes of intercepts of the least squares linear fit to the region of data fitted yielding lines having slopes approaching 0 were plotted as functions of mass ratio between LPS and carbon per particle, mass of LPS per particle and total mass of LPS plus carbon per particle respectively (Figure 3.35, Figure 3.36, Figure 3.37).

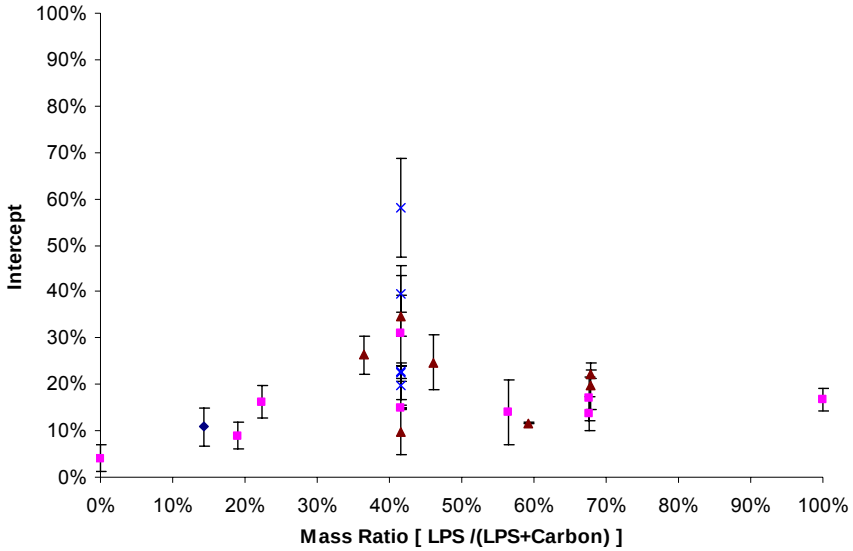

Figure 3.35 Plot of the relative magnitude of intercept of the least squares linear fit to the region of data fitted to a line having a slope approaching 0 as a function of mass ratio between LPS and carbon per particle. Particles with ~340 pg (♦), ~1200 pg (■), ~2400 pg (▲) and ~3700 pg (x) total mass of LPS plus carbon per particle were generated and deposited onto the cells. Error bars represent the standard deviation of the intercept.

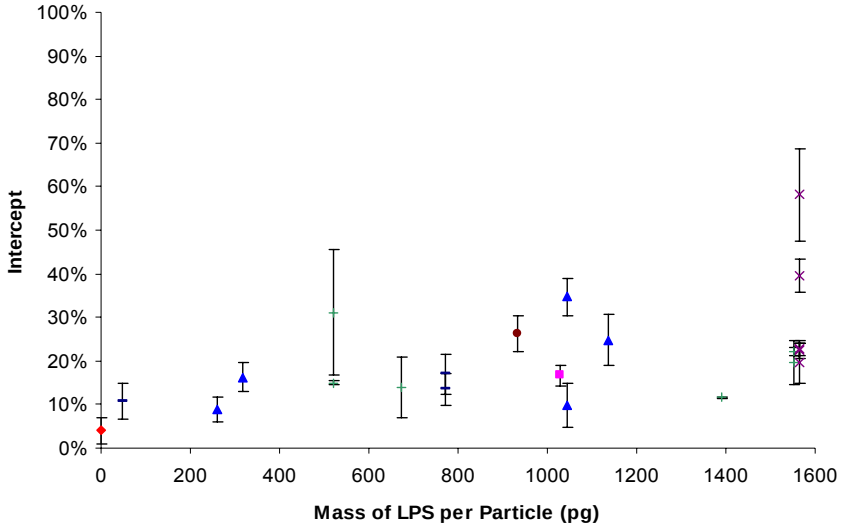

Figure 3.36 Plot of the relative magnitude of intercept of the least squares linear fit to the region of data fitted to a line having a slope approaching 0 as a function of mass of LPS per particle. Particles with 0 pg LPS but ~1200 pg carbon (♦), 0 pg carbon but ~1200 pg LPS (■), < 500 pg carbon (—), 500 pg to 1000 pg carbon (+), 1000 pg to 1500 pg carbon (▲), 1500 pg to 2000 pg carbon (●) and ~2200 pg carbon (x) per particle were generated and deposited onto the cells. Error bars represent the standard deviation of the intercept.

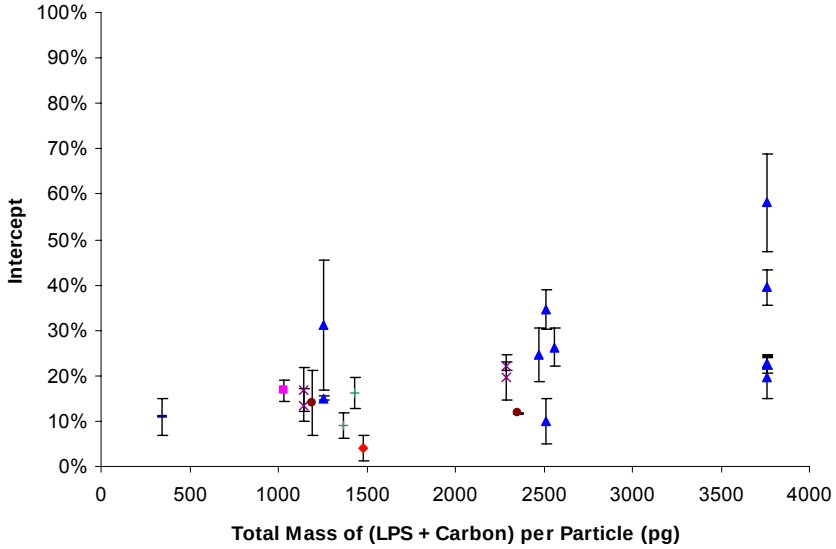

Figure 3.37 Plot of the relative magnitude of intercept of the least squares linear fit to the region of data fitted to a line having a slope approaching 0 as a function of total mass of LPS plus carbon per particle. Particles with 0% of LPS to total mass (♦), 100% of LPS to total mass (■), ~15% of LPS to total mass (—), ~20% of LPS to total mass (+), ~40% of LPS to total mass (▲), ~60% of LPS to total mass (●) and ~70% of LPS to total mass (x) per particle were generated and deposited onto the cells. Error bars represent the standard deviation of the intercept.

3.7.3.3 Cropping of an individual cell from each image and background subtraction before fluorescence signal relative to positive control

Although using previous methodologies, the trend could be seen when relative fluorescence intensities verses the number of deposited particles was plotted, the differences between test samples and negative control were small.

In an effort to treat the results in a different manner, the brightest 28 μm by 28 μm square was cropped from each of the 9 pictures taken in array (Figure 3.38) prior to obtaining an average of the fluorescence intensities. Background subtraction (method shown in section 3.7.3.2) was then performed to set the negative control to 0%. The relative fluorescence intensity was plotted as a function of number of particles deposited onto the cells (Figure 3.39). It was observed that there were also two distinct regions able to be fitted with least squares linear regression lines: a region of positive slope, and a region of data points able to be fitted to a line which had a slope approaching 0. Because it was plotted in a different way, the magnitude of Y axis in figure 3.39 (~40%) was more extended than in figure 3.31 (~20%) and figure 3.23 (~10%), yet a similar trend as observed figure 3.31 and figure 3.23 was apparent.

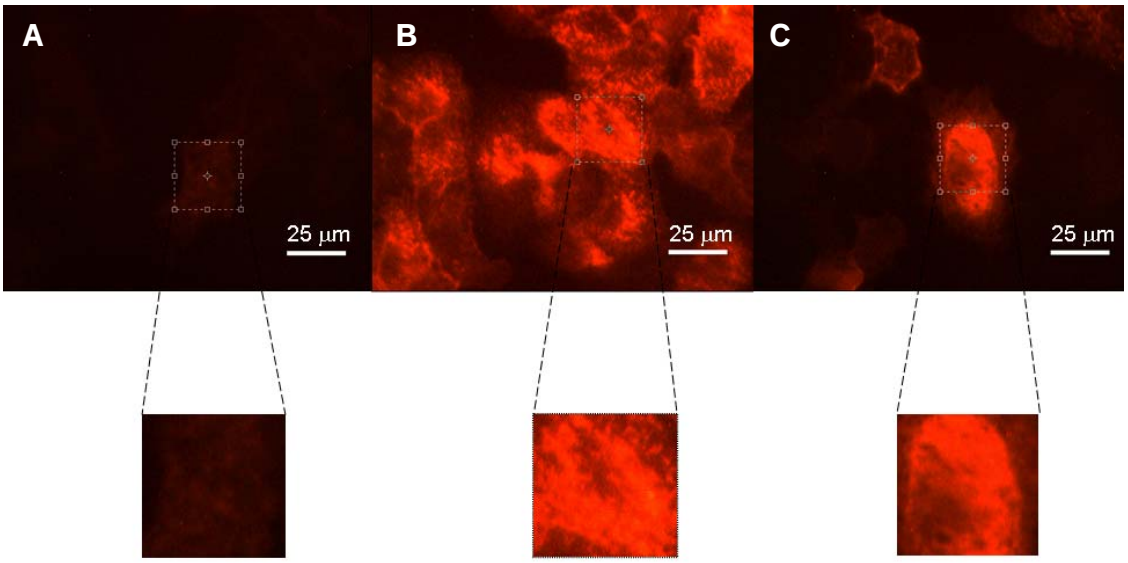

Figure 3.38 Fluorescence images after ICAM-1 antibody staining to A549 cells. The brightest 28 μm by 28 μm square was cropped from Negative control (A), Positive control (B) and test sample (C) respectively. Images were taken using an objective magnification of 40X.

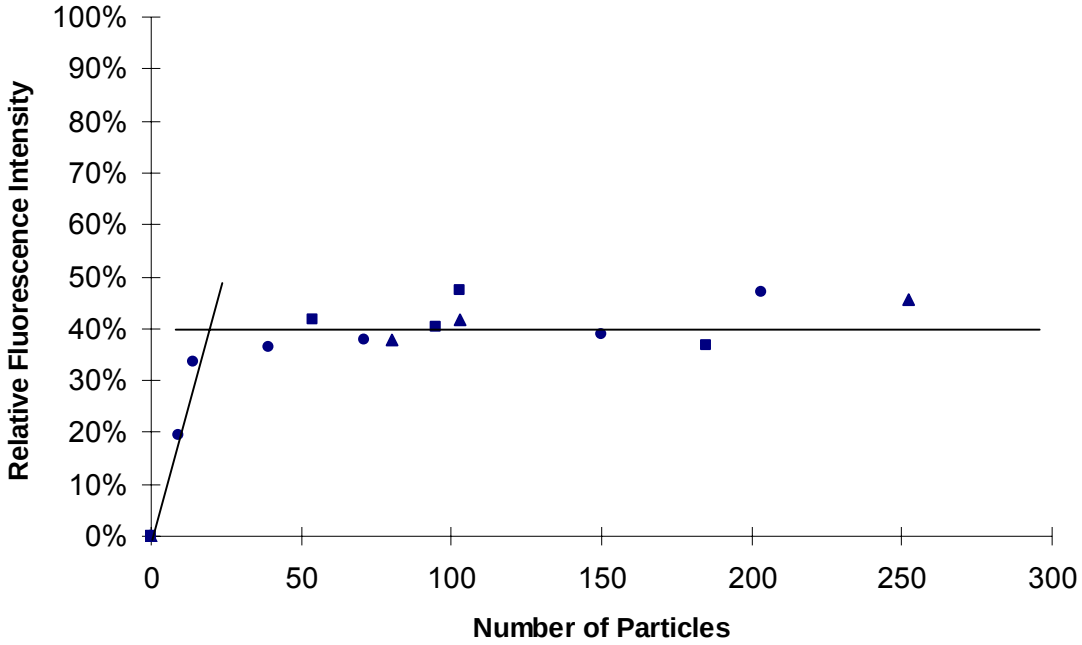

Figure 3.39 Plot of the relative ICAM-1 antibody fluorescence intensity (after cropping ~ one cell and background subtraction) as a function of number of particles. Different numbers of particles containing 1570 pg LPS, 2200 pg carbon and 6 pg FluoSpheres per particle were deposited onto the cells. (■) (●) (▲) indicate replicates.

Again, two numbers were used to present ICAM-1 expressions: the magnitude of the slope of the least squares linear fit to the region of data fitted to a positive slope and the magnitude of the intercept of the least squares linear fit to the region of data fitted to a line having a slope approaching 0.

3.7.3.3.1 Results from the region of positive slope of a least squares linear fit

A549 cells were cultured in centre-well organ dishes and dosed with different compositions of particles containing LPS and carbon and incubated for 24 hours before being fixed and stained with ICAM-1 fluorescence antibodies. After cropping ~ one cell and background subtraction, the relative fluorescence intensities were plotted as a function of the number of particles for each individual experiment. The magnitude of the slope of the least squares linear fit to the region of data fitted to a positive slope from each type of particles were plotted as functions of mass ratio between LPS and carbon per particle, mass of LPS per particle and total mass of LPS plus carbon per particle respectively (Figure 3.40, Figure 3.41, Figure 3.42).

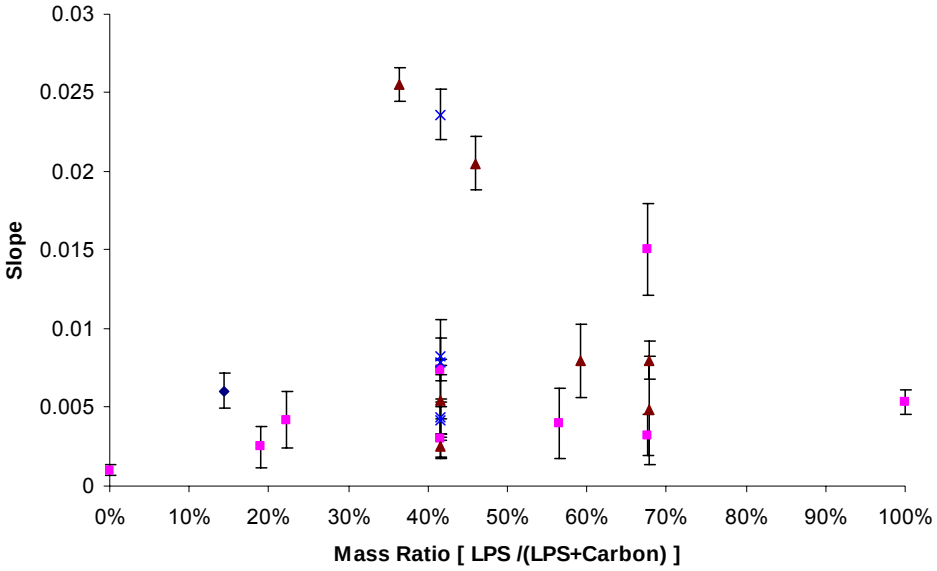

Figure 3.40 The magnitude of the slope of the least squares linear fit to the region of data fitted to a positive slope as a function of mass ratio between LPS and carbon per particle. Particles with ~340 pg (♦), ~1200 pg (■), ~2400 pg (▲) and ~3700 pg (x) total mass of LPS plus carbon per particle were generated and deposited onto the cells. Error bars represent the error of slopes.

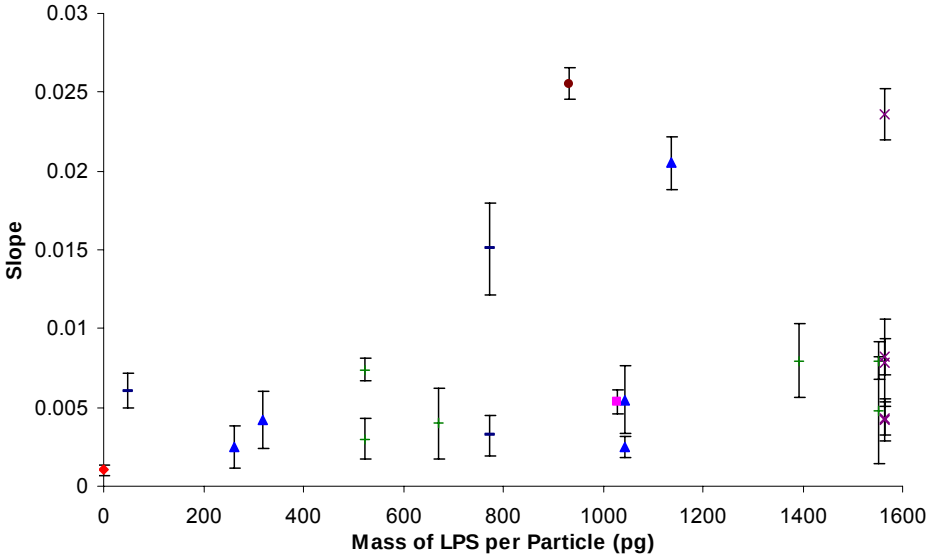

Figure 3.41 The magnitude of the slope of the least squares linear fit to the region of data fitted to a positive slope as a function of mass of LPS per particle. Particles with 0 pg LPS but ~1200 pg carbon (♦), 0 pg carbon but ~1200 pg LPS (■), < 500 pg carbon (—), 500 pg to 1000 pg carbon (+), 1000 pg to 1500 pg carbon (▲), 1500 pg to 2000 pg carbon (●) and ~2200 pg carbon (x) per particle were generated and deposited onto the cells. Error bars represent the error of slopes.

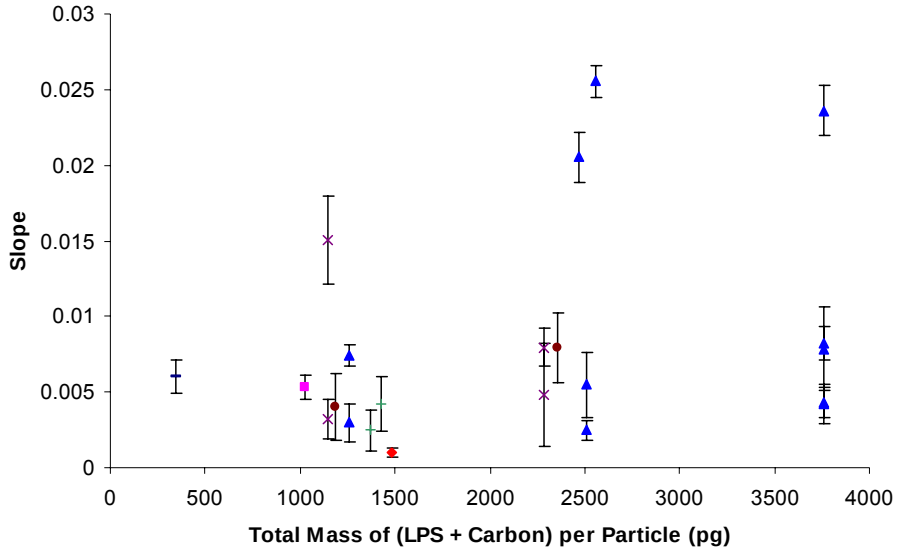

Figure 3.42 The magnitude of the slope of the least squares linear fit to the region of data fitted to a positive slope as a function of total mass of LPS plus carbon per particle. Particles with 0% of LPS to total mass (♦), 100% of LPS to total mass (■), ~15% of LPS to total mass (—), ~20% of LPS to total mass (+), ~40% of LPS to total mass (▲), ~60% of LPS to total mass (●) and ~70% of LPS to total mass (x) per particle were generated and deposited onto the cells. Error bars represent the error of slopes.

3.7.3.3.2 Results from the region of data that was fitted to a least squares linear fit to data that yielded a line having a slope approaching 0

A549 cells were cultured in centre-well organ dishes and dosed with different compositions of particles containing LPS and carbon and incubated for 24 hours before being fixed and stained with ICAM-1 fluorescence antibodies. After cropping ~ one cell and background subtraction, the relative fluorescence intensities were plotted as a function of the number of particles for each individual experiment. The intercept of the least squares linear fits, that all had slopes approaching 0, were plotted for each type of particle. The intercept of negative control was 0 because of background subtraction. The relative magnitudes of intercepts of the least squares linear fit to these region of data were plotted as functions of mass ratio between LPS and carbon per particle, mass of LPS per

particle and total mass of LPS plus carbon per particle respectively (Figure 3.43, Figure 3.44, Figure 3.45).

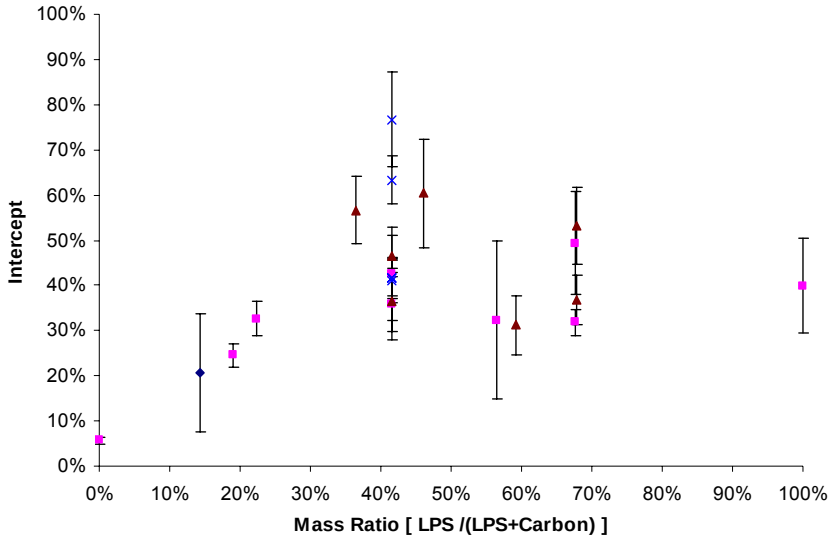

Figure 3.43 Plot of the relative magnitude of intercept of the least squares linear fit to the region of data fitted to a line having a slope approaching 0 regions as a function of mass ratio between LPS and carbon per particle. Particles with ~340 pg (♦), ~1200 pg (■), ~2400 pg (▲) and ~3700 pg (x) total mass of LPS plus carbon per particle were generated and deposited onto the cells. Error bars represent the standard deviation of the intercept.

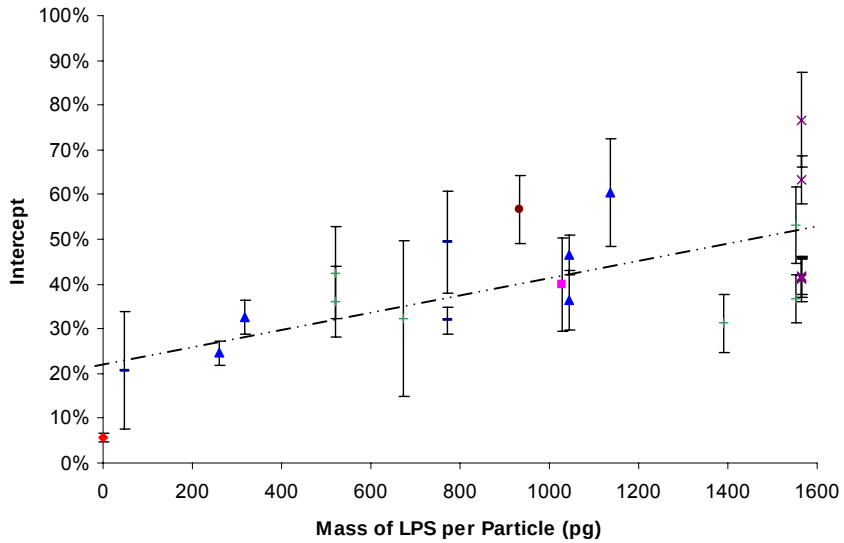

Figure 3.44 Plot of the relative magnitude of intercept of the least squares linear fit to the region of data fitted to a line having a slope approaching 0 as a function of mass of LPS per particle. Particles with 0 pg LPS but ~1200 pg carbon (♦), 0 pg carbon but ~1200 pg LPS (■), < 500 pg carbon (—), 500 pg to 1000 pg carbon (+), 1000 pg to 1500 pg carbon (▲), 1500 pg to 2000 pg carbon (●) and ~2200 pg carbon (x) per particle were generated and deposited onto the cells. Error bars represent the standard deviation of the intercept. The equation of the least squares linear fit was y = 0.0002x + 0.2249.

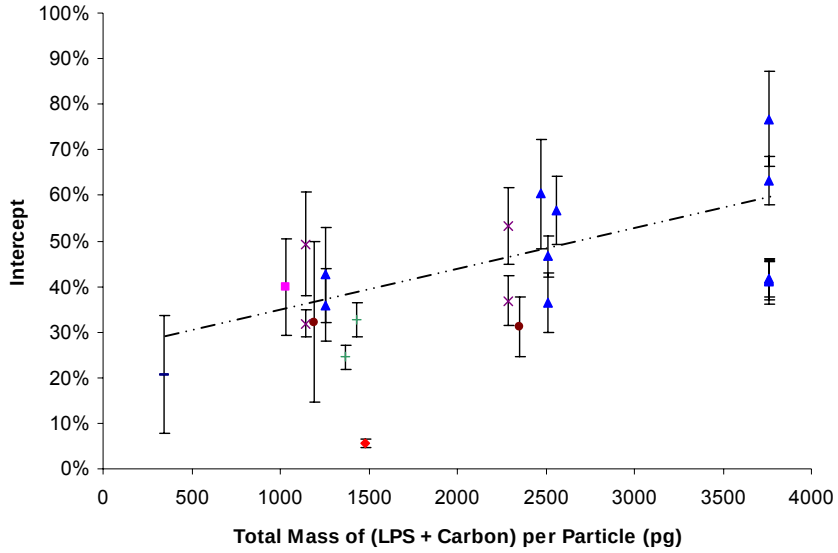

Figure 3.45 Plot of the relative magnitude of intercept of the least squares linear fit to the region of data fitted to a line having a slope approaching 0 as a function of total mass of LPS plus carbon per particle. Particles with 0% of LPS to total mass (♦), 100% of LPS to total mass (■), ~15% of LPS to total mass (—), ~20% of LPS to total mass (+), ~40% of LPS to total mass (▲), ~60% of LPS to total mass (●) and ~70% of LPS to total mass (x) per particle were generated and deposited onto the cells. Error bars represent the standard deviation of the intercept. The equation of the least squares linear fit was y = 0.00008x + 0.2312.

3.7.3.3.3 Other observations using these image processing methodologies

3.7.3.3.3.1 Same particle composition with different incubation period

A549 cells were cultured in centre-well organ dishes and dosed with different numbers of particles containing 50 pg LPS and 290 pg carbon per particle and incubated in incubator with 250 µL SFM. Cells were incubated for 24, 48 or 72 hours before fixed and stained with ICAM-1 fluorescence antibodies. After cropping ~ one cell and background subtraction, the relative fluorescence intensities were plotted as a function of number of particles (Figure 3.46). The data from different incubation periods followed the same trend as previously observed (eg. similar to figure 3.15 MALDI-TOF-MS's data), which is different incubation periods did not affect the cellular responses as long as cells were dosed with the same composition of particles.

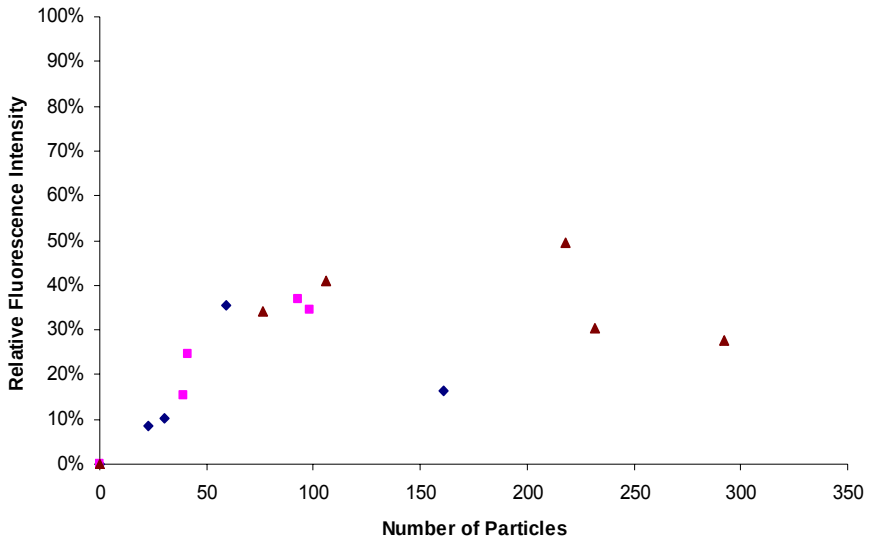

Figure 3.46 Plot of the relative ICAM-1 antibody fluorescence intensity (after cropping ~ one cell and background subtraction) as a function of number of particles. A549 cells were cultured in centre-well organ dishes and dosed with different numbers of particles containing 50 pg LPS and 290 pg carbon per particle and incubated in incubator with 250 µL SFM for 24 (♦), 48 (■) and 72 (▲) hours before fixed and stained with ICAM-1 fluorescence antibodies.

3.7.3.4 Establishing a threshold to do background subtraction

The previous sections introduced a background subtraction methodology, which was to subtract the fluorescence signals of negative control from the fluorescence signals of both positive control and test samples. In this section, a different background subtraction method was examined.

The fluorescence signals from negative control and cells dosed with particles containing LPS and carbon were calculated by Image J. 0 to 255 levels were used to express fluorescence signal intensities. The number of pixels was plotted as a function of fluorescence intensity levels (Figure 3.47). It was observed that negative controls had only one peak at lower than level 20 while samples with particles had two peaks with one close to but higher than the peak of negative controls and the other one at about level 100.

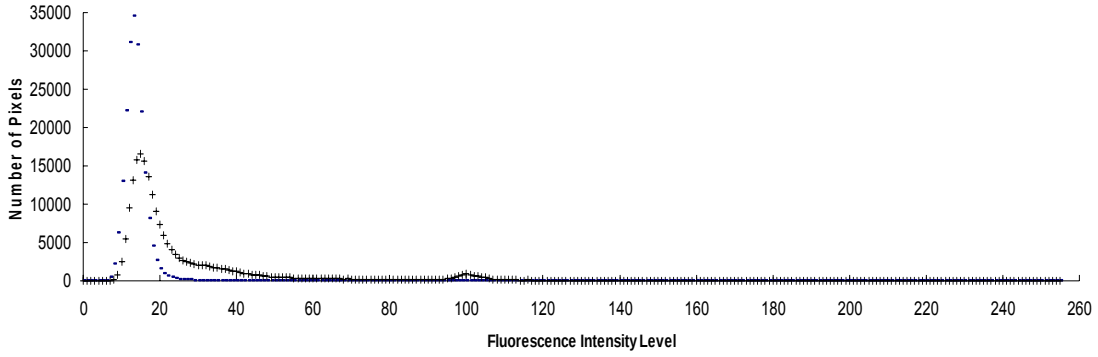

Figure 3.47 Plot of number of pixels as a function of fluorescence intensity level. A fluorescence image of negative controls (-) and a fluorescence image of cell cultures dosed with particles containing 770 pg LPS, 370 pg carbon and 6 pg FluoSpheres per particle (+) were used.

If the peak of negative control could be avoided when doing integration, the results from negative control would be 0. A method to do background subtraction was to establish a threshold when doing integration in replacement of integrating from level 0 to level 255.

3.7.3.4.1 Establishing a threshold at level 66

A threshold of level 66 was established since it was the level that most negative control plots became 0 and therefore the integration from level 67 to level 255 of negative control was close to 0. The fluorescence image from cells dosed with particles was also integrated from level 67 to level 255. Absolute fluorescence signal intensity was plotted as a function of number of particles deposited onto the cells (Figure 3.48). It was observed that there were also two distinct regions able to be fitted with least squares linear regression lines: a region of positive slope, and a region of data points able to be fitted to a line which had a slope approaching 0. But the data points were scattered more than other image processing methodologies.

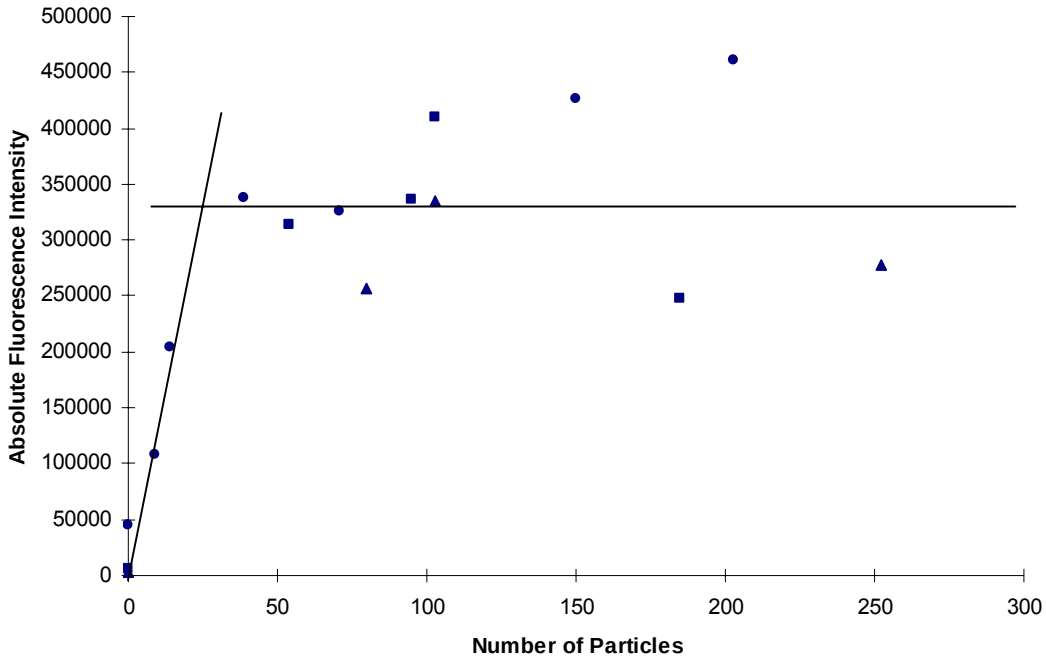

Figure 3.48 Plot of absolute ICAM-1 antibody fluorescence intensity (after establishing a threshold of level 66) as a function of number of particles. Different numbers of particles containing 1570 pg LPS, 2200 pg carbon and 6 pg FluoSpheres per particle were deposited onto the cells. (■) (●) (▲) indicate replicates.

Again, two numbers were used to present ICAM-1 expressions: the magnitude of the slope of the least squares linear fit to the region of data fitted to a positive slope and the magnitude of the intercept of the least squares linear fit to the region of data fitted to a line having a slope approaching 0.

3.7.3.4.1.1 Results from the region of positive slope of a least squares linear fit

A549 cells were cultured in centre-well organ dishes and dosed with different compositions of particles containing LPS and carbon and incubated for 24 hours before being fixed and stained with ICAM-1 fluorescence antibodies. After establishing a threshold of level 66, the absolute fluorescence intensities were plotted as a function of the number of particles for each individual experiment. The magnitude of the slope of the

least squares linear fit to the region of data fitted to a positive slope from each type of particles were plotted as functions of mass ratio between LPS and carbon per particle, mass of LPS per particle and total mass of LPS plus carbon per particle respectively (Figure 3.49, Figure 3.50, Figure 3.51).

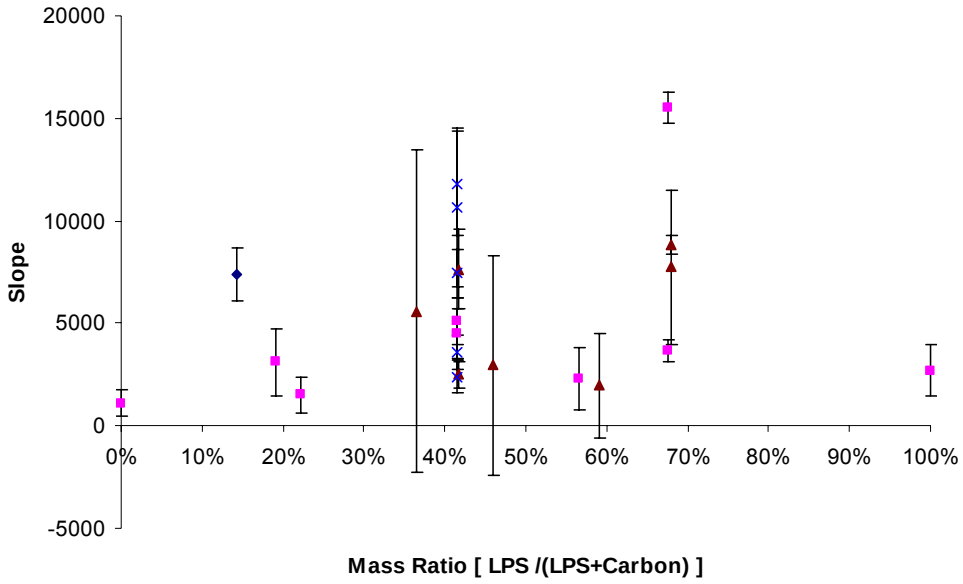

Figure 3.49 The magnitude of the slope of the least squares linear fit to the region of data fitted to a positive slope as a function of mass ratio between LPS and carbon per particle. Particles with ~340 pg (♦), ~1200 pg (■), ~2400 pg (▲) and ~3700 pg (x) total mass of LPS plus carbon per particle were generated and deposited onto the cells. Error bars represent the error of slopes.

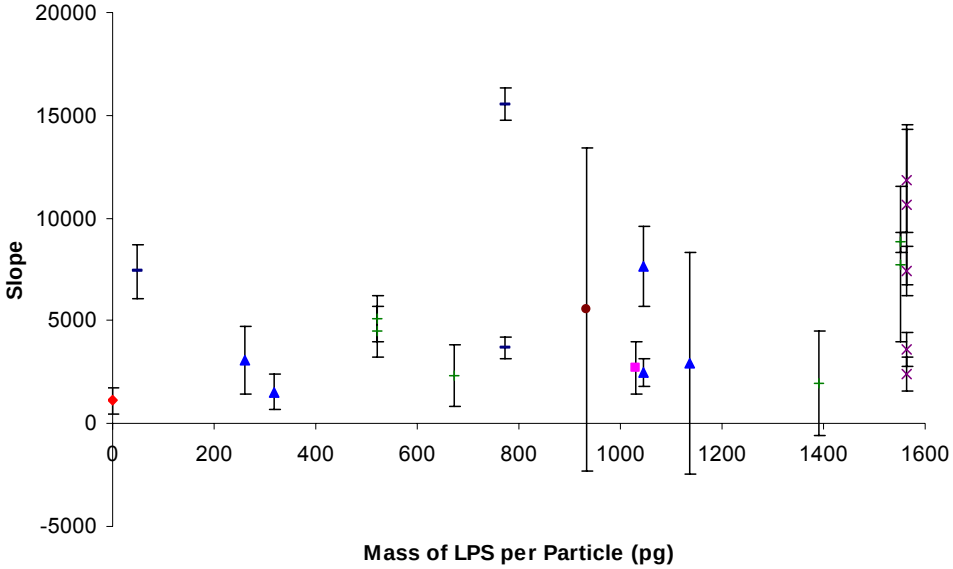

Figure 3.50 The magnitude of the slope of the least squares linear fit to the region of data fitted to a positive slope as a function of mass of LPS per particle. Particles with 0 pg LPS but ~1200 pg carbon (♦), 0 pg carbon but ~1200 pg LPS (■), < 500 pg carbon (—), 500 pg to 1000 pg carbon (+), 1000 pg to 1500 pg carbon (▲), 1500 pg to 2000 pg carbon (●) and ~2200 pg carbon (x) per particle were generated and deposited onto the cells. Error bars represent the error of slopes.

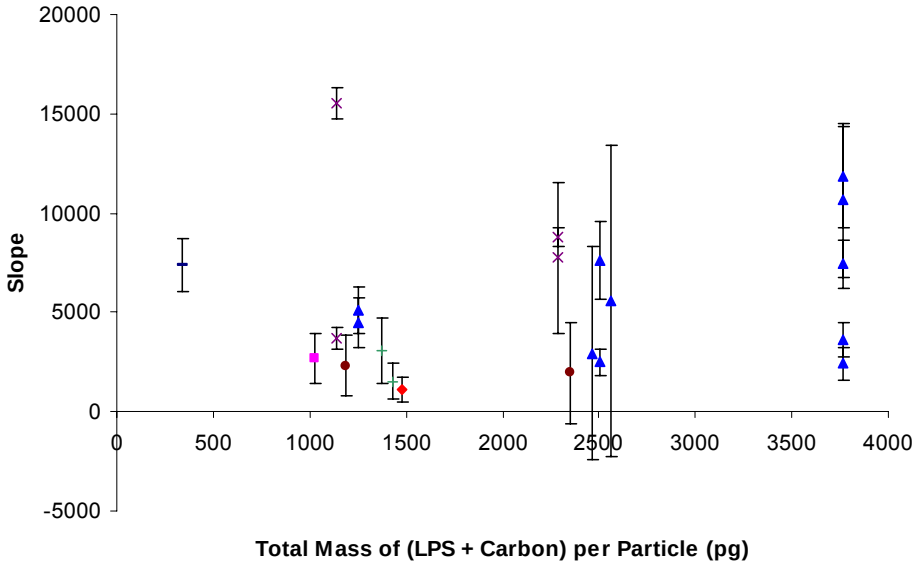

Figure 3.51 The magnitude of the slope of the least squares linear fit to the region of data fitted to a positive slope as a function of total mass of LPS plus carbon per particle. Particles with 0% of LPS to total mass (♦), 100% of LPS to total mass (■), ~15% of LPS to total mass (—), ~20% of LPS to total mass (+), ~40% of LPS to total mass (▲), ~60% of LPS to total mass (●) and ~70% of LPS to total mass (x) per particle were generated and deposited onto the cells. Error bars represent the error of slopes.

3.7.3.4.1.2 Results from the region of data that was fitted to a least squares linear fit to data that yielded a line having a slope approaching 0

A549 cells were cultured in centre-well organ dishes and dosed with different compositions of particles containing LPS and carbon and incubated for 24 hours before being fixed and stained with ICAM-1 fluorescence antibodies. After establishing a threshold of level 66, the absolute fluorescence intensities were plotted as a function of the number of particles for each individual experiment. The intercept of the least squares linear fits, that all had slopes approaching 0, were plotted for each type of particle. The absolute magnitudes of intercepts of the least squares linear fit to the region of data fitted to a line having a slope approaching 0 were plotted as functions of mass ratio between LPS and carbon per particle, mass of LPS per particle and total mass of LPS plus carbon per particle respectively (Figure 3.52, Figure 3.53, Figure 3.54).

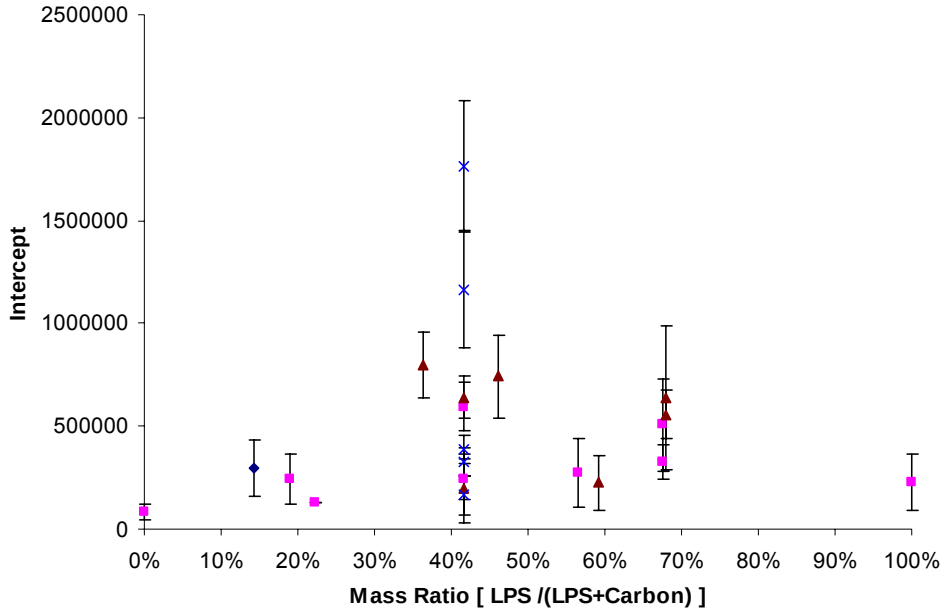

Figure 3.52 Plot of absolute magnitude of intercept of the least squares linear fit to the region of data fitted to a line having a slope approaching 0 as a function of mass ratio between LPS and carbon per particle. Particles with ~340 pg (♦), ~1200 pg (■), ~2400 pg (▲) and ~3700 pg (x) total mass of LPS plus carbon per particle were generated and deposited onto the cells. Error bars represent the standard deviation of the intercept.

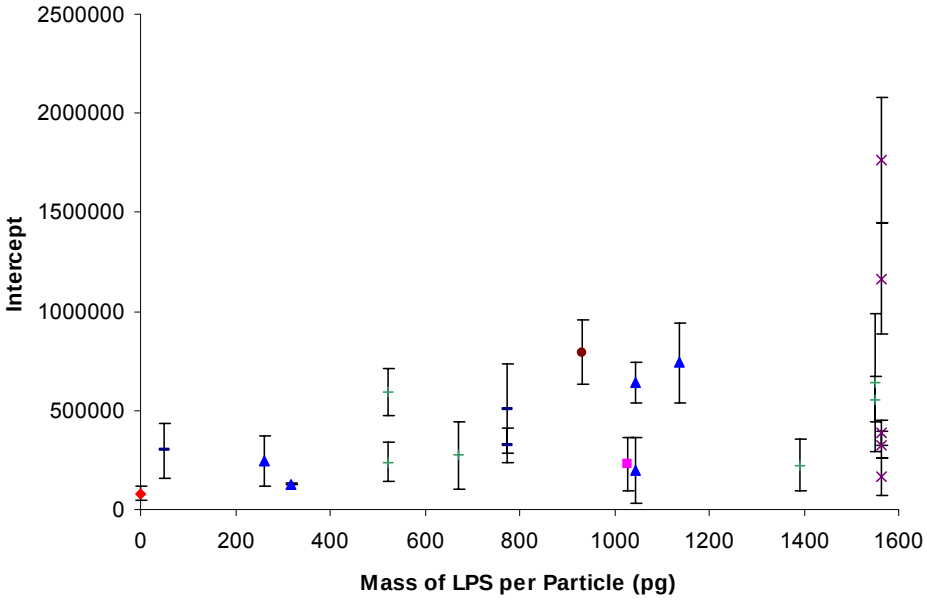

Figure 3.53 Plot of absolute magnitude of intercept of the least squares linear fit to the region of data fitted to a line having a slope approaching 0 as a function of mass of LPS per particle. Particles with 0 pg LPS but ~1200 pg carbon (♦), 0 pg carbon but ~1200 pg LPS (■), < 500 pg carbon (—), 500 pg to 1000 pg carbon (+), 1000 pg to 1500 pg carbon (▲), 1500 pg to 2000 pg carbon (●) and ~2200 pg carbon (x) per particle were generated and deposited onto the cells. Error bars represent the standard deviation of the intercept.

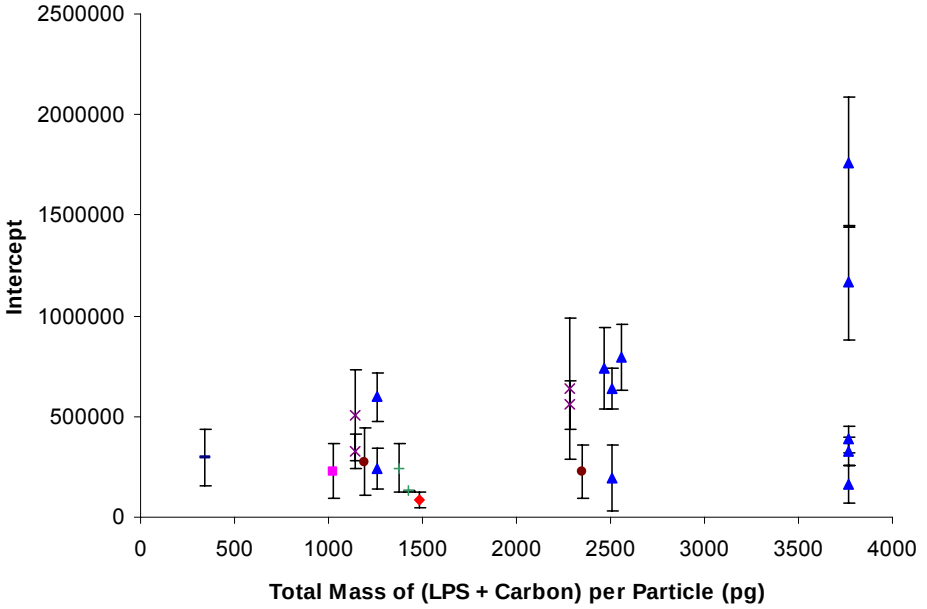

Figure 3.54 Plot of absolute magnitude of intercept of the least squares linear fit to the region of data fitted to a line having a slope approaching 0 as a function of total mass of LPS plus carbon per particle. Particles with 0% of LPS to total mass (♦), 100% of LPS to total mass (■), ~15% of LPS to total mass (—), ~20% of LPS to total mass (+), ~40% of LPS to total mass (▲), ~60% of LPS to total mass (●) and ~70% of LPS to total mass (x) per particle were generated and deposited onto the cells. Error bars represent the standard deviation of the intercept.

3.7.3.4.2 Establishing a threshold at level 22

From figure 3.47, it was observed that although negative controls were not exactly 0, they were closed to 0 from level 22. It was also observed that cells dosed with particles had more pixels than negative control in the region from level 22 to level 66. Therefore, if the threshold was established at level 66, some information may be lost. A threshold of level 22 was established in replacement of level 66. The fluorescence image was integrated from level 23 to level 255. Absolute fluorescence signal intensity was plotted as a function of number of particles deposited onto the cells (Figure 3.55). It was observed that there were also two distinct regions able to be fitted with least squares linear regression lines: a region of positive slope, and a region of data points able to be fitted to a line which had a slope approaching 0. In addition, the data points were less scattered as compared to figure 3.48.

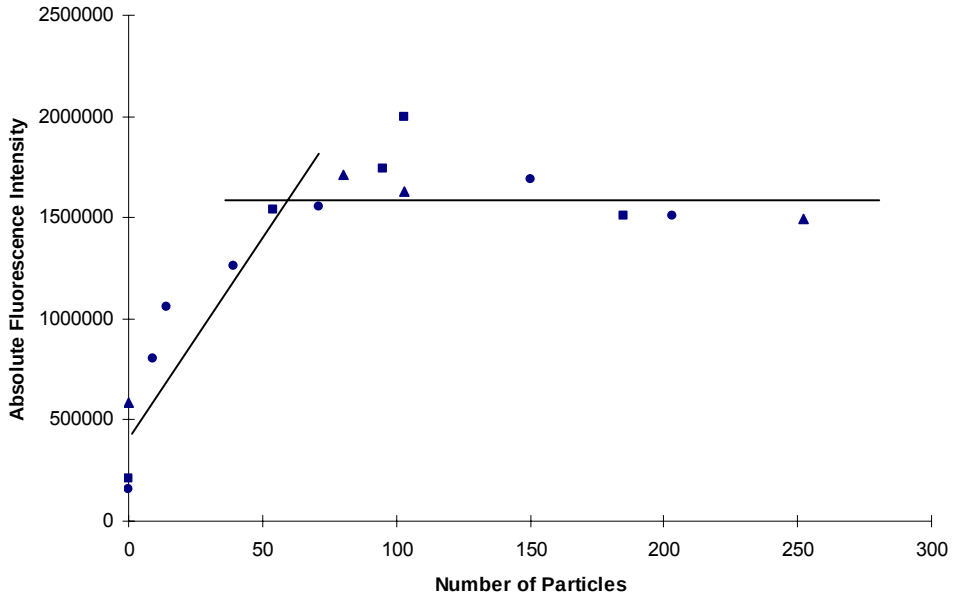

Figure 3.55 Plot of absolute ICAM-1 antibody fluorescence intensity (after establishing a threshold of level 22) as a function of number of particles. Different numbers of particles containing 1570 pg LPS, 2200 pg carbon and 6 pg FluoSpheres per particle were deposited onto the cells. (■) (●) (▲) indicate replicates.

Again, two numbers were used to present ICAM-1 expressions: the magnitude of the slope of the least squares linear fit to the region of data fitted to a positive slope and the magnitude of the intercept of the least squares linear fit to the region of data fitted to a line having a slope approaching 0.

3.7.3.4.2.1 Results from the region of positive slope of a least squares linear fit

A549 cells were cultured in centre-well organ dishes and dosed with different compositions of particles containing LPS and carbon and incubated for 24 hours before being fixed and stained with ICAM-1 fluorescence antibodies. After establishing a threshold of level 22, the absolute fluorescence intensities were plotted as a function of the number of particles for each individual experiment. The magnitude of the slope of the least squares linear fit to the region of data fitted to a positive slope from each type of particles were plotted as functions of mass ratio between LPS and carbon per particle, mass of LPS per particle and total mass of LPS plus carbon per particle respectively (Figure 3.56, Figure 3.57, Figure 3.58).

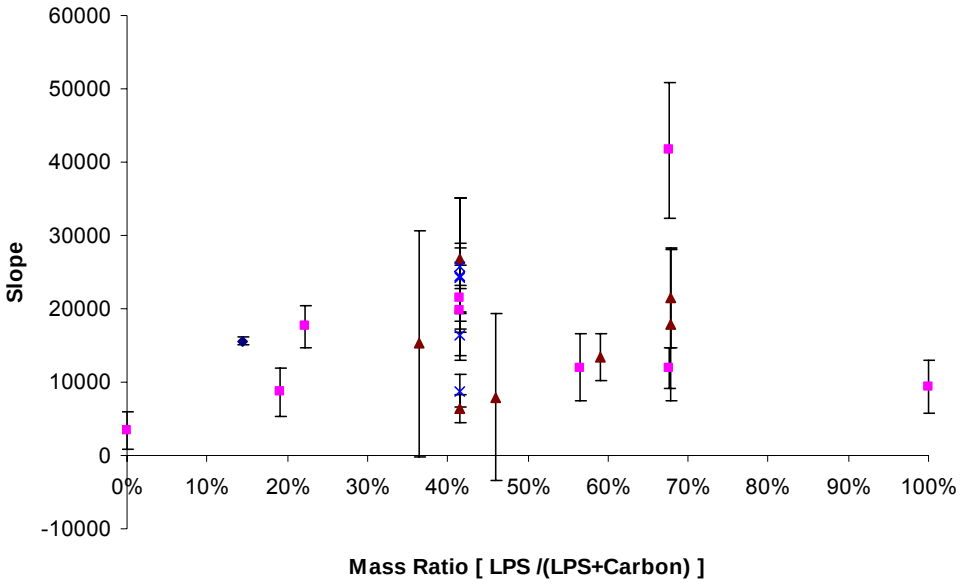

Figure 3.56 The magnitude of the slope of the least squares linear fit to the region of data fitted to a positive slope as a function of mass ratio between LPS and carbon per particle. Particles with ~340 pg (♦), ~1200 pg (■), ~2400 pg (▲) and ~3700 pg (x) total mass of LPS plus carbon per particle were generated and deposited onto the cells. Error bars represent the error of slopes.

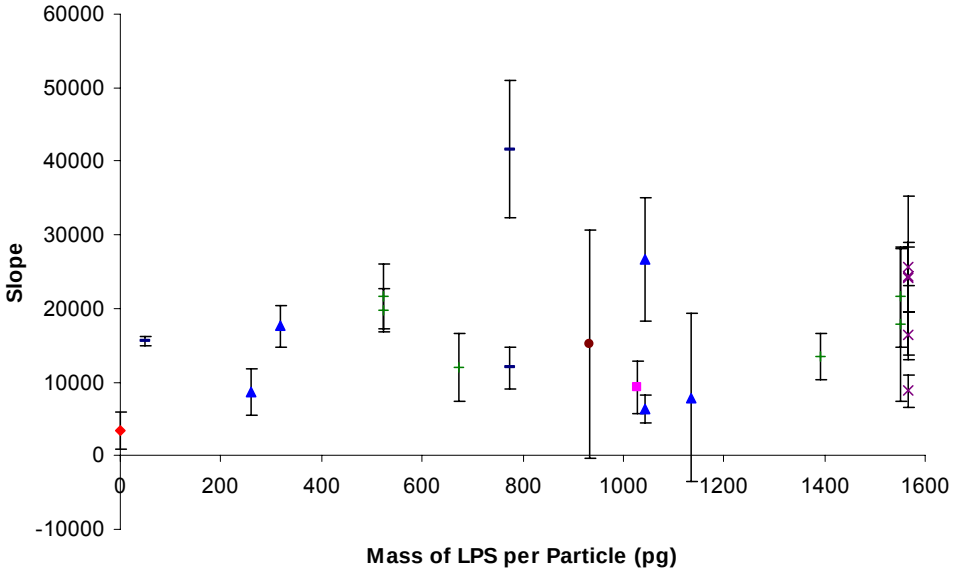

Figure 3.57 The magnitude of the slope of the least squares linear fit to the region of data fitted to a positive slope as a function of mass of LPS per particle. Particles with 0 pg LPS but ~1200 pg carbon (♦), 0 pg carbon but ~1200 pg LPS (■), < 500 pg carbon (—), 500 pg to 1000 pg carbon (+), 1000 pg to 1500 pg carbon (▲), 1500 pg to 2000 pg carbon (●) and ~2200 pg carbon (x) per particle were generated and deposited onto the cells. Error bars represent the error of slopes.

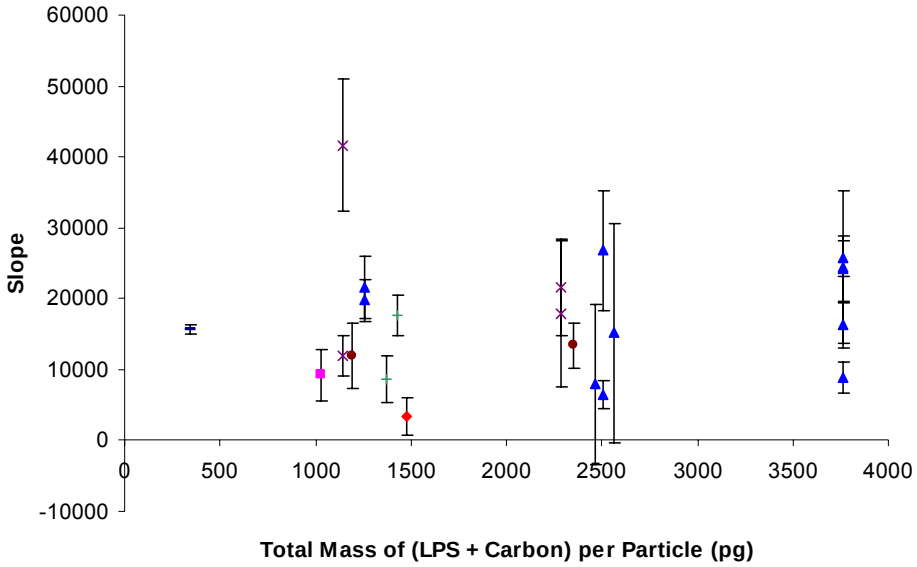

Figure 3.58 The magnitude of the slope of the least squares linear fit to the region of data fitted to a positive slope as a function of total mass of LPS plus carbon per particle. Particles with 0% of LPS to total mass (♦), 100% of LPS to total mass (■), ~15% of LPS to total mass (—), ~20% of LPS to total mass (+), ~40% of LPS to total mass (▲), ~60% of LPS to total mass (●) and ~70% of LPS to total mass (x) per particle were generated and deposited onto the cells. Error bars represent the error of slopes.

3.7.3.4.2.2 Results from the region of data that was fitted to a least squares linear fit to data that yielded a line having a slope approaching 0

A549 cells were cultured in centre-well organ dishes and dosed with different compositions of particles containing LPS and carbon and incubated for 24 hours before being fixed and stained with ICAM-1 fluorescence antibodies. After establishing a threshold of level 22, the absolute fluorescence intensities were plotted as a function of the number of particles for each individual experiment. The intercept of the least squares linear fits, that all had slopes approaching 0, were plotted for each type of particle. The absolute magnitudes of intercepts of the least squares linear fit to the region of data fitted to a line having a slope approaching 0 were plotted as functions of mass ratio between

LPS and carbon per particle, mass of LPS per particle and total mass of LPS plus carbon per particle respectively (Figure 3.59, Figure 3.60, Figure 3.61).

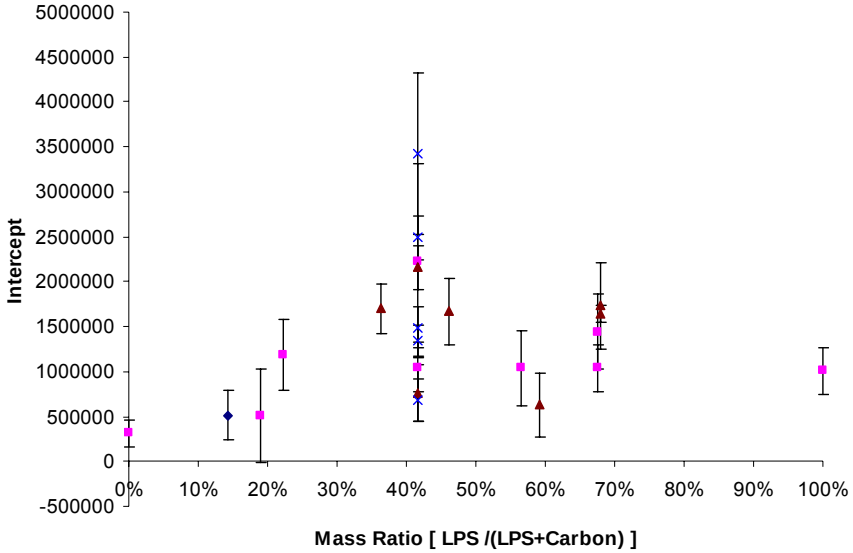

Figure 3.59 Plot of absolute magnitude of intercept of the least squares linear fit to the region of data fitted to a line having a slope approaching 0 as a function of mass ratio between LPS and carbon per particle. Particles with ~340 pg (♦), ~1200 pg (■), ~2400 pg (▲) and ~3700 pg (x) total mass of LPS plus carbon per particle were generated and deposited onto the cells. Error bars represent the standard deviation of the intercept.

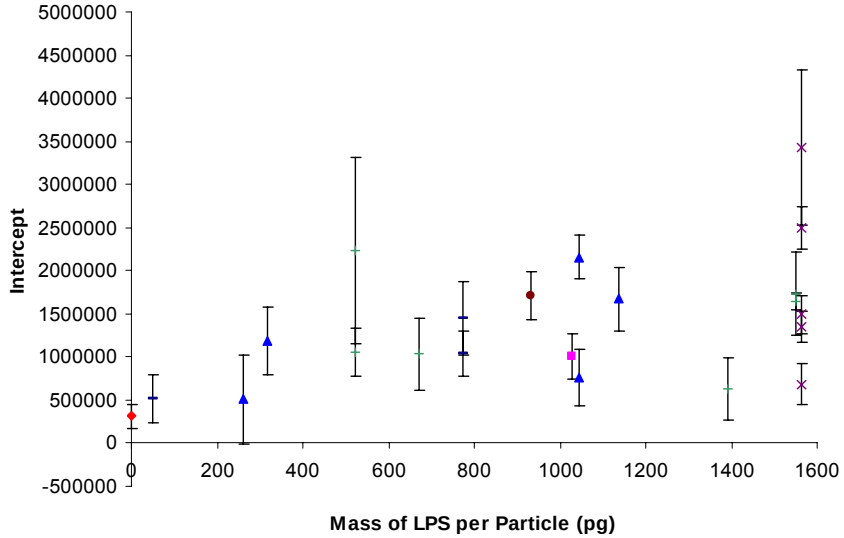

Figure 3.60 Plot of absolute magnitude of intercept of the least squares linear fit to the region of data fitted to a line having a slope approaching 0 as a function of mass of LPS per particle. Particles with 0 pg LPS but ~1200 pg carbon (♦), 0 pg carbon but ~1200 pg LPS (■), < 500 pg carbon (—), 500 pg to 1000 pg carbon (+), 1000 pg to 1500 pg carbon (▲), 1500 pg to 2000 pg carbon (●) and ~2200 pg carbon (x) per particle were generated and deposited onto the cells. Error bars represent the standard deviation of the intercept.

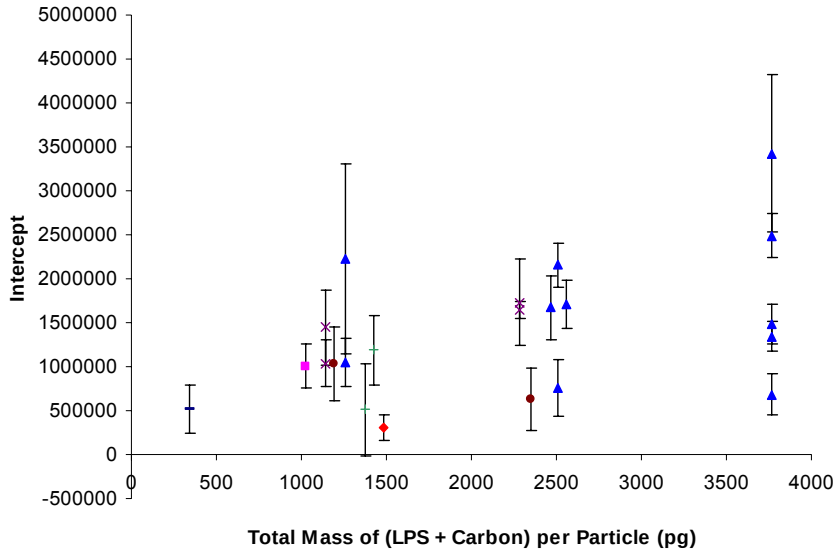

Figure 3.61 Plot of absolute magnitude of intercept of the least squares linear fit to the region of data fitted to a line having a slope approaching 0 as a function of total mass of LPS plus carbon per particle. Particles with 0% of LPS to total mass (♦), 100% of LPS to total mass (■), ~15% of LPS to total mass (—), ~20% of LPS to total mass (+), ~40% of LPS to total mass (▲), ~60% of LPS to total mass (●) and ~70% of LPS to total mass (x) per particle were generated and deposited onto the cells. Error bars represent the standard deviation of the intercept.

3.7.3.5 Discussion

Five different methodologies were used to process the images of ICAM-1 antibody fluorescence intensities. The resultant data were plotted as a function of number of particles showed in the above sections. It was observed that there were two distinct regions in all of the plots that able to be fitted with least squares linear regression lines: a region of positive slope, and a region of data points able to be fitted to a line which had a slope approaching 0 (eg. figure 3.39). Therefore, the magnitude of the slope of the least squares linear fit to the region of data fitted to a positive slope and the magnitude of the intercept of the least squares linear fit to the region of data fitted to a line having a slope approaching 0 were used to present ICAM-1 expression levels respectively. It was observed that the shapes of the plots from the five different image processing methodologies were similar. The only difference was the dynamic range of Y axis. The

reason why the resultant data were parted to two distinct regions remains unknown. I speculate that the cells rapidly reach to their highest ICAM-1 response to one specific type of particle. In the region of data points that able to be fitted to a line with a slope approaching 0, when the number of particles increased, the cells would not bother express more ICAM-1. But if the type of particle was changed, the cells would rapidly reach to a new highest ICAM-1 response to that new specific type of particle.

Since the purpose of this study was to learn what was more important in affecting cellular responses, three factors were monitored: mass ratio between LPS and carbon per particle, mass of LPS per particle and total mass of LPS plus carbon per particle. By observing the region of positive slope (eg. figure 3.40, figure 3.41, figure 3.42), there was no obvious trend from any of these three factors. It was concluded that these three factors did not affect the region of positive slope. It was also concluded that the different LPS plus carbon particle compositions did not affect this region. However, there were not many data points collected in this region, which may contribute the large scatter in the data, with points for similar x axis numbers frequently not agreeing within experimental error.

By observing the magnitude of intercept of the least squares linear fit to the region of data fitted to a line having a slope approaching 0, the plot with mass ratio between LPS and carbon per particle had two distinct regions able to be fitted with least squares linear regression lines: a region of positive slope, and a region of data points able to be fitted to a line which had a slope approaching 0 (eg. figure 3.43). It was concluded that in a low mass ratio, increasing the ratio of LPS would increase the ICAM-1 expressions however after passing a certain mass ratio, ICAM-1 expressions were no longer related to the mass

ratio, or even can be observed decreasing when increasing the mass ratio. Both the plots with mass of LPS per particle and total mass of LPS plus carbon per particle could be fitted with least squares linear regression lines with a positive slope (eg. figure 3.44, figure 3.45). It was concluded that if the mass of carbon was kept relatively the same, increasing the mass of LPS per particle could increase the ICAM-1 expressions. If the mass ratio was kept relatively the same, increasing the total mass of the particle could also increase the ICAM-1 expressions. Therefore, both the mass of LPS per particle and the total mass of the particle could affect the ICAM-1 expressions. Increasing either of them could increase the ICAM-1 expressions.

3.8 Other observations of ICAM-1 and CXCL-5 expression

Previous studies indicated the ICAM-1 results from antibody assays and the CXCL-5 results from MALDI-TOF-MS were consistent. LPS is an activator of neutrophils [108], and CXCL-5 is chemokine that can recruit neutrophils [109], ICAM-1 is known as an adhesion molecule that can bind with neutrophils to assist in their movement from the blood to the inflammation sites [25, 110]. Both ICAM-1 and CXCL-5 could be regulated by transcription factor nuclear factor κB (NF-κB) [27, 37] and NF-κB could be activated by LPS [111]. Therefore, ICAM-1 results and CXCL-5 results agreed with each other when the cells were incubated with particles containing LPS and carbon. However, whether ICAM-1 and CXCL-5 expressions still have correlations under other conditions (eg. cell death) remains unknown. To address this question, A549 cells were dried to death intentionally. ICAM-1 and CXCL-5 were monitored relative to the negative control.

A549 cells were grown to approximately 90% or more confluence on an 18 mm × 18 mm glass coverslip in a 6-well plate. Growth medium was aspirated with a water

faucet driven vacuum aspirator. Cells were incubated for 24 hours with no medium added during the incubation period. Therefore, these cells were not viable after the incubation period because of lack of moisture (described in section 3.4.1.2). The negative control was as per all steps of the procedure described above except that instead of no medium added, 200 µL SFM was immediately added to the cell culture after growth medium was aspirated. Cells in a negative control were therefore viable after the incubation period. The supernatant of a negative control was collected and 200 µL SFM was used to wash the surface of the dried cells and collected as its supernatant. Both supernatants were monitored using MALDI-TOF-MS (Figure 3.62). ICAM-1 antibody assays were performed on both samples and images were taken using an inverted fluorescence microscope (Figure 3.62).

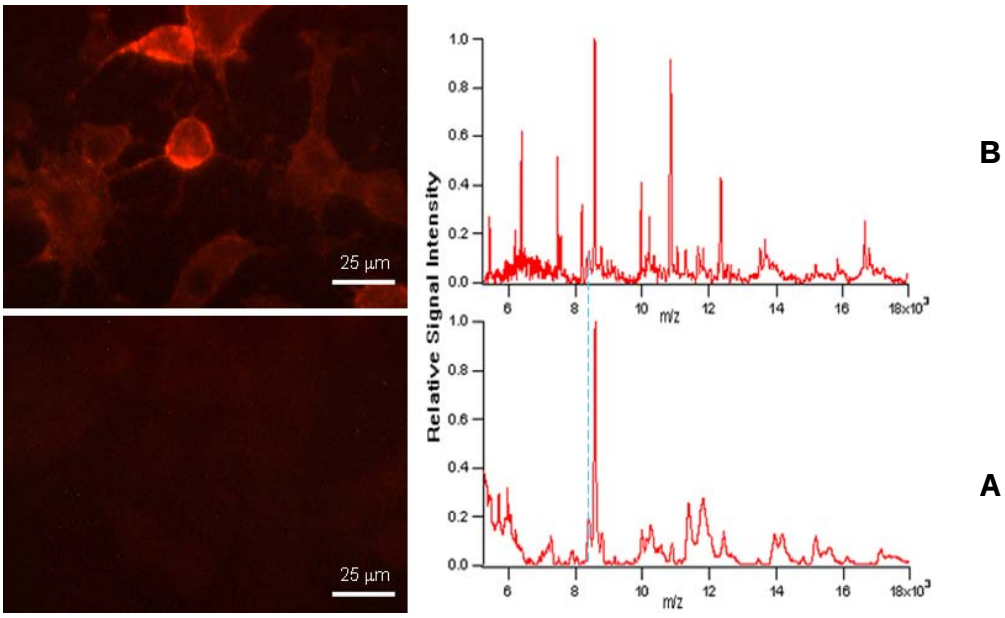

Figure 3.62 ICAM-1 antibodies fluorescence images (on the left) and MALDI-TOF mass spectra of the supernatants (on the right) of A549 cell cultures. Red colour represented ICAM-1 expressions. Cells were grown to approximately 90% or more confluence on an 18 mm × 18 mm glass coverslip in a 6-well plate. Growth medium was aspirated with a water faucet driven vacuum aspirator. 0 µL (B) or 200 µL (A) SFM was immediately added to the cell culture. Cells were then incubated for 24 hours. Supernatants were collected for MALDI-TOF-MS analysis and CXCL-5 was monitored. Cells were stained with ICAM-1 antibodies. Fluorescence images were taken using an objective magnification of 40X.

Figure 3.62 indicated that both the dead cells and the negative control did not secrete CXCL-5, however the ICAM-1 expression from the dead cells was much stronger than the negative control and it was effected by every single cell. Therefore, the ICAM-1 and CXCL-5 expression levels do not always agree with each other in this cell line. I suspected that it may because ICAM-1 could be regulated by some mediator other than the one which could regulate both ICAM-1 and CXCL-5. There was also a possibility that when cells were drying out, the cell membrane was destroyed and the biomolecules that used to be inside the cells came out and the strong signal intensities of those biomolecules suppressed the signal intensity of CXCL-5.

3.9 Entire procedure of the optimized methodology

3.9.1 Chemicals preparing

3.9.1.1 Growth medium

F-12K Medium was prepared from F-12K medium powder (Sigma-Aldrich, N3520-10X1L, Oakvillle, ON, Canada) according to instructions provided by the supplier. 11.1 g F-12K powder and 2.5 g sodium bicarbonate ($NaHCO_3$) were added to 900 mL of 15-20 ºC Milli-Q water while gently stirring the water. The desired pH for cell culture was 7.0-7.6. Since filtration may raise the pH by 0.1-0.3, the pH was adjusted to 7.2 using 1N sodium hydroxide (NaOH) or 1N hydrochloric acid (HCl) while stirring. The solution was filtered in a sterile biological safety cabinet with a 0.22 microns filter (Nalge Nunc International Corp., 291-4520, Rochester, NY, USA) and dispensed into a sterile container followed by adding 100 mL FBS to the solution making the final volume to 1 L.

3.9.1.2 SFM

SFM contained everything found in the growth medium except the last 100 mL. Instead of FBS, 0.22 microns filtered Milli-Q water was added to the solution.

3.9.1.3 Cryoprotectant medium

Cryoprotectant medium was prepared by adding 1 mL of Dimethyl sulfoxide (DMSO) to 9 mL of growth medium.

3.9.1.4 TNF-α solution

10 μg TNF-α powder was dissolved in 1 mL 0.22 microns filtered Milli-Q water making the final concentration 10 μg/mL and stored at -80 ºC. To avoid repeated freezing and thawing, each 100 μL aliquot was stored in separated autoclaved micro centrifuge vials.

3.9.1.5 0.01M (1X) PBS solution

Ten PBS tablets (Oxoid Limited, BR0014G, Basingstoke, Hampshire, UK), in total containing 8.0 g sodium chloride (NaCl), 0.2 g potassium chloride (KCl), 1.15 g disodium hydrogen phosphate (Na_2HPO_4) and 0.2 g potassium dihydrogen phosphate (KH_2PO_4), were dissolved in 1 L of Milli-Q water and autoclaved for 10 minutes at 115°C or filtered with a 0.22 microns filter to be sterile. The PBS solution mentioned in the whole thesis was 1X PBS solution.

3.9.1.6 4% (w/v) PFA/PBS (pH 7.4) solution

4 g PFA powder (Polysciences Inc., 00380-1, Warrington, PA, USA) was dissolved in 80 mL PBS solution and a small volume (about 1 mL) of 1 N NaOH at 60 ºC or lower

with stirring [112]. pH of the solution was adjusted to 7.4 with 1 N HCl. A final volume of 100 mL was obtained by adding PBS solution. The solution was filtered with a 0.22 micrometer syringe filter and stored at -20 ºC for further fixation use.

3.9.1.7 Diluted antibody solution

1% (w/v) BSA/PBS solution was prepared by adding 1 g BSA powder to 100 mL PBS solution and stored at 4 ºC for primary antibody dilution. 2 µL of 0.2 mg/mL primary antibody (mouse anti-human ICAM-1 antibody) (Invitrogen Canada Inc., MHCD5400, Burlington, ON, Canada) was added to 200 µL 1% (w/v) BSA/PBS solution for each cell culture's staining.

2 µL of 2 mg/mL secondary antibody (fluorescence goat anti-mouse IgG antibody) was added to 200 µL PBS solution for each cell culture's staining.

According to the instruction by the supplier, the diluted antibody solution was to be fresh made every time, or at most, stored for one week maximum at 4 ºC.

3.9.2 Cell culture

3.9.2.1 Start from frozen cells

In an effort to avoid excessive alkalinity of the medium, a 100 mm × 20 mm cell culture dish (BD Falcon, 353003, Mississauga, ON, Canada) with 10 mL growth medium was placed into the incubator (with 5% CO_2) for 15 minutes to allow the medium to reach its normal pH. Each vial containing frozen cells was thawed by bathing in a 37 ºC water bath for approximately 2 minutes. The vial was sprayed with 70% ethanol and all of the operations from this point on were carried in a sterile biological safety cabinet. Thawed suspension was added into the cell culture dish with the 10 mL pre-warmed medium. The

culture dish was shaken to make the cell pellets evenly suspended prior to incubation in the incubator until the cells attached to the growth surface (approximately 4 hours). Culture medium was removed and discarded since the cryoprotectant medium containing DMSO was harmful to cells. 10 mL of fresh growth medium was added to the cell culture dish.

3.9.2.2 Subculturing cells

Cell passage was performed when cells reached 80% confluence or more and it was performed in a biological safety cabinet with sterilizing the area with 70% ethanol. Culture medium was removed and discarded. 4 mL 37 ºC PBS solution was used to briefly rinse the cell layer and to remove Ca^{2+} and Mg^{2+} that were needed for cell attachment to the surface [113, 114], and the rinse also removed the serum in the growth medium which contained trypsin inhibitor. 1 mL 37 ºC 0.05% (w/v) (1X) Trypsin/EDTA•4Na (Invitrogen Canada Inc., 25300-112, Burlington, ON, Canada) solution was then added to the culture dish and incubated for no more than 5 minutes. Trypsin was a protease that could cleave the adhesion proteins that kept the cells on the surface [115]. Cells were observed under an inverted microscope every 2 minutes until the cell layer was dispersed and cells were observed to be round in appearance. Rocking back and forth, or knocking the culture plate against a table slightly could help the cells detach from the plate. 5 mL growth medium was added to the culture dish and the suspension was transferred into a 15 mL capped centrifuge tube (Corning, 430791, Lowell, MA, USA) and centrifuged at rcf of 1000 g for 2 minutes to spin down the cell pellets. The supernatant was removed and discarded. The cell pellets were resuspended with 6 mL of growth medium. A certain volume of suspension (dependent on the time I

wanted the cells to be 80% confluence and the percentage confluence of the previous passage) was added to a new cell culture dish containing 8 mL of 37 ºC fresh growth medium for passage, or to a new centre-well organ culture dish (BD Falcon, 353037, Mississauga, ON, Canada) containing 1 mL of 37 ºC fresh growth medium for study of dosing cells with particles. Culture dishes were shaken to make cells evenly suspended in the dishes. According to the instruction by ATCC, A549 cell line's doubling time was 22 hours and the recommended subculture ratio was 1:3 to 1:8. Culture dishes were incubated in 5% CO_2 at 37 ºC and 100% humidity incubator. If not passed, cells were fed by removing and discarding the culture medium and adding 10 mL 37 ºC fresh growth medium two or three times per week.

3.9.2.3 Storing cells

The procedure for storing cells were the same as subculturing cells until the step of cell resuspension. Instead of adding 6 mL of growth medium, 1 mL of cryoprotectant medium was added to resuspend the cell pellets. The 1 mL suspension was transferred to a 2 mL cryogenic vial (VWR, 16001-102, Mississauga, ON, Canada). In an effort to avoid reducing viability of the cells, the resuspending and transferring steps were performed quickly (approximately 2 minutes). The cryogenic vial was immediately placed in a -80 ºC fridge for 15 hours and then transferred into a liquid nitrogen tank for further storage.

3.9.3 Particle generation and deposition onto lung cells *in vitro*

Cells were grown to approximately 90% or more confluence in a centre-well organ culture dish. 2 mL of 0.22 microns filtered Milli-Q water was added in the moat of the

dish. With a population of particles generated and levitated using an EDLT (as described in chapter 2), the culture medium was removed and discarded with a 1000 μL pipettor by tilting the dish to ~45° followed by aspirating 1000 μL each time until no more medium was able to be aspirated by the pipettor. 60 μL fresh SFM was gently added into the culture drop by drop to the centre of the culture while SFM could be seen spreading to the whole culture. The cell culture was immediately placed on the bottom electrode under the AC trap. The particles were then deposited from the AC trap directly onto the cell culture. If multiple populations of particle depositions were needed, the total time from removing medium to the end of the particle deposition step was no more than 5 minutes. Cell culture was then centrifuged at rcf of 1200 g for 1 minute and 190 μL additional fresh SFM was added slowly into the culture dish against the wall. Cell culture was then incubated in the incubator with 5% CO_2 at 37 ºC and 100% humidity for 24 hours incubation period.

The negative control was cell cultures grown to approximately 90% or more confluence in a centre-well organ culture dish that followed all steps of the procedure described above except deposition of the particles. The positive control was cell cultures grown to approximately 90% or more confluence in a centre-well organ culture dish bathed in 240 μL of SFM with 10 μL of TNF-α solution (concentration of TNF-α added = 400 ng/mL, total moles TNF-α added = 5.9 pmol) and incubated for 24 hours incubation period.

Trypan blue assay was performed to one random culture after a 24 hours incubation period by removing and discarding the culture SFM and briefly rinsing with PBS solution prior to adding 50 μL 0.4% (w/v) trypan blue solution and swirling to even. Trypan blue

solution was removed and discarded after 5 minutes. The culture was rinsed with PBS solution and observed with an inverted microscope. Blue colour cells were none viable and transparent colour cells were viable.

3.9.4 Collection of the Supernatant and MALDI-TOF-MS sample preparation and data acquisition

After a 24 hours incubation period, 20 μL supernatant was collected. The supernatant was stored in a micro-centrifuge tube at -20 ºC until analysis.

A C_{18} ZipTip was used to purify and concentrate the biomolecules in the supernatant. ZipTip was a 10 μL pipette tip with a small amount of chromatography media fixed at the end with no dead volume. 5 μL of 10 μg/mL lysozyme was added into the 20 μL supernatant as internal standard. 6.5 μL of 2.5% (v/v) trifluoroacetic acid (TFA) was added into the supernatant to acidify the supernatant. The final TFA concentration was 0.5% at a pH of <4. According to the instruction by the supplier, the pipettor for ZipTip was used by fully depressing the pipettor plunger to a dead stop using a volume setting of 10 μL. Wetting solution, ACN, was aspirated into the ZipTip and dispensed to waste twice without introducing air into the tip. Washing solution, 0.1% (v/v) TFA in Milli-Q water, was then aspirated into ZipTip and dispensed to waste twice without introducing air into the tip to equilibrate the ZipTip. The biomolecules were retained on the Ziptip's stationary phase by aspirating and dispensing the supernatant for 10 cycles without introducing air into the tip. Washing solution was then aspirated and dispensed to waste twice again without introducing air into the tip. The elution solution was prepared by adding excess SA powder into 50 μL ACN with 50 μL 0.1% (v/v) TFA mixture solution to make SA saturate. Followed a centrifugation at rcf of 2000 g for 5 minutes, the

supernatant without solid SA was used for elution. ZipTip was aspirated and dispensed 5 cycles in a 4 μL elution solution without introducing air. The 4 μL elution solution was directly transferred onto a sample well of a stainless steel MALDI plate. MALDI-TOF-MS was operated with a nitrogen laser with a wavelength of 337 nm. The software used for MALDI-TOF-MS was MassLynx. The instrument was operated in positive ion linear mode with a sampling rate of 5 ns and a time lag focusing (TLF) delay of 500 ns. The micro-channel plate detector voltage (MCP) was at 1850 V. The matrix suppression delay was at 1009 mass units. The source voltage was at 15000 V and the pulse voltage was at 1400 V. Spectral profiles were collected in the mass range 5000 – 18000 Da, acquiring 5 shots per spectrum at a laser firing rate of 5 Hz. 60 spectra from random spots were collected for each sample. Standards were 1 μL 1 mg/mL myoglobin from equine heart (Sigma-Aldrich, M1882-1G, Oakvillle, ON, Canada) with exact mass of 16951.49 Da [116] and 1 μL 1 mg/mL cytochrome c from equine heart (Sigma-Aldrich, C7752-50MG, Oakvillle, ON, Canada) with exact mass of 12384 Da with 2 μL saturated SA in ACN/TFA solution directly dispensed onto a sample well of the MALDI target plate.

3.9.5 MALDI-TOF-MS data processing

MALDI-TOF-MS data processing was performed with MassLynx software. The 60 spectral profiles collected for each sample were combined. This process enhanced mass accuracy and produced a more reproducible spectrum for the sample [117]. The combined spectrum was calibrated with the two standards masses. It was background subtracted using a polynomial order of 5, 20% below the curve and smoothed with a Savitzky-Golay algorithm by setting to 20 channels once. To compare the data, the

relative abundance of every ion in a spectrum was normalized to the abundance of the internal standard ion signal intensity.

3.9.6 Immunocytochemistry assay

After the collection of supernatant, the cells in the centre-well organ culture dish were rinsed with PBS solution twice and fixed with 200 μL 37 ºC 4% (w/v) PFA/PBS (pH 7.4) solution for 20 minutes at room temperature for each culture. Cells were rinsed with PBS solution for three times (each time with ~1 mL PBS solution) prior to adding 200 μL room temperature serum-free protein block (DakoCytomation Inc., X0909, Carpinteria, CA, USA) to each culture for 20 minutes. Protein block was to reduce non-specific stainings [118, 119]. 200 μL room temperature primary antibody was added to each culture directly after removing and discarding the protein block without rinsing. The staining period was 1 hour at room temperature. Cells were rinsed with PBS solution three times by adding and removing ~1 mL PBS solution each time. The second rinsing, PBS solution was retained with cells for 5 minutes at room temperature before being removed. 200 μL room temperature secondary antibody was added to cells and the staining period was 30 minutes at room temperature in dark. Cells were then rinsed with PBS solution for three times by adding and removing ~1 mL PBS solution each time. The second rinsing, PBS solution was retained with cells for 1 hour at room temperature in dark before being removed. ~1 mL of PBS solution was added to each culture prior to storing cells at 4 ºC until analysis. According to the instructions by the supplier of the immunocytochemistry reagents, the cells were to be analyzed within 18 hours of staining.

3.9.7 Image from fluorescence microscopy and data analysis

An inverted fluorescence microscope with an Epi-FI filter block was used for observing and capturing images of the fluorescently labeled cell cultures. In section 3.7.3, five data process methodologies were compared. Since the results from the five methodologies were similar, one method with the largest dynamic range of Y axis was selected for use in the studies described in chapter 4 and 5. 9 pictures were taken in array. The brightest 28 μm by 28 μm square (about one cell big) was cropped from each of the 9 pictures. The intensity of the fluorescence emission in the cropped image was calculated using Image J software and integrated using Excel by multiplying intensity by the number of pixels with that intensity and summing all the products. The average of the 9 intensities for each culture relatives to positive control was expressed as a percentage. A background subtraction was performed to set the negative control to 0% prior to plotting relative fluorescence intensities as a function of the numbers of particles deposited.

Chapter 4 Adjuvant Potential

4.1 Introduction

Adjuvants are agents used in vaccines because it has been observed to increase the immune response leading to improved vaccine efficacy [120-122]. Adjuvants are defined as "agents that act non-specifically to increase the specific immune response or responses to an antigen" in dictionary of immunology [120, 121]. From the website of the U.S. National Cancer Institute, a vaccine adjuvant is defined as "a substance added to a vaccine to improve the immune response so that less vaccine is needed". Adjuvants have been used from the 1920s [122, 123], however the mechanisms of how they work are poorly understood [120, 124-128]. The immune response is composed of two branches: cell-mediated immunity (CMI) and humoral immunity [129, 130]. T helper type 1 (Th1) cells lead to CMI responses [120, 122, 131], while T helper type 2 (Th2) cells lead to humoral immune responses [120, 122, 127, 131-134].

Studies have demonstrated that aluminum salts used as adjuvants to activate Th2 cells [120, 122, 127, 131-134], while LPS is an adjuvant in activating Th1 cells [120, 122, 131]. One recent study has concluded that mixing LPS and an aluminum salt, added to act as an adjuvant, can impair Th2-mediated allergic responses while not inducing a Th1 pattern of inflammation [131]. Other studies have investigated this further and concluded that the toxicity is reduced if the LPS is adsorbed to aluminum-containing adjuvant in the vaccine [126, 135-137]. Some studies have demonstrated that blocking ICAM-1 and its ligand LFA-1 interaction can increase Th2 cytokines secretion and suppress Th1 cytokines. Other studies have concluded that Th2 cytokines can induce ICAM-1

expression [138, 139], which suggests a correlation between ICAM-1 expression and Th2 responses. (Th2 cytokines are low molecular weight proteins, such as Interleukin 4 (IL-4), Interleukin 5 (IL-5) and Interleukin 10 (IL-10), which are produced by Th2 cells [140-142]. Th1 cytokines are low molecular weight proteins, such as Interferon gamma (IFN-γ) and Interleukin 2 (IL-2), which are produced by Th1 cells [141, 142].)

Many studies have demonstrated that soluble forms of transition metals, a class of compounds of ambient particles, are responsible for effecting lung cell injury and inflammation in animals [61, 143-149]. Although as a class, transition metals have similar properties to each other, their different physical and chemical behavior effects different degrees of pulmonary inflammation [61, 145-147]. Several studies conclude that Ottawa dust of Environmental Health Centre-93 (EHC-93), which contain numerous transition metals [150], has adjuvant activity [56, 151, 152]. One of these studies concluded that EHC-93 was an equally potent adjuvant as alum for the production of specific antibodies when mice were immunized with a specific vaccine [152].

Studies have shown that although sodium salts themselves have low potential to cause lung irritation in animals [146, 153], when they are mixed with other compositions, they can cause higher lung cell responses [50, 153]. Sodium is also found in EHC-93 [150].

In this chapter, I made an attempt to study the adjuvant potential in a different aspect: ICAM-1 expression and CXCL-5 expression were monitored as opposed to the more commonly monitored Th2 cell and Th2 cytokine responses and expression levels respectively. Aluminum hydroxide $Al(OH)_3$, a commonly used adjuvant in vaccines [120, 122, 125-127, 131], together with two transition metal salts: Zinc (Zn) and Nickel (Ni),

and one sodium salt, were investigated for their potential to effect a cellular response by monitoring ICAM-1 expression using the methodology developed in chapter 3. Each of these metals are present in EHC-93, and EHC-93 has been shown to induce pulmonary inflammation in animals [61, 147].

4.2 Experimental

4.2.1 A549 cells incubated with different particles

4.2.1.1 A549 cells incubated with $Al(OH)_3$ gel and particles containing LPS plus carbon

A549 cells were grown to approximately 90% or more confluence in centre-well organ culture dishes. Different numbers of particles containing 1570 pg LPS, 2200 pg carbon and 6 pg FluoSpheres per particle were deposited onto the cells as per all steps of the procedure described in section 3.9.3, except that the SFM was replaced with SFM containing 5 μg/mL $Al(OH)_3$ gel (Sigma-Aldrich, A8222, Oakvillle, ON, Canada) [154]. The negative control and positive controls were as per the steps of the procedure described in section 3.9.3. Two more controls were used in this study. One control was as per the same steps of the procedure as negative control except that the SFM was replaced with SFM containing 5 μg/mL $Al(OH)_3$ gel. The other control was cell cultures dosed with different numbers of particles containing LPS plus carbon as described above and incubated in SFM without $Al(OH)_3$ gel.

4.2.1.2 A549 cells incubated with particles containing nickel nitrate ($Ni(NO_3)_2$)

A549 cells were grown to approximately 90% or more confluence in centre-well organ culture dishes. Different numbers of particles containing 1550 pg LPS, 2180 pg carbon, 1 pg $Ni(NO_3)_2$ and 6 pg FluoSpheres per particle were deposited onto the cells as per all steps of the procedure described in section 3.9.3. The negative control and positive controls were as per the steps of the procedure described in section 3.9.3. One more control was used in this study. The control was cell cultures grown to approximately 90% or more confluence in centre-well organ culture dishes and dosed with different numbers of particles containing 1570 pg LPS, 2200 pg carbon and 6 pg FluoSpheres per particle without $Ni(NO_3)_2$. Ni has been measured at 69.6 μg/g dust in EHC-93 [150], and the Ni was 69 μg/g in the particle mimics used.

4.2.1.3 A549 cells incubated with particles containing sodium chloride (NaCl)

A549 cells were grown to approximately 90% or more confluence in centre-well organ culture dishes. Different numbers of particles containing 1550 pg LPS, 2180 pg carbon, 210 pg NaCl and 6 pg FluoSpheres per particle were deposited onto the cells as per all steps of the procedure described in section 3.9.3. The negative control and positive controls were as per the steps of the procedure described in section 3.9.3. One more control was used in this study. The control was cell cultures grown to approximately 90% or more confluence in centre-well organ culture dishes and dosed with different numbers of particles containing 1570 pg LPS, 2200 pg carbon and 6 pg FluoSpheres per particle without NaCl. Na has been measured at 20.6 mg/g dust in EHC-93 [150], and the Na was 21 mg/g in the particle mimics used.

4.2.1.4 A549 cells incubated with particles containing zinc nitrate ($Zn(NO_3)_2$)

A549 cells were grown to approximately 90% or more confluence in centre-well organ culture dishes. Different numbers of particles containing 520 pg LPS, 740 pg carbon, 50 pg $Zn(NO_3)_2$ and 6 pg FluoSpheres per particle were deposited onto the cells as per all steps of the procedure described in section 3.9.3. The reason for using lower mass of each compound in these particle mimics was because higher concentration of $Zn(NO_3)_2$ in the starting solution caused the ink nanoparticles to aggregate and precipitate. The negative control and positive controls were as per the steps of the procedure described in section 3.9.3. One more control was used in this study. The control was cell cultures grown to approximately 90% or more confluence in centre-well organ culture dishes and dosed with different numbers of particles containing 520 pg LPS, 730 pg carbon and 6 pg FluoSpheres per particle without $Zn(NO_3)_2$. Zn has been measured at 10.4 mg/g dust in EHC-93 [150], and the Zn was 12 mg/g in the particle mimics used.

4.2.2 Immunocytochemistry assay, image taken from fluorescence microscopy and data analysis

Procedures used in this study all were as per the procedures described in section 3.9.6 and section 3.9.7.

4.2.3 CXCL-5 monitored by MALDI-TOF-MS

A549 cells were grown to approximately 90% or more confluence directly on a 6-well plate surface. Growth medium was aspirated with a water faucet driven vacuum aspirator. 200 μL SFM containing 20 μg/mL $Al(OH)_3$ gel was added to cell culture followed by a 24-hour incubation period. A population of particles containing 2590 pg

NaCl and 520 pg carbon per particle were deposited onto the cells followed by a 2-hour incubation period. Supernatant was collected and analyzed using MALDI-TOF-MS as per the procedures described in section 3.9.4 and 3.9.5. Two controls were used in this study. The negative control was as per all steps of the procedure described above except that no $Al(OH)_3$ gel added to the SFM and no deposition of the particles onto the cells. One more control was as per all steps of the procedure described above except that no $Al(OH)_3$ gel added to the SFM.

4.3 Results

4.3.1 $Al(OH)_3$ gel did not increase ICAM-1 expression notably

Following deposition of particles containing LPS plus carbon, cell cultures were incubated with SFM containing $Al(OH)_3$ gel, or not containing $Al(OH)_3$ gel (the test experiment and the control experiment), and relative ICAM-1 antibody fluorescence intensities were measured and plotted as a function of number of particles. It was observed that both of the plots had two distinct regions able to be fitted with least squares linear regression lines: a region of positive slope, and a region of data points able to be fitted to a line which had a slope approaching 0, similar to figure 3.39. The relative magnitudes of intercepts of the least squares linear fit to the region of data fitted yielded lines having slopes approaching 0 from both plots are plotted in figure 4.1. Cells incubated with SFM containing $Al(OH)_3$ gel without dosing particles was another control experiment. The average relative ICAM-1 antibody fluorescence intensity was calculated from the 9 pictures array (described in section 3.9.7) and shown in Figure 4.1.

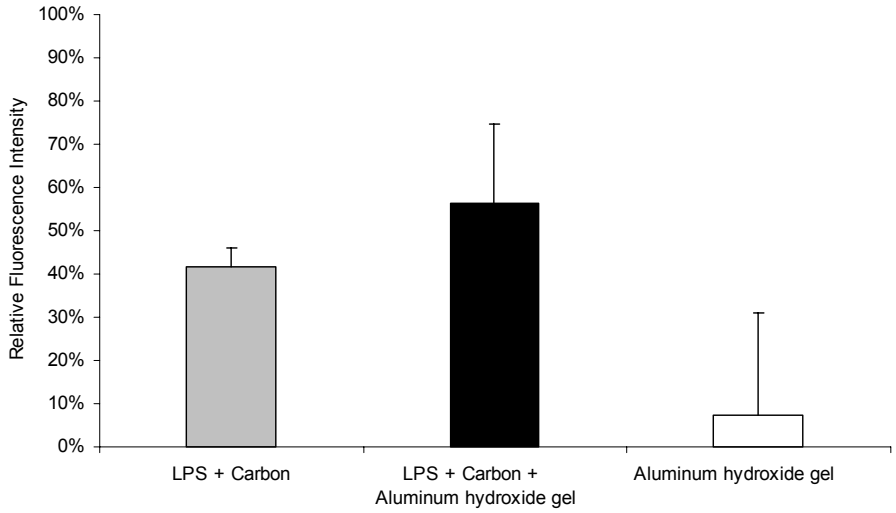

Figure 4.1 Effect of $Al(OH)_3$ gel on ICAM-1 expressions. A549 cells were grown to approximately 90% or more confluence in centre-well organ culture dishes. Different numbers of particles containing 1570 pg LPS, 2200 pg carbon and 6 pg FluoSpheres per particle were deposited onto the cells ( ) ( ). SFM containing 5 µg/mL $Al(OH)_3$ gel ( ) ( ) or not containing $Al(OH)_3$ gel ( ) were used to incubate the cells for 24 hours. The relative magnitudes of intercepts of the least squares linear fit to the region of data fitted yielding lines having slopes approaching 0 of ICAM-1 expressions were plotted ( ) ( ) and the error bars for the two data points were the standard deviation of the intercept. The average relative fluorescence intensity from 9 pictures array was plotted ( ) and the error bar for this data point was the standard deviation of the 9 pictures.

Figure 4.1 indicated that $Al(OH)_3$ gel itself suppressed ICAM-1 expression, however when it was incubated with LPS plus carbon particles, the ICAM-1 expression increased marginally over that expressed when incubated with LPS plus carbon particles.

4.3.2 $Zn(NO_3)_2$ did not increase ICAM-1 expression

Following deposition of particles containing LPS and carbon with $Zn(NO_3)_2$, or particles containing LPS and carbon without $Zn(NO_3)_2$, cell cultures were incubated with SFM, and relative ICAM-1 antibody fluorescence intensities were measured and plotted as a function of number of particles. It was observed that both of the plots had two distinct regions able to be fitted with least squares linear regression lines: a region of positive slope, and a region of data points able to be fitted to a line which had a slope approaching 0, similar to figure 3.39. The relative magnitudes of intercepts of the least

squares linear fit to the region of data fitted yielding lines having slopes approaching 0 from both plots are plotted in figure 4.2.

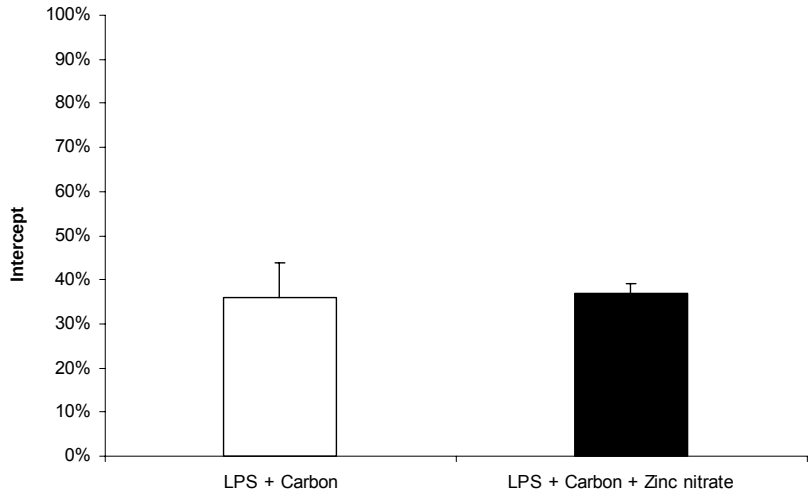

Figure 4.2 Effect of $Zn(NO_3)_2$ on ICAM-1 expressions. A549 cells were grown to approximately 90% or more confluence in centre-well organ culture dishes. Different numbers of particles containing 520 pg LPS, 730 pg carbon and 6 pg FluoSpheres per particle or different numbers of particles containing 520 pg LPS, 740 pg carbon, 50 pg $Zn(NO_3)_2$ and 6 pg FluoSpheres per particle were deposited onto the cells and incubated with cells for 24 hours. The relative magnitudes of intercepts of the least squares linear fit to the region of data fitted yielding lines having slopes approaching 0 of ICAM-1 expressions were plotted and the error bars for the data points were the standard deviation of the intercept.

Figure 4.2 indicated that ICAM-1 expression did not increase when $Zn(NO_3)_2$ was added to the LPS plus carbon particles.

4.3.3 $Ni(NO_3)_2$ and NaCl increased ICAM-1 expression

Following deposition of particles containing LPS and carbon with $Ni(NO_3)_2$, or particles containing LPS and carbon with NaCl, cell cultures were incubated with SFM, and relative ICAM-1 antibody fluorescence intensities were measured and plotted as a function of number of particles. It was observed that both of the plots had two distinct regions able to be fitted with least squares linear regression lines: a region of positive slope, and a region of data points able to be fitted to a line which had a slope approaching

0, similar as figure 3.39. The relative magnitudes of intercepts of the least squares linear fit to the region of data fitted yielding lines having slopes approaching 0 from both plots, together with the first two histograms in figure 4.1 are plotted in figure 4.3 for direct visual comparison.

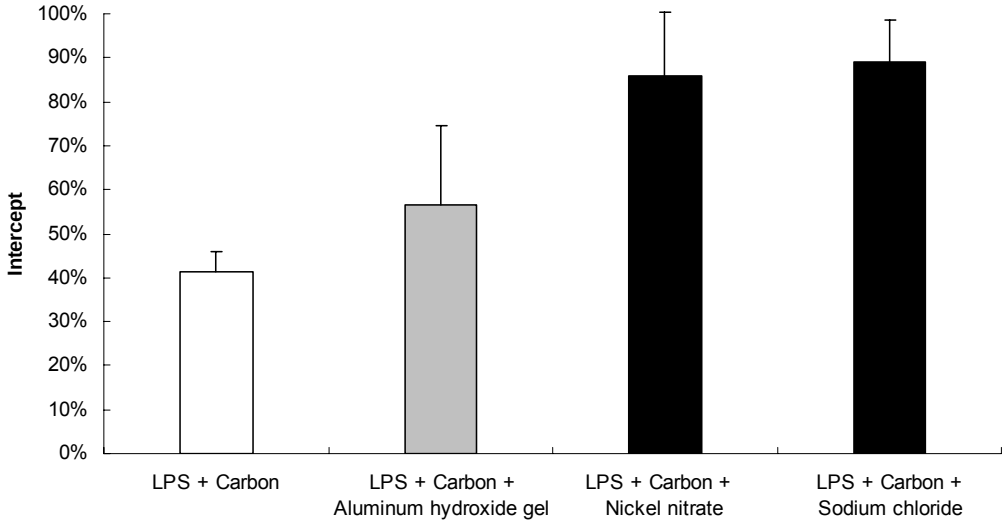

Figure 4.3 Effect of $Ni(NO_3)_2$ and NaCl on ICAM-1 expressions. A549 cells were grown to approximately 90% or more confluence in centre-well organ culture dishes. Different numbers of particles containing 1570 pg LPS, 2200 pg carbon and 6 pg FluoSpheres per particle (□) (▒) or different numbers of particles containing 1550 pg LPS, 2180 pg carbon, 1 pg $Ni(NO_3)_2$ and 6 pg FluoSpheres per particle or different numbers of particles containing 1550 pg LPS, 2180 pg carbon, 210 pg NaCl and 6 pg FluoSpheres per particle were deposited onto the cells. SFM containing 5 µg/mL $Al(OH)_3$ gel (▒) or not containing $Al(OH)_3$ gel (□) (■) were used to incubated the cells for 24 hours. The relative magnitudes of intercepts of the least squares linear fit to the region of data fitted yielding lines having slopes approaching 0 of ICAM-1 expressions were plotted and the error bars for the data points were the standard deviation of the intercept.

Figure 4.3 indicated that ICAM-1 expression increased when $Ni(NO_3)_2$ or NaCl was added to the LPS plus carbon particles relative to $Al(OH)_3$ gel incubated with LPS plus carbon particles.

4.3.4 $Al(OH)_3$ gel primed the cells

MALDI-TOF-MS was used to study if aluminium hydroxide gel could prime cells by increasing CXCL-5 expressions. Cell supernatants were collected and characterized by MALDI-TOF-MS (Figure 4.4). The ion signal intensity labelled with dashed line represented CXCL-5.

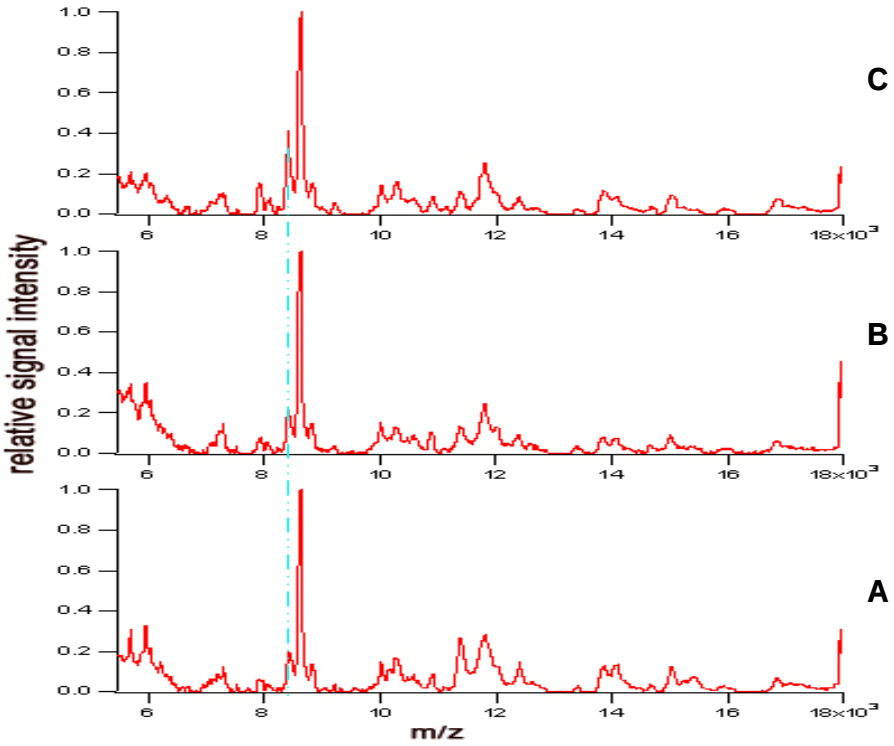

Figure 4.4 MALDI-TOF mass spectra of the supernatants of A549 cell cultures. Cells were grown to approximately 90% or more confluence directly on a 6-well plate surface. 200 µL SFM containing 20 µg/mL $Al(OH)_3$ gel (C) or 200 µL SFM not containing $Al(OH)_3$ gel (A) (B) was used to incubate with cells for a 24-hour incubation period. ~50 particles containing 2590 pg NaCl and 520 pg carbon per particle were deposited onto the cells (B) (C) followed by a 2-hour incubation period. The supernatants were each processed using a C_{18} ZipTip prior to co-crystallization with SA matrix on a MALDI target plate.

Figure 4.4 indicates that both negative control and the cells dosed with NaCl plus carbon particles without incubating with $Al(OH)_3$ gel prior to deposition of particles did not produce measurably different CXCL-5 secretions whereas the cells incubated with

$Al(OH)_3$ gel for 24 hours and then dosed with particles produced more CXCL-5 than the negative control.

4.4 Discussion

In this chapter, I made an attempt to study the adjuvant potential in a different aspect: ICAM-1 expression and CXCL-5 expression were monitored as opposed to the more commonly monitored Th2 cell and Th2 cytokine responses and expression levels respectively.

$Al(OH)_3$ gel itself suppressed ICAM-1 expression, however when it was incubated with LPS plus carbon particles, the ICAM-1 expression increased marginally over that expressed when incubated with LPS plus carbon particles. As documented in the literature, $Al(OH)_3$ was a Th2 adjuvant while LPS was a Th1 adjuvant [120, 122]. Since two adjuvants worked together, a great increasing of ICAM-1 expression was expected. The result indicated increasing ICAM-1 expression, however, the increase was marginal. I speculate that the marginally increased ICAM-1 expression may have been due to the two adjuvants working together and neutralizing their own adjuvant activity. It may also explain previous results that concluded $Al(OH)_3$ could decrease the toxicity of LPS [126, 135-137].

$Al(OH)_3$ gel primed cells produced more CXCL-5 than $Al(OH)_3$ gel non-primed cells when they were subsequently dosed with particles containing NaCl and carbon. CXCL-5 is a known chemokine whose function is reported to recruit and activate neutrophils [109] and its activity can be inhibited by IFN-γ [26], which is a Th1 cytokine [141]. Since Th1 and Th2 responses inhibit each other [122], CXCL-5 was reported to be inhibited by Th1 cytokines [26], $Al(OH)_3$ was reported as a Th2 adjuvant [120, 122], and

the result from my experiment suggested that $Al(OH)_3$ was able to induce CXCL-5, there was a possibility that CXCL-5 was also a T cell chemoattractant besides a neutrophil chemoattractant [109].

Zn, Ni and Na were added to the LPS plus carbon particles, at respective levels as have been measured in EHC-93. Zn did not increase the ICAM-1 expression at this level, however Ni and Na increased the ICAM-1 expression when added to LPS plus carbon particles. This agreed with previous studies, which showed adjuvant activity of EHC-93 as a mixture [151, 152].

NaCl has been reported to have low potential to cause lung irritation in animals by itself [146, 153]. However, in this study, it indicated together with other compounds, even the mass percentage of Na in the ambient air, it could cause an increase of ICAM-1 expression.

The number of mole of Ni per particle was much lower than the Na, and it also caused an increasing of ICAM-1 expression when added to LPS plus carbon particles. Literatures suggested that the ICAM-1 expression in A549 cells only depends on NF-κB pathway [37]. However, there are many different ways to activate NF-κB pathway [27, 29-32]. Therefore, I speculate that the Ni and Na were through different mechanisms to activate the NF-κB pathway in an effort to enhance the ICAM-1 expression. There is a possibility that Ni is a transition metal and it triggers the oxidative stress while Na does not, which might explain why Ni is more potent than Na.

4.5 Future direction

CXCL-5 and IL-8 were both members of the C-X-C family and their structures are similar. IL-8 was reported as both a neutrophil and T cell chemoattractant in earlier

studies [33, 155, 156] however no investigator reported CXCL-5 as a T cell chemoattractant. Since the result from my experiment suggested that there was a possibility that CXCL-5 was also a T cell chemoattractant, it would be informative to investigate further using T cells. If CXCL-5 is both neutrophil and T cell chemoattractant, it could be a potential biomarker for research into alternative compounds as adjuvants in vaccines.

Since Ni and Na increased the ICAM-1 expression when added to LPS plus carbon particles, it would be informative to investigate further the adjuvant activities of Ni and Na based on measuring IL-4 and IFN-γ, two important cytokines in adjuvant studies [129, 154], changing the cell lines to dendritic cells because of their ability to initiate immune response and regulate T cell-mediated immune response [157], Co-culture with naïve T cells, and experiments *in vivo*.

It would be also informative to investigate the pathways that different metals triggered to study the mechanisms of how the metals affect the ICAM-1 expressions.

Chapter 5 Incubation of Sulfates Containing Carbon Particles with Human Lung Cells (A549) and Measurement of ICAM-1 and CXCL-5 Expressions

5.1 Introduction

Sulfates comprise a significant portion of PM [158, 159]. Sulfates are mainly formed by the oxidation of sulfur dioxide (SO_2), which is emitted from either natural sources, such as oceans, wetlands, volcanoes [160] and in the combustion of carbonaceous fossil fuels (coal, heavy petroleum distillates) [158-160]. Ammonium sulfate ($(NH_4)_2SO_4$) and sulfuric acid (H_2SO_4) have been identified as the major persistent sulfate species in ambient air [158, 159]. $(NH_4)_2SO_4$ is the product of H_2SO_4 neutralization by ammonia (NH_3) gas [158]. Sodium sulfate (Na_2SO_4) can be readily found in suspended particles near coastal areas and after de-icing compounds are applied to the road in winter [17, 18]. Na_2SO_4 is the product when H_2SO_4 reacts with NaCl in sea salt and de-icing compounds [17, 18].

Carbon is also a major component of PM [17, 18, 159]. It is an abundant species in the emissions of high temperature combustion sources [17, 92, 161]. Studies have shown that large amounts of sulfate accompanied by similar amounts of carbonaceous material with other low concentration compounds constitute a majority of PM by mass [159].

Early *in vivo* studies have provided an order of pulmonary irritant potency of sulfates, which is sulfuric acid > ammonium sulfate ~ sodium sulfate, as determined using the method of respiratory mechanics (pulmonary flow resistance and compliance) as the readout [146, 158]. However no such comparison studies were performed *in vitro*, and no studies have characterized the order of pulmonary irritant potency after sulfates are combined with other components. Sodium is commonly used in toxicological studies

as negative controls [160] because of its perceived comparatively low toxicity [146, 153], but it cause greater lung cell responses when it is mixed with other compounds [50, 153].

In this chapter, sulfuric acid (H_2SO_4), ammonium sulfate ($(NH_4)_2SO_4$) and sodium sulfate (Na_2SO_4) alone, or together with carbon, were used to create mimics of ambient particles. Expression levels of CXCL-5 and ICAM-1 were compared using the methodology developed in chapter 3. In an effort to compare the irritant potency of the three compounds, in one study the masses of carbon, glycerol and FluoSpheres were fixed as base components of the particles, with one of the three sulfates added as an additional compound for each type of particle. The sulfate concentration in the starting solutions was constant, and by analogy, in each particle, the number of moles of sulfates was also constant.

5.2 Experimental

5.2.1 A549 cells incubated with different particles

A549 cells were grown to approximately 90% or more confluence in centre-well organ culture dishes. Different numbers of particles contained either 10 pg (~0.1 pmol) H_2SO_4, or 20 pg (~0.1 pmol) $(NH_4)_2SO_4$, or 20 pg (~0.1 pmol) Na_2SO_4, plus 60 pg carbon, 160 pg glycerol and 6 pg FluoSpheres per particle. These resultant particles were deposited onto the cells as per all steps of the procedure described in section 3.9.3, except that no additional 190 μL SFM was added to the cell cultures during the 24 hours incubation period in an effort to enable the particles to make contact with the cells. SO_4^{2-} has been measured at 44.5 mg/g dust in EHC-93 [150], and the SO_4^{2-} was 42 mg/g in the particle mimics used. In addition, the reason for using such low concentration of each

component in the particle was because higher concentrations of H_2SO_4 in the starting solution caused the ink nanoparticles to aggregate and precipitate. In an effort to have the same number of moles of sulfates per particle, the concentration of $(NH_4)_2SO_4$ and Na_2SO_4 were lowered to the same as H_2SO_4, although higher concentrations of the $(NH_4)_2SO_4$ and Na_2SO_4 did not cause precipitation of ink in starting solution. In an effort to have the SO_4^{2-} abundance per particle at the level as it has been measured in EHC-93, the total mass of the starting solution needed to be increased instead of decreasing the sulfate concentration since the sulfate concentration was extremely low. However higher concentrations of ink in the starting solution with H_2SO_4 also caused precipitation. Glycerol had been used in cell studies in a previous study and showed no harm to cell cultures [162] and therefore it was used to complete the total mass of the particle mimics.

The negative control was as per the steps of the procedure described above except for the deposition of particles. The positive control was cell cultures grown to approximately 90% or more confluence in a centre-well organ culture dish and bathed in 60 μL of SFM with 400 ng/mL TNF-α (total moles TNF-α added = 1.4 pmol) and incubated for 24 hours incubation period. One more control was used in this study. The control was cell cultures grown to approximately 90% or more confluence in a centre-well organ culture dish and bathed in 60 μL of SFM with 3.0 ng/μL carbon, 8.4 ng/μL glycerol and 0.3 ng/μL FluoSpheres, whose dosage was approximately equivalent to 3000 of the above particles without the sulfates, and then incubated for 24 hours.

Another experiment was also performed in this study. A549 cells were grown to approximately 90% or more confluence in centre-well organ culture dishes. Different numbers of particles containing higher dosages of sulfates but no carbon and no glycerol

per particle (3160 pg (~32 pmol) H_2SO_4 and 6 pg FluoSpheres per particle, or 4260 pg (~32 pmol) $(NH_4)_2SO_4$ and 6 pg FluoSpheres per particle, or 4580 pg (~32 pmol) Na_2SO_4 and 6 pg FluoSpheres per particle) were deposited onto the cells as per all steps of the procedure described above.

5.2.2 Supernatant collection and CXCL-5 monitored by MALDI-TOF-MS

The procedures used in this study were all as per the procedures described in section 3.9.4 and section 3.9.5.

5.2.3 Immunocytochemistry assay, image taken from fluorescence microscopy and data analysis

The procedures used in this study were all as per the procedures described in section 3.9.6 and section 3.9.7.

5.3 Results

5.3.1 Images of the particles

Representative images of the cell cultures that immediately after their deposition of the particles, or images of particles deposition onto glass slides are shown in figure 5.1. The observations of $(NH_4)_2SO_4$ and Na_2SO_4 particles were similar when deposited onto the glass slides, however Na_2SO_4 particles were not found under fluorescence microscope, which might because of their faster dissolving in the SFM. Therefore, only images of $(NH_4)_2SO_4$ are shown in figure 5.1. The particles with carbon could be observed using an optical microscope when they were deposited onto the cells, however the particles without carbon could only be observed by fluorescence microscope with the aid of

FluoSpheres to indicate particle location in the SFM. The particles with carbon were ~6 μm in diameter and particles without carbon were ~16 μm in diameter because there were more than 300 times more sulfates in particles without carbon than in particles with carbon.

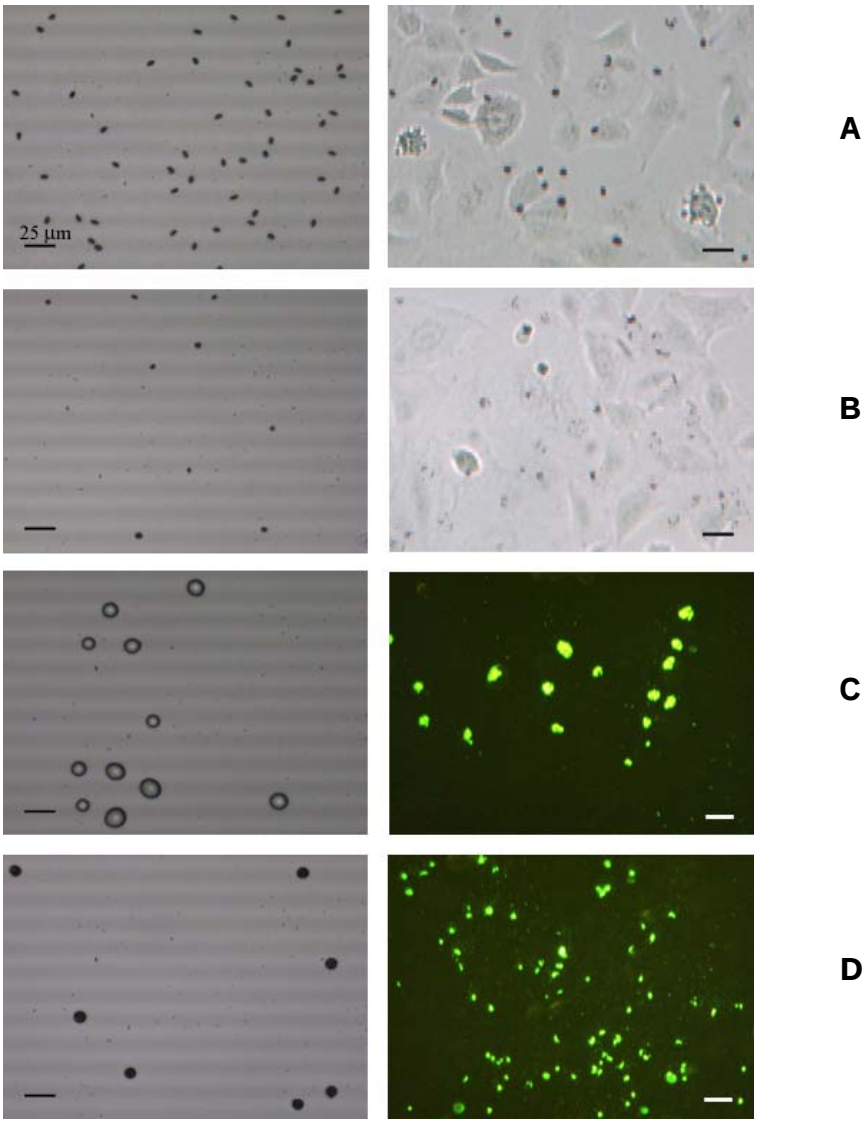

Figure 5.1 Photomicrographs of particles containing 10 pg H_2SO_4, 60 pg carbon, 160 pg glycerol and 6 pg FluoSpheres per particle (A), or 20 pg $(NH_4)_2SO_4$, 60 pg carbon, 160 pg glycerol and 6 pg FluoSpheres per particle (B), or 3160 pg H_2SO_4 and 6 pg FluoSpheres per particle (C), or 4260 pg $(NH_4)_2SO_4$ and 6 pg FluoSpheres per particle (D), on glass slide (left), or on cells (right). For the particles without carbon, fluorescence images of FluoSpheres (green colour) were taken after depositions of particles onto the cells.

5.3.2 ICAM-1 expressions induced by different sulfates particles

Following deposition of particles containing carbon, glycerol, FluoSpheres and different sulfates, cell cultures were incubated with SFM, and relative ICAM-1 antibody fluorescence intensities were measured and plotted as a function of the number of particles for each type of particles respectively. It was observed that each data set was able to be fitted with a least squares linear regression line. To illustrate the data generated by these experiments, the relative fluorescence intensity of ICAM-1 expressions induced by particles containing 10 pg H_2SO_4, or 20 pg $(NH_4)_2SO_4$, or 20 pg Na_2SO_4, plus 60 pg carbon, 160 pg glycerol and 6 pg FluoSpheres per particle were plotted as a function of number of particles deposited onto the cells respectively (Figure 5.2).

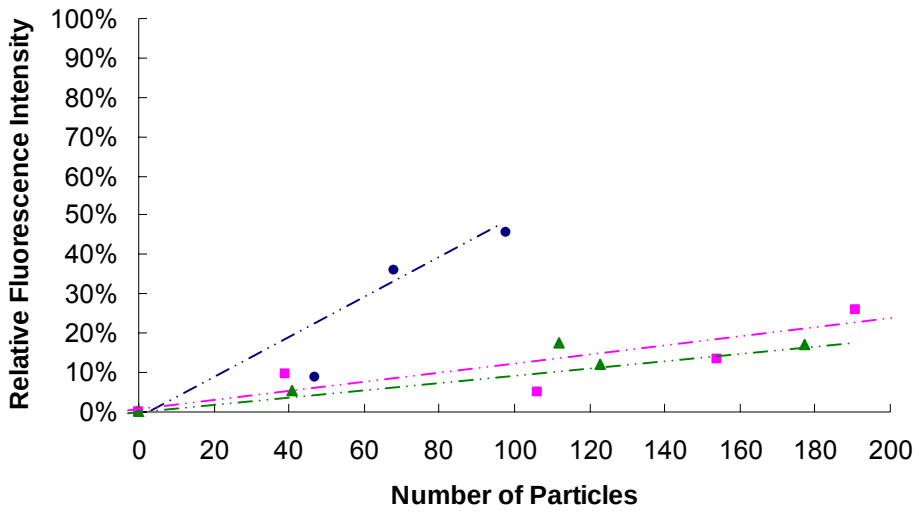

Figure 5.2 Plot of the relative ICAM-1 antibody fluorescence intensity as a function of number of particles. Different numbers of particles contained either 10 pg H_2SO_4 (●), or 20 pg $(NH_4)_2SO_4$ (■), or 20 pg Na_2SO_4 (▲), plus 60 pg carbon, 160 pg glycerol and 6 pg FluoSpheres per particle. These resultant particles were deposited onto the cells. The relative fluorescence intensities of ICAM-1 expressions were plotted as a function of number of particles deposited onto the cells respectively. The equations of the least squares linear fits were $y = 0.0049x - 0.037$ for H_2SO_4, $y = 0.0011x + 0.0037$ for $(NH_4)_2SO_4$, and $y = 0.0010x + 0.013$ for Na_2SO_4.

Following deposition of particles containing FluoSpheres and different sulfates, cell cultures were incubated with SFM, and relative ICAM-1 antibody fluorescence intensities were measured and plotted as a function of the number of particles for each type of particles respectively. It was also observed that each data set was able to be fitted with a least squares linear regression line (Figure 5.3).

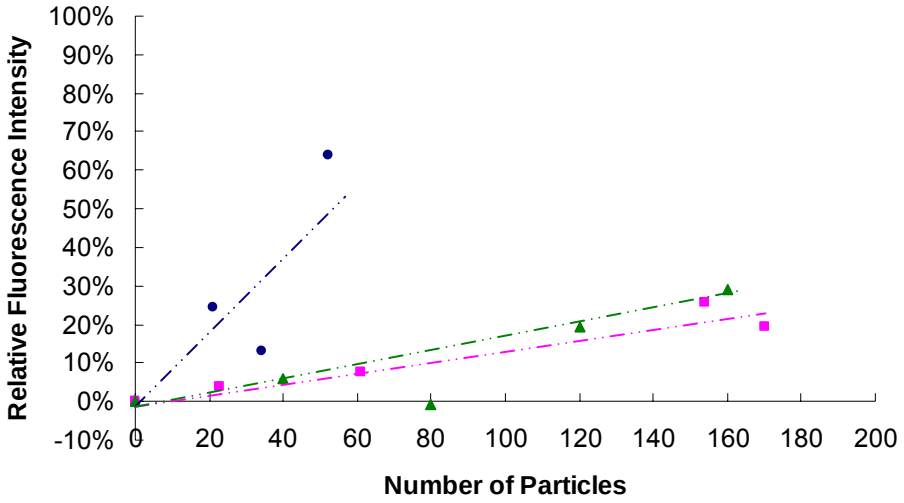

Figure 5.3 Plot of the relative ICAM-1 antibody fluorescence intensity as a function of number of particles. Different numbers of particles contained either 3160 pg H_2SO_4 (●), or 4260 pg $(NH_4)_2SO_4$ (■), or 4580 pg Na_2SO_4 (▲), plus 6 pg FluoSpheres per particle. These resultant particles were deposited onto the cells. The relative fluorescence intensities of ICAM-1 expressions were plotted as a function of number of particles deposited onto the cells respectively. The equations of the least squares linear fits were y = 0.0109x - 0.0382 for H_2SO_4, y = 0.0013x + 0.0027 for $(NH_4)_2SO_4$, and y = 0.0018x + 0.0359 for Na_2SO_4.

5.3.3 Comparison of ICAM-1 differential expressions

Since the relative fluorescence intensity of ICAM-1 expressions versus the numbers of particles could be fitted using a linear relationship for each different composition of particle, the magnitudes of slopes of the least squares linear fits from all types of particles were used to divide by the number of moles of sulfates per particle and then plotted in figure 5.4 for comparison. The relative fluorescence intensity of ICAM-1 expression in

the control experiment, in which was cells bathed with 3.0 ng/μL carbon, 8.4 ng/μL glycerol and 0.3 ng/μL FluoSpheres, was 3% lower than the negative control. It indicated carbon, glycerol and FluoSpheres themselves did not effect measurably differential ICAM-1 expression. Since the dosage of the control experiment was approximately equivalent to 3000 particles without the sulfates, a data point at approximately 3000 particles was assigned to enable the calculation of a representative slope of the least squares linear fit for the control experiment. Another data point from chapter 3, which was cells dosed with different numbers of particles containing 1480 pg carbon plus 6 pg FluoSpheres per particle, was used for comparison.

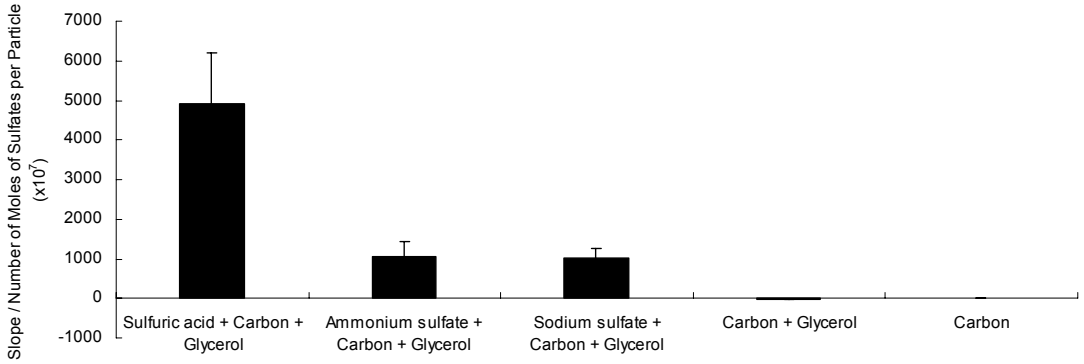

Figure 5.4 Effect of H_2SO_4, $(NH_4)_2SO_4$, and Na_2SO_4 on ICAM-1 expressions. A549 cells were grown to approximately 90% or more confluence in centre-well organ culture dishes. Different numbers of particles contained either 10 pg H_2SO_4, or 20 pg $(NH_4)_2SO_4$, or 20 pg Na_2SO_4, plus 60 pg carbon, 160 pg glycerol and 6 pg FluoSpheres per particle. These resultant particles were deposited onto the cells and incubated with cells for 24 hours. The control experiment was cells bathed in 60 μL of SFM with 3.0 ng/μL carbon, 8.4 ng/μL glycerol and 0.3 ng/μL FluoSpheres and incubated for 24 hours. Another data point was cells dosed with different numbers of particles containing 1480 pg carbon plus 6 pg FluoSpheres per particle. The magnitudes of slopes of the least squares linear fits of ICAM-1 expressions were used to divide by the number of moles of sulfates per particle and then plotted. Error bars represent the error of slopes. The Y-axis value for carbon particle was 0.13 and therefore can not be observed from the diagram.

The magnitudes of slopes of the least squares linear fits from another experiment, which was cells dosed with particles containing 3160 pg H_2SO_4 and 6 pg FluoSpheres per particle, or 4260 pg $(NH_4)_2SO_4$ and 6 pg FluoSpheres per particle, or 4580 pg Na_2SO_4

and 6 pg FluoSpheres per particle, were used to divide by the number of moles of sulfates per particle and then plotted in figure 5.5.

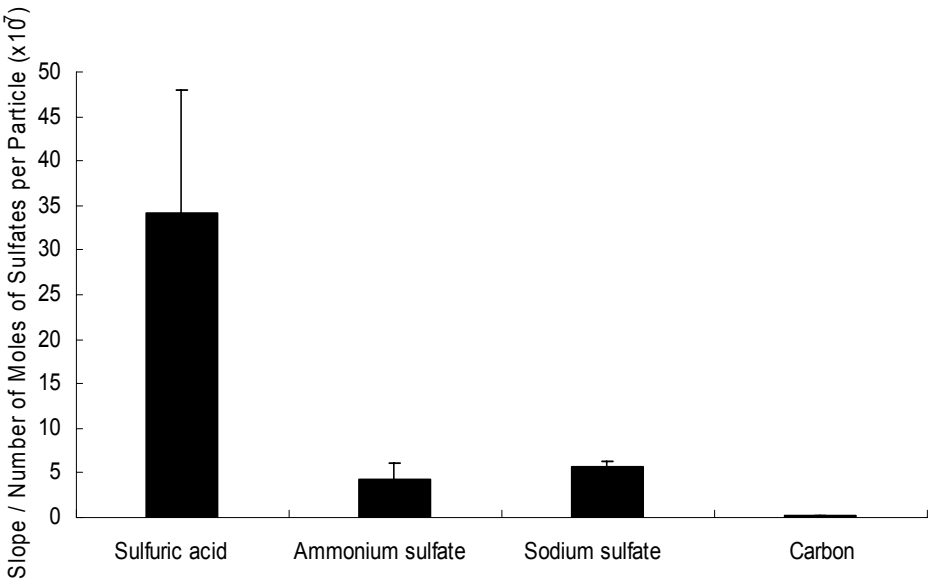

Figure 5.5 Effect of H_2SO_4, $(NH_4)_2SO_4$, and Na_2SO_4 on ICAM-1 expressions. A549 cells were grown to approximately 90% or more confluence in centre-well organ culture dishes. Different numbers of particles containing 3160 pg H_2SO_4 and 6 pg FluoSpheres per particle, or 4260 pg $(NH_4)_2SO_4$ and 6 pg FluoSpheres per particle, or 4580 pg Na_2SO_4 and 6 pg FluoSpheres per particle were deposited onto the cells and incubated with cells for 24 hours. Another data point was cells dosed with different numbers of particles containing 1480 pg carbon plus 6 pg FluoSpheres per particle. The magnitudes of slopes of the least squares linear fits of ICAM-1 expressions were used to divide by the number of moles of sulfates per particle and then plotted. Error bars represent the error of slopes.

Figure 5.4 indicated that H_2SO_4 + carbon particles induced ICAM-1 expression 4.6 times higher than $(NH_4)_2SO_4$ + carbon particles and 4.9 times higher than Na_2SO_4 + carbon particles. Figure 5.5 indicated that H_2SO_4 particles induced ICAM-1 expression was 8.1 times higher than $(NH_4)_2SO_4$ particles and 6.1 times higher than Na_2SO_4 particles. Both of the figures indicated the order of ICAM-1 expression induced by sulfates was $H_2SO_4 > (NH_4)_2SO_4 \sim Na_2SO_4$. This result agreed with the early *in vivo* studies [146, 158].

The two figures also indicated that carbon, which was an insoluble component in particles, did not change the order of irritant potency of the sulfates, which were soluble components in particles.

Furthermore, the relative slopes (absolute slope divided by the number of moles of sulfates per particle) are shown in figure 5.4 and figure 5.5. When the number of moles of sulfates per particle was increased by a factor of approximately 300, the relative slope of the ICAM-1 expression was decreased by a factor of approximately 150. The difference between the two particle types was that the former one contained carbon and the later one did not. Therefore, there was a possibility that the carbon, which did not effect measurably different ICAM-1 expression by itself, helped increase the ICAM-1 expression when it was present in sulfates + carbon particles.

5.3.4 Comparison of CXCL-5 differential expressions

Following collection of the supernatants, MALDI-TOF-MS was used to monitor CXCL-5. The relative CXCL-5 signal intensities were plotted as a function of the number of particles for each type of particle respectively. It was also observed that each plot was able to be fitted with a least squares linear regression line individually. The magnitudes of slopes of the least squares linear fits from all types of particles were used to divide by the number of moles of sulfates per particle and then plotted in figure 5.6 for comparison. Since the dosage of the control experiment was approximately equivalent to 3000 particles without the sulfates, a data point at approximately 3000 particles was assigned to permit an estimate for a slope of a least squares linear fit for the control experiment.

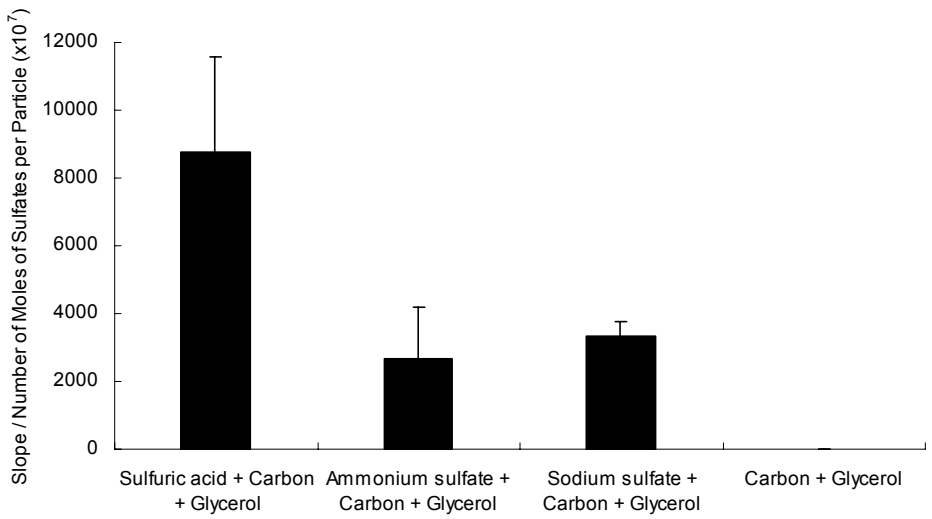

Figure 5.6 Effect of H_2SO_4, $(NH_4)_2SO_4$, and Na_2SO_4 on CXCL-5 expressions. A549 cells were grown to approximately 90% or more confluence in centre-well organ culture dishes. Different numbers of particles contained either 10 pg H_2SO_4, or 20 pg $(NH_4)_2SO_4$, or 20 pg Na_2SO_4, plus 60 pg carbon, 160 pg glycerol and 6 pg FluoSpheres per particle. These resultant particles were deposited onto the cells and incubated with cells for 24 hours. The control experiment was cells bathed in 60 µL of SFM with 3.0 ng/µL carbon, 8.4 ng/µL glycerol and 0.3 ng/µL FluoSpheres and incubated for 24 hours. The magnitudes of slopes of the least squares linear fits of CXCL-5 expressions were used to divide by the number of moles of sulfates per particle and then plotted. Error bars represent the error of slopes. The Y-axis value for carbon + glycerol was 17.

The CXCL-5 data presented in figure 5.6 followed the same trend as the ICAM-1 data plotted in figure 5.4. It indicated that H_2SO_4 with carbon particles induced CXCL-5 expression 3.3 times higher than $(NH_4)_2SO_4$ with carbon particles and 2.6 times higher than Na_2SO_4 with carbon particles. The order of CXCL-5 expression induced by sulfates was $H_2SO_4 > (NH_4)_2SO_4 \sim Na_2SO_4$. This result also agreed with the early *in vivo* studies [146, 158].

5.4 Discussion

In this chapter, I made an attempt to study the ICAM-1 and CXCL-5 expressions from A549 cells induced by different sulfates alone, or in a carbon aggregate host.

The result in my ICAM-1 study indicated that H_2SO_4 particles induced ICAM-1 expression 8.1 times higher than $(NH_4)_2SO_4$ particles and 6.1 times higher than Na_2SO_4 particles. It agreed with previous *in vivo* studies, which had given an order of pulmonary irritant potency of pure sulfates: $H_2SO_4 > (NH_4)_2SO_4 \sim Na_2SO_4$ [146, 158]. However, both of the previous *in vivo* studies reported H_2SO_4 had 10 times more pulmonary irritant potency than $(NH_4)_2SO_4$, which were higher than the ICAM-1 result in my study. However, it was within my experimental error. Furthermore, between the two previous studies, one reported $(NH_4)_2SO_4$ had similar pulmonary irritant potency with Na_2SO_4 [158], which was similar to the result of my study, whereas another study reported $(NH_4)_2SO_4$ had 10 times more pulmonary irritant potency than Na_2SO_4 [146].

The results from ICAM-1 and CXCL-5 expressions agreed with each other and indicated carbon, which was an insoluble component in particles, did not change the order of irritant potency of the sulfates which were soluble components in particles. However, the data plotted in figure 5.4 and figure 5.5 demonstrated that there is a possibility that the carbon, which did not effect measurably different ICAM-1 expression by itself, helped increase the ICAM-1 expression in sulfates particles.

This study used the *in vitro* methodology developed in our group to validate an existing pulmonary irritant potency result from previous *in vivo* studies, although the experimental endpoints used were totally different. Furthermore, this study characterized the order of pulmonary irritant potency of sulfates in a carbon aggregate host from the perspective of the ability of inducing ICAM-1 and CXCL-5 expressions.

5.5 Future direction

This study was based on particle sizes of 6 ~ 16 μm diameter. It would be informative to investigate the sulfates using fine particle sizes since sulfates were abundant in $PM_{2.5}$ fraction [17].

Chapter 6 Conclusion

Inhalation of particulate matter is associated with adverse effects on human health. This thesis is based on a hypothesis that different chemicals in a particle cause measurably different ICAM-1 and CXCL-5 responses.

Allen Haddrell, a previous graduate student, developed a methodology to assess the ICAM-1 expression of ambient particles, *in vitro*. However problems with this methodology were identified, and the majority of this thesis was to find solutions to these problems. After a systematic study, most of the challenges were conquered. Table 6.1 represents the differences between the Haddrell methodology and the improved methodology. However, the problem of data processing of ICAM-1 expression remained unsolved. Five different methodologies were used to process the images of ICAM-1 antibody fluorescence intensities. Only through one processing methodology, the trends of the data can be observed. The data from the other four processing methodologies were too scattered to make strong conclusions.

Haddrell Methodology	Improved Methodology
Cells cultured on a coverslip	Cells cultured in center-well organ dish
Remove growth medium	Remove growth medium Add serum free medium (SFM) Add water in the moat
Dose cells with particles and incubate	Dose cells with particles, centrifuge and incubate
Collect supernatant and ziptip	Collect supernatant, add internal standard, and ziptip
Characterize with MALDI-MS	Characterize with MALDI-MS
Fixing cells with 1% acetone solution	Fixing cells with 4% (w/v) paraformaldehyde (PFA)
ICAM-1 antibodies staining	ICAM-1 antibodies staining

Table 6.1 Comparison of the Haddrell methodology and the improved methodology. Red colour represents the changes in the methodology.

Zn, Ni and Na were added to the LPS plus carbon particles, at respective levels as have been measured in EHC-93. Zn did not increase the ICAM-1 expression at this level, however Ni and Na increased the ICAM-1 expression when added to LPS plus carbon particles.

I also made an attempt to study the ICAM-1 and CXCL-5 expressions from A549 cells induced by different sulfates alone, or in a carbon aggregate host. The result in my ICAM-1 study indicated that H_2SO_4 particles induced ICAM-1 expression 8.1 times

higher than $(NH_4)_2SO_4$ particles and 6.1 times higher than Na_2SO_4 particles. It agreed with previous *in vivo* studies, which had given an order of pulmonary irritant potency of pure sulfates: $H_2SO_4 > (NH_4)_2SO_4 \sim Na_2SO_4$ [146, 158]. The results also indicated carbon did not change the order of irritant potency of the sulfates. However, there is a possibility that the carbon, which did not effect measurably different ICAM-1 expression by itself, helped increase the ICAM-1 expression in sulfates particles. This study used the *in vitro* methodology developed in our group to validate an existing pulmonary irritant potency result from previous *in vivo* studies, although the experimental endpoints used were totally different. Furthermore, this study characterized the order of pulmonary irritant potency of sulfates in a carbon aggregate host from the perspective of the ability of inducing ICAM-1 and CXCL-5 expressions.

The contribution of this thesis is to improve the existing *in vitro* methodology to assess the ICAM-1 and CXCL-5 expressions of ambient particles and understand more about how A549 cells respond to the different particle compositions.

REFERENCES

1. Linn, W.S., Gong, H., Clark, K.W., and Anderson, K.R. (1999). Day-to-day particulate exposures and health changes in Los Angeles area residents with severe lung disease. Journal of the Air & Waste Management Association *49*, 108-115.
2. Choi, J.H., Xu, Q.S., Park, S.Y., Kim, J.H., Hwang, S.S., Lee, K.H., Lee, H.J., and Hong, Y.C. (2007). Seasonal variation of effect of air pollution on blood pressure. Journal of Epidemiology and Community Health *61*, 314-318.
3. Ibald-Mulli, A., Stieber, J., Wichmann, H.E., Koenig, W., and Peters, A. (2001). Effects of air pollution on blood pressure: A population-based approach. American Journal of Public Health *91*, 571-577.
4. Dvonch, J.T., Kannan, S., Schulz, A.J., Keeler, G.J., Mentz, G., House, J., Benjamin, A., Max, P., Bard, R.L., and Brook, R.D. (2009). Acute Effects of Ambient Particulate Matter on Blood Pressure Differential Effects Across Urban Communities. Hypertension *53*, 853-859.
5. Dockery, D.W., and Pope, C.A. (1994). Acute Respiratory Effects of Particulate Air-Pollution. Annual Review of Public Health *15*, 107-132.
6. Gauderman, W.J., Gilliland, G.F., Vora, H., Avol, E., Stram, D., McConnell, R., Thomas, D., Lurmann, F., Margolis, H.G., Rappaport, E.B., Berhane, K., and Peters, J.M. (2002). Association between air pollution and lung function growth in Southern California children - Results from a second cohort. American Journal of Respiratory and Critical Care Medicine *166*, 76-84.
7. Dockery, D.W., Pope, C.A., Xu, X.P., Spengler, J.D., Ware, J.H., Fay, M.E., Ferris, B.G., and Speizer, F.E. (1993). An Association between Air-Pollution and Mortality in 6 United-States Cities. New England Journal of Medicine *329*, 1753-1759.
8. Sarnat, J.A., Schwartz, J., and Suh, H.H. (2001). Fine particulate air pollution and mortality in 20 US cities. New England Journal of Medicine *344*, 1253-1254.
9. Reichhardt, T. (1995). Weighing the Health Risks of Airborne-Particulates. Environmental Science & Technology *29*, A360-A364.
10. Gordian, M.E., Ozkaynak, H., Xue, J.P., Morris, S.S., and Spengler, J.D. (1996). Particulate air pollution and respiratory disease in Anchorage, Alaska. Environmental Health Perspectives *104*, 290-297.
11. Spurny, K.R. (1996). Chemical mixtures in atmospheric aerosols and their correlation to lung diseases and lung cancer occurence in the general population. Toxicology Letters *88*, 271-277.
12. Brook, R.D., Franklin, B., Cascio, W., Hong, Y.L., Howard, G., Lipsett, M., Luepker, R., Mittleman, M., Samet, J., Smith, S.C., and Tager, I. (2004). Air pollution and cardiovascular disease - A statement for healthcare professionals

from the expert panel on population and prevention science of the American Heart Association. Circulation *109*, 2655-2671.
13. Delfino, R.J., Sioutas, C., and Malik, S. (2005). Potential role of ultrafine particles in associations between airborne particle mass and cardiovascular health. Environmental Health Perspectives *113*, 934-946.
14. Rodriguez, R.A.S., Gavillan, J.G., Perez, E.S., and Mattei, H. (2007). Is cardiovascular and respiratory mortality related to PM10 in Puerto Rico? pp. S157-S157, Lippincott Williams & Wilkins.
15. Romieu, I., Castro-Giner, F., Kunzli, N., and Sunyer, J. (2008). Air pollution, oxidative stress and dietary supplementation: a review. European Respiratory Journal *31*, 179-196.
16. Brunekreef, B., and Holgate, S.T. (2002). Air pollution and health. Lancet *360*, 1233-1242.
17. Chow, J.C., and Watson, J.G. (August 1998). Guideline on Speciated Particulate Monitoring, Prepared for Office of Air Quality Planning and Standards (MD-14), U.S. Environmental Protection Agency, Research Triangle Park, North Carolina by Desert Research Institute, Reno, Nevada.
18. Chong, N.-S., Sivaramakrishnan, K., Wells, M., and Jones, K. (2002). Characterization of Inhalable Particulate Matter in Ambient Air by Scanning Electron Microscopy and Energy-Dispersive X-ray Analysis. Electronic Journal of Environmental, Agricultural and Food Chemistry *1*, 145-164.
19. Ravishankara, A.R. (1997). Heterogeneous and multiphase chemistry in the troposphere. Science *276*, 1058-1065.
20. Nathan, C. (2002). Points of control in inflammation. Nature *420*, 846-852.
21. Medzhitov, R. (2008). Origin and physiological roles of inflammation. Nature *454*, 428-435.
22. Pathak, S., and Palan, U. (2005). Immunology: Essential And Fundamental 2 edition (January 30, 2005) Edition (Science Publishers, Inc.).
23. van Eeden, S.F., and Hogg, J.C. (2002). Systemic inflammatory response induced by particulate matter air pollution: The importance of bone-marrow stimulation. Journal of Toxicology and Environmental Health-Part A *65*, 1597-1613.
24. Blankenberg, S., Barbaux, S., and Tiret, L. (2003). Adhesion molecules and atherosclerosis. Atherosclerosis *170*, 191-203.
25. Fakler, C.R., Wu, B., McMicken, H.W., Geske, R.S., and Welty, S.E. (2000). Molecular mechanisms of lipopolysaccharide induced ICAM-1 expression in A549 cells. Inflammation Research *49*, 63-72.
26. Persson, T., Monsef, N., Andersson, P., Bjartell, A., Malm, J., Calafat, J., and Egesten, A. (2003). Expression of the neutrophil-activating CXC chemokine ENA-78/CXCL5 by human eosinophils. Clinical and Experimental Allergy *33*, 531-537.
27. Pold, M., Zhu, L.X., Sharma, S., Burdick, M.D., Lin, Y., Lee, P.P.N., Pold, A., Luo, J., Krysan, K., Dohadwala, M., Mao, J.T., Batra, R.K., Strieter, R.M., and Dubinett, S.M. (2004). Cyclooxygenase-2-dependent expression of angiogenic CXC chemokines ENA-78/CXC ligand (CXCL) 5 and interleukin-8/CXCL8 in human non-small cell lung cancer. Cancer Research *64*, 1853-1860.

28. Imaizumi, T., Hatakeyama, M., Taima, K., Ishikawa, A., Yamashita, K., Yoshida, H., and Satoh, K. (2004). Effect of double-stranded RNA on the expression of epithelial neutrophil activating peptide-78/CXCL-5 in human endothelial cells. Inflammation *28*, 215-219.
29. Brasier, A.R. (2006). The NF-kappa B regulatory network. Cardiovascular Toxicology *6*, 111-130.
30. Haddad, J.J. (2002). Antioxidant and prooxidant mechanisms in the regulation of redox(y)-sensitive transcription factors. Cellular Signalling *14*, 879-897.
31. Harris, A.L. (2002). Hypoxia - A key regulatory factor in tumour growth. Nature Reviews Cancer *2*, 38-47.
32. Karin, M., Cao, Y.X., Greten, F.R., and Li, Z.W. (2002). NF-kappa B in cancer: From innocent bystander to major culprit. Nature Reviews Cancer *2*, 301-310.
33. Taub, D.D., and Oppenheim, J.J. (1993). Review of the Chemokine Meeting the 3rd International-Symposium of Chemotactic Cytokines. Cytokine *5*, 175-179.
34. Kacimi, R., Karliner, J.S., Koudssi, F., and Long, C.S. (1998). Expression and regulation of adhesion molecules in cardiac cells by cytokines - Response to acute hypoxia. Circulation Research *82*, 576-586.
35. Staunton, D.E., Marlin, S.D., Stratowa, C., Dustin, M.L., and Springer, T.A. (1988). Primary Structure of Icam-1 Demonstrates Interaction between Members of the Immunoglobulin and Integrin Supergene Families. Cell *52*, 925-933.
36. Staunton, D.E., Dustin, M.L., and Springer, T.A. (1989). Functional Cloning of Icam-2, a Cell-Adhesion Ligand for Lfa-1 Homologous to Icam-1. Nature *339*, 61-64.
37. Holden, N.S., Catley, M.C., Cambridge, L.M., Barnes, P.J., and Newton, R. (2004). ICAM-1 expression is highly NF-kappa B-dependent in A549 cells - No role for ERK and p38 MAPK. European Journal of Biochemistry *271*, 785-791.
38. Mills, P.R., Davies, R.J., and Devalia, J.L. (1999). Airway epithelial cells, cytokines, and pollutants. American Journal of Respiratory and Critical Care Medicine *160*, S38-S43.
39. Lieber, M., Smith, B., Szakal, A., Nelsonrees, W., and Todaro, G. (1976). Continuous Tumor-Cell Line from a Human Lung Carcinoma with Properties of Type-Ii Alveolar Epithelial Cells. International Journal of Cancer *17*, 62-70.
40. Javois, L.C. (1994). Immunocytochemical methods and protocols (Humana Press Inc.).
41. Reyzer, M.L., and Caprioli, R.M. (2005). MALDI mass spectrometry for direct tissue analysis: A new tool for biomarker discovery. Journal of Proteome Research *4*, 1138-1142.
42. Griffiths, W.J., Jonsson, A.P., Liu, S.Y., Rai, D.K., and Wang, Y.Q. (2001). Electrospray and tandem mass spectrometry in biochemistry. Biochemical Journal *355*, 545-561.
43. Walch, A., Rauser, S., Deininger, S.O., and Hofler, H. (2008). MALDI imaging mass spectrometry for direct tissue analysis: a new frontier for molecular histology. Histochemistry and Cell Biology *130*, 421-434.
44. Aebersold, R., and Mann, M. (2003). Mass spectrometry-based proteomics. Nature *422*, 198-207.

45. Gonnet, F., Lemaitre, G., Waksman, G., and Tortajada, J. (2003). MALDI/MS peptide mass fingerprinting for proteome analysis: identification of hydrophobic proteins attached to eucaryote keratinocyte cytoplasmic membrane using different matrices in concert. Proteome Science *1*, 2.
46. Feng, X., and Agnes, G.R. (2000). Single isolated droplets with net charge as a source of ions. Journal of the American Society for Mass Spectrometry *11*, 393-399.
47. Bogan, M.J., Bakhoum, S.F.W., and Agnes, G.R. (2005). Promotion of alpha-cyano-4-hydroxycinnamic acid and peptide cocrystallization within levitated droplets with net charge. Journal of the American Society for Mass Spectrometry *16*, 254-262.
48. Haddrell, A.E., Ishii, H., van Eeden, S.F., and Agnes, G.R. (2005). Apparatus for preparing mimics of suspended particles in the troposphere and their controlled deposition onto individual lung cells in culture with measurement of downstream biological response. Analytical Chemistry *77*, 3623-3628.
49. Haddrell, A.E., van Eeden, S.F., and Agnes, G.R. (2006). Dose-response studies involving controlled deposition of less than 100 particles generated and levitated in an ac trap onto lung cells, in vitro, and quantitation of ICAM-1 differential expression. Toxicology in Vitro *20*, 1030-1039.
50. Eleghasim, N.M., Haddrell, A.E., van Eeden, S., and Agnes, G.R. (2006). The preparation of < 100 particles per trial having the same mole fraction of 12 inorganic compounds at diameters of 6.8, 3.8, or 2.6 mu m followed by their deposition onto human lung cells (A549) with measurement of the relative downstream differential expression of ICAM-1. International Journal of Mass Spectrometry *258*, 134-141.
51. Davis, E.J. (1997). A history of single aerosol particle levitation. Aerosol Science and Technology *26*, 212-254.
52. March, R.E. (1997). An introduction to quadrupole ion trap mass spectrometry. Journal of Mass Spectrometry *32*, 351-369.
53. Kardjaputri, A.J. (2009). Dose response relationship between the chemical composition of 2.4±0.1 μm particles and human lung cell (A549) cytokine expression, Simon Fraser University, Burnaby.
54. Hillenkamp, F., Karas, M., Beavis, R.C., and Chait, B.T. (1991). Matrix-Assisted Laser Desorption Ionization Mass-Spectrometry of Biopolymers. Analytical Chemistry *63*, A1193-A1202.
55. Fenn, J.B. (1993). Ion Formation from Charged Droplets - Roles of Geometry, Energy, and Time. Journal of the American Society for Mass Spectrometry *4*, 524-535.
56. Steerenberg, P.A., Withagen, C.E.T., van Dalen, W.J., Dormans, J., and van Loveren, H. (2004). Adjuvant activity of ambient particulate matter in macrophage activity-suppressed, N-acetylcysteine-treated, iNOS- and IL-4-deficient mice. Inhalation Toxicology *16*, 835-843.
57. Adamson, I.Y.R., Prieditis, H., and Vincent, R. (1999). Pulmonary toxicity of an atmospheric particulate sample is due to the soluble fraction. Toxicology and Applied Pharmacology *157*, 43-50.

58. Vincent, R., Bjarnason, S.G., Adamson, I.Y.R., Hedgecock, C., Kumarathasan, P., Guenette, J., Potvin, M., Goegan, P., and Bouthillier, L. (1997). Acute pulmonary toxicity of urban particulate matter and ozone. American Journal of Pathology *151*, 1563-1570.
59. Fujii, T., Hayashi, S., Hogg, J.C., Vincent, R., and Van Eeden, S.F. (2001). Particulate matter induces cytokine expression in human bronchial epithelial cells. American Journal of Respiratory Cell and Molecular Biology *25*, 265-271.
60. Dye, J.A., Adler, K.B., Richards, J.H., and Dreher, K.L. (1999). Role of soluble metals in oil fly ash-induced airway epithelial injury and cytokine gene expression. American Journal of Physiology-Lung Cellular and Molecular Physiology *277*, L498-L510.
61. Rice, T.M., Clarke, R.W., Godleski, J.J., Al-Mutairi, E., Jiang, N.F., Hauser, R., and Paulauskis, J.D. (2001). Differential ability of transition metals to induce pulmonary inflammation. Toxicology and Applied Pharmacology *177*, 46-53.
62. Simon-Deckers, A., Gouget, B., Mayne-L'Hermite, M., Herlin-Boime, N., Reynaud, C., and Carriere, M. (2008). In vitro investigation of oxide nanoparticle and carbon nanotube toxicity and intracellular accumulation in A549 human pneumocytes. Toxicology *253*, 137-146.
63. Swain, P., Nayak, S.K., Nanda, P.K., and Dash, S. (2008). Biological effects of bacterial lipopolysaccharide (endotoxin) in fish: A review. Fish & Shellfish Immunology *25*, 191-201.
64. Thorn, J. (2001). The inflammatory response in humans after inhalation of bacterial endotoxin: a review. Inflammation Research *50*, 254-261.
65. Mueller-Anneling, L., Avol, E., Peters, J.M., and Thorne, P.S. (2004). Ambient endotoxin concentrations in PM10 from Southern California. Environmental Health Perspectives *112*, 583-588.
66. Rizzo, M.C., Naspitz, C.K., Fernandez-Caldas, E., Lockey, R.F., Mimica, I., and Sole, D. (1997). Endotoxin exposure and symptoms in asthmatic children. Pediatric Allergy and Immunology *8*, 121-126.
67. Loppnow, H., Libby, P., Freudenberg, M., Krauss, J.H., Weckesser, J., and Mayer, H. (1990). Cytokine Induction by Lipopolysaccharide (Lps) Corresponds to Lethal Toxicity and Is Inhibited by Nontoxic Rhodobacter-Capsulatus Lps. Infection and Immunity *58*, 3743-3750.
68. Carty, C.L., Gehring, U., Cyrys, J., Bischof, W., and Heinrich, J. (2003). Seasonal variability of endotoxin in ambient fine particulate matter. Journal of Environmental Monitoring *5*, 953-958.
69. Liebers, V., Raulf-Heimsoth, M., and Bruning, T. (2008). Health effects due to endotoxin inhalation (review). Archives of Toxicology *82*, 203-210.
70. Park, J.H., Gold, D.R., Spiegelman, D.L., Burge, H.A., and Milton, D.K. (2001). House dust endotoxin and wheeze in the first year of life. American Journal of Respiratory and Critical Care Medicine *163*, 322-328.
71. Bischof, W., Koch, A., Gehring, U., Fahlbusch, B., Wichmann, H.E., and Heinrich, J. (2002). Predictors of high endotoxin concentrations in the settled dust of German homes. Indoor Air *12*, 2-9.

72. Wickens, K., Douwes, J., Siebers, R., Fitzharris, P., Wouters, I., Doekes, G., Mason, K., Hearfield, M., Cunningham, M., and Crane, J. (2003). Determinants of endotoxin levels in carpets in New Zealand homes. Indoor Air *13*, 128-135.
73. Vogelzang, P.F.J., van der Gulden, J.W.J., Folgering, H., Kolk, J.J., Heederik, D., Preller, L., Tielen, M.J.M., and van Schayck, C.P. (1998). Endotoxin exposure as a major determinant of lung function decline in pig farmers. American Journal of Respiratory and Critical Care Medicine *157*, 15-18.
74. Hasday, J.D., Bascom, R., Costa, J.J., Fitzgerald, T., and Dubin, W. (1999). Bacterial endotoxin is an active component of cigarette smoke. Chest *115*, 829-835.
75. Morrison, D.C., and Ryan, J.L. (1992). Bacterial Endotoxic Lipopolysaccharides: Molecular Biochemistry and Cellular Biology (CRC Press).
76. Dentener, M.A., Vreugdenhil, A.C.E., Hoet, P.H.M., Vernooy, J.H.J., Nieman, F.H.M., Heumann, D., Janssen, Y.M.W., Buurman, W.A., and Wouters, E.F.M. (2000). Production of the acute-phase protein lipopolysaccharide-binding protein by respiratory type II epithelial cells - Implications for local defense to bacterial endotoxins. American Journal of Respiratory Cell and Molecular Biology *23*, 146-153.
77. Gereda, J.E., Klinnert, M.D., Price, M.R., Leung, D.Y.M., and Liu, A.H. (2001). Metropolitan home living conditions associated with indoor endotoxin levels. Journal of Allergy and Clinical Immunology *107*, 790-796.
78. Milton, D.K., Wypij, D., Kriebel, D., Walters, M.D., Hammond, S.K., and Evans, J.S. (1996). Endotoxin exposure-response in a fiberglass manufacturing facility. American Journal of Industrial Medicine *29*, 3-13.
79. Schwartz, D.A., Thorne, P.S., Yagla, S.J., Burmeister, L.F., Olenchock, S.A., Watt, J.L., and Quinn, T.J. (1995). The Role of Endotoxin in Grain Dust-Induced Lung-Disease. American Journal of Respiratory and Critical Care Medicine *152*, 603-608.
80. Rylander, R. (1997). Evaluation of the risk of endotoxin exposure. International Journal of Occupational and Environmental Health *3*, S32-S36.
81. Swan, J.R.M., Kelsey, A., Crook, B., and Gilbert, E.J. (2003). Occupational and environmental exposure to bioaerosols from composts and potential health effects - A critical review of published data, Prepared for the Health and Safety Executive, Norwich, UK, by The Composting Association, Northamptonshire, UK and Health and Safety Laboratory, Sheffield, UK
82. Jornitz, M.W., and Meltzer, T.H. (2007). Filtration and Purification in the Biopharmaceutical Industry 2Edition (Informa HealthCare).
83. Hochstein, H.D., Mills, D.F., Outschoorn, A.S., and Rastogi, S.C. (1983). The Processing and Collaborative Assay of a Reference Endotoxin. Journal of Biological Standardization *11*, 251-260.
84. Poole, S., Dawson, P., and Das, R.E.G. (1997). Second international standard for endotoxin: calibration in an international collaborative study. Journal of Endotoxin Research *4*, 221-231.
85. Guillot, L., Medjane, S., Le-Barillec, K., Balloy, V., Danel, C., Chignard, M., and Si-Tahar, M. (2004). Response of human pulmonary epithelial cells to lipopolysaccharide involves Toll-like receptor 4 (TLR4)-dependent signaling

pathways - Evidence for an intracellular compartmentalization of TLR4. Journal of Biological Chemistry *279*, 2712-2718.
86. Monick, M.M., Yarovinsky, T.O., Powers, L.S., Butler, N.S., Carter, A.B., Gudmundsson, G., and Hunninghake, G.W. (2003). Respiratory syncytial virus up-regulates TLR4 and sensitizes airway epithelial cells to endotoxin. Journal of Biological Chemistry *278*, 53035-53044.
87. MacRedmond, R., Greene, C., Taggart, C.C., McElvaney, N., and O'Neill, S. (2005). Respiratory epithelial cells require Toll-like receptor 4 for induction of human b-defensin 2 by lipopolysaccharide. Respiratory Research *6*, 11.
88. Abate, W., Alghaithy, A.A., Parton, J., Jones, K.P., and Jackson, S.K. (2010). Surfactant lipids regulate LPS-induced interleukin-8 production in A549 lung epithelial cells by inhibiting translocation of TLR4 into lipid raft domains. Journal of Lipid Research *51*, 334-344.
89. Donnarumma, G., Paoletti, I., Buommino, E., Iovene, M.R., Tudisco, L., Cozza, V., and Tufano, M.A. (2007). Anti-ninflammatory effects of moxifloxacin and human beta-defensin 2 association human lung epithelial cell line (A549) stimulated with lipopolysaccharide. Peptides *28*, 2286-2292.
90. Peterson, A.A., and McGroarty, E.J. (1985). High-Molecular-Weight Components in Lipopolysaccharides of Salmonella-Typhimurium, Salmonella-Minnesota, and Escherichia-Coli. Journal of Bacteriology *162*, 738-745.
91. Jann, B., Reske, K., and Jann, K. (1975). Heterogeneity of Lipopolysaccharides - Analysis of Polysaccharide Chain Lengths by Sodium Dodecylsulfate Polyacrylamide Gel-Electrophoresis. European Journal of Biochemistry *60*, 239-246.
92. Gray, H.A. (7 February 1986). Control of Atmospheric Fine Primary Carbon Particle Concentrations, Prepared for California Air Resources Board by Environmental Quality Laboratory, California Institute of Technology, Pasadena, California.
93. Siegla, D.C., and Smith, G.W. (1981). Particulate Carbon: Formation During Combustion (Basic Books).
94. (IARC), I.A.f.R.o.C. (1996). carbon black. IARC Monogr Eval Carcinog Risks Hum *65*, 149-262.
95. Althouse, R., Huff, J., Tomatis, L., and Wilbourn, J. (1980). An Evaluation of Chemicals and Industrial Processes Associated with Cancer in Humans Based on Human and Animal Data International Agency for Research on Cancer Monographs Volumes 1-20. Cancer Research *40*, 1-12.
96. Carero, A.D.P., Hoet, P.H.M., Verschaeve, L., Schoeters, G., and Nemery, B. (2001). Genotoxic effects of carbon black particles, diesel exhaust particles, and urban air particulates and their extracts on a human alveolar epithelial cell line (A549) and a human monocytic cell line (THP-1). Environmental and Molecular Mutagenesis *37*, 155-163.
97. Haddrell, A.E. (2007). Developing an in vitro methodology to study the inflammation potential of ambient particle types, Simon Fraser University, Burnaby.
98. Chen, C.C., Chou, C.Y., Sun, Y.T., and Huang, W.C. (2001). Tumor necrosis factor alpha-induced activation of downstream NF-kappa B site of the promoter

mediates epithelial ICAM-1 expression and monocyte adhesion: Involvement of PKC alpha, tyrosine kinase, and IKK2, but not MAPKs, pathway. Cellular Signalling *13*, 543-553.
99. Pelletier, M., and Girard, D. (2005). Interleukin-15 increases neutrophil adhesion onto human respiratory epithelial A549 cells and attracts neutrophils in vivo. Clinical and Experimental Immunology *141*, 315-325.
100. Pelletier, M., Lavastre, V., and Girard, D. (2002). Activation of human epithelial lung A549 cells by the pollutant sodium sulfite: Enhancement of neutrophil adhesion. Toxicological Sciences *69*, 210-216.
101. Hannun, Y.A., and Boustany, R.-M. (1998). Apoptosis in Neurobiology, 1 Edition (CRC Press).
102. Green, F.J. (1990). The Sigma-Aldrich Handbook of Stains, Dyes and Indicators (Aldrich Chem Co Library).
103. Clarke, C.J., Truong, T.G., and Hannun, Y.A. (2007). Role for neutral sphingomyelinase-2 in tumor necrosis factor alpha-stimulated expression of vascular cell adhesion molecule-1 (VCAM) and intercellular adhesion molecule-1 (VCAM) in lung epithelial cells - p38 MAPK is an upstream regulator of nSMase2. Journal of Biological Chemistry *282*, 1384-1396.
104. Sun, G.P., Xu, X.F., Wang, Y.S., Shen, X.Y., Chen, Z.M., and Yang, J. (2008). Mycoplasma pneumoniae infection induces reactive oxygen species and DNA damage in A549 human lung carcinoma cells. Infection and Immunity *76*, 4405-4413.
105. Haddrell, A.E., van Eeden, S., and Agnes, G.R. (2008). MALDI-MS monitoring of differential biomolecule secretion from human lung cells in vitro following incubation with < 150 particles. Journal of Proteome Research *7*, 2539-2545.
106. Steinkamp, J.A., Wilson, J.S., Saunders, G.C., and Stewart, C.C. (1982). Phagocytosis - Flow Cytometric Quantitation with Fluorescent Microspheres. Science *215*, 64-66.
107. Harmsen, A.G., Mason, M.J., Muggenburg, B.A., Gillett, N.A., Jarpe, M.A., and Bice, D.E. (1987). Migration of Neutrophils from Lung to Tracheobronchial Lymph-Node. Journal of Leukocyte Biology *41*, 95-103.
108. Parker, L.C., Prince, L.R., and Sabroe, I. (2007). Translational mini-review series on Toll-like receptors: Networks regulated by Toll-like receptors mediate innate and adaptive immunity. Clinical and Experimental Immunology *147*, 199-207.
109. Heshmat, N.M., Mostafal, G.A., A-Aziz, M.M.A., and El-Bary, E.M.A. (2007). Sputum epithelial cell-derived neutrophil-activating peptide-78 (ENA-78/CXCL5) in asthmatic children. pp. 536, Mosby-Elsevier.
110. Bella, J., and Rossmann, M.G. (1999). Review: Rhinoviruses and their ICAM receptors. pp. 69-74, Academic Press Inc.
111. Kim, H.J., Lee, H.S., Chong, Y.H., and Kang, J.L. (2006). p38 mitogen-activated protein kinase up-regulates LPS-induced NF-kappa B activation in the development of lung injury and RAW 264.7 macrophages. Toxicology *225*, 36-47.
112. Karnovsky, M.J. (1965). A Formaldehyde-Glutaraldehyde Fixative of High Osmolality for Use in Electron Microscopy. Journal of Cell Biology *27*, 137A-138A.

113. Klebe, R.J., Hall, J.R., Rosenberger, P., and Dickey, W.D. (1977). Cell Attachment to Collagen - Ionic Requirements. Experimental Cell Research *110*, 419-425.
114. Hoang, A.M., Klebe, R.J., Steffensen, B., Ryu, O.H., Simmer, J.P., and Cochran, D.L. (2002). Amelogenin is a cell adhesion protein. Journal of Dental Research *81*, 497-500.
115. Noone, P.G., Zhou, Z.Q., Silverman, L.M., Jowell, P.S., Knowles, M.R., and Cohn, J.A. (2001). Cystic fibrosis gene mutations and pancreatitis risk: Relation to epithelial ion transport and trypsin inhibitor gene mutations. Gastroenterology *121*, 1310-1319.
116. Zaia, J., Annan, B.S., and Biemann, K. (1992). The Correct Molecular-Weight of Myoglobin, a Common Calibrant for Mass-Spectrometry. Rapid Communications in Mass Spectrometry *6*, 32-36.
117. Carrina J. Keys, D.J.D., Helen Sutton, Graeme Wells, Martin Lunt, Therese McKenna, Mark McDowall, Haroun N. Shah (2004). Compilation of a MALDI-TOF mass spectral database for the rapid screening and characterisation of bacteria implicated in human infectious diseases. Infection, Genetics and Evolution *4*, 221-242.
118. Tacha, D.E., and Mckinney, L. (1992). Casein Reduces Nonspecific Background Staining in Immunolabeling Techniques. Journal of Histotechnology *15*, 127-132.
119. Kenna, J.G., Major, G.N., and Williams, R.S. (1985). Methods for Reducing Nonspecific Antibody-Binding in Enzyme-Linked Immunosorbent Assays. Journal of Immunological Methods *85*, 409-419.
120. Brewer, J.M. (2006). (How) do aluminium adjuvants work? Immunology Letters *102*, 10-15.
121. Rosen, F.S., Steiner, L.A., and Unanue, E.R. (1989). Dictionary of immunology (The Macmillan Press Ltd.).
122. Cox, J.C., and Coulter, A.R. (1997). Adjuvants - A classification and review of their modes of action. Vaccine *15*, 248-256.
123. Glenny, A.T., Pope, C.G., Waddington, H., and Wallace, U. (1926). Immunological notes XVLL.-XXIV. Journal of Pathology and Bacteriology *29*, 31-40.
124. Janeway, C.A. (1989). Approaching the Asymptote - Evolution and Revolution in Immunology. Cold Spring Harbor Symposia on Quantitative Biology *54*, 1-13.
125. HogenEsch, H. (2002). Mechanisms of stimulation of the immune response by aluminum adjuvants. pp. S34-S39, Elsevier Sci Ltd.
126. Lindblad, E.B. (2004). Aluminium adjuvants - in retrospect and prospect. Vaccine *22*, 3658-3668.
127. Gupta, R.K. (1998). Aluminum compounds as vaccine adjuvants. Advanced Drug Delivery Reviews *32*, 155-172.
128. Sokolovska, A., Hem, S.L., and HogenEsch, H. (2007). Activation of dendritic cells and induction of CD4(+) T cell differentiation by aluminum-containing adjuvants. Vaccine *25*, 4575-4585.
129. Audibert, F. (2003). Adjuvants for vaccines, a quest. pp. 1187-1193, Elsevier Science Bv.

130. Mauk, K.L. (2006). Gerontological Nursing: Competencies For Care (Jones & Bartlett Publishers).
131. Bortolatto, J., Borducchi, E., Rodriguez, D., Keller, A.C., Faquim-Mauro, E., Bortoluci, K.R., Mucida, D., Gomes, E., Christ, A., Schnyder-Candrian, S., Schnyder, B., Ryffel, B., and Russo, M. (2008). Toll-like receptor 4 agonists adsorbed to aluminium hydroxide adjuvant attenuate ovalbumin-specific allergic airway disease: role of MyD88 adaptor molecule and interleukin-12/interferon-gamma axis. Clinical and Experimental Allergy *38*, 1668-1679.
132. Mancino, D., and Ovary, Z. (1980). Adjuvant Effects of Amorphous Silica and of Aluminum Hydroxide on Ige and Igg1 Antibody-Production in Different Inbred Mouse Strains. International Archives of Allergy and Applied Immunology *61*, 253-258.
133. Hamaoka, T., Katz, D.H., Bloch, K.J., and Benacerr.B (1973). Hapten-Specific Ige Antibody-Responses in Mice .1. Secondary Ige Responses in Irradiated Recipients of Syngeneic Primed Spleen-Cells. Journal of Experimental Medicine *138*, 306-311.
134. Hamaoka, T., Katz, D.H., and Benacerr.B (1973). Hapten-Specific Ige Antibody-Responses in Mice .2. Cooperative Interactions between Adoptively Transferred T and B Lymphocytes in Development of Ige Response. Journal of Experimental Medicine *138*, 538-556.
135. Shi, Y., HogenEsch, H., Regnier, F.E., and Hem, S.L. (2001). Detoxification of endotoxin by aluminum hydroxide adjuvant. Vaccine *19*, 1747-1752.
136. Norimatsu, M., Ogikubo, Y., Aoki, A., Takahashi, T., Watanabe, G., Taya, K., Sasamoto, S., Tsuchiya, M., and Tamura, Y. (1995). Effects of Aluminum Adjuvant on Systemic Reactions of Lipopolysaccharides in Swine. Vaccine *13*, 1325-1329.
137. Lindblad, E.B. (2004). Aluminium compounds for use in vaccines. Immunology and Cell Biology *82*, 497-505.
138. Bianco, A., Sethi, S.K., Allen, J.T., Knight, R.A., and Spiteri, M.A. (1998). Th2 cytokines exert a dominant influence on epithelial cell expression of the major group human rhinovirus receptor, ICAM-1. European Respiratory Journal *12*, 619-626.
139. Weigel, G., Bertalanffy, P., Dubsky, P., Griesmacher, A., and Wolner, E. (1999). Mycophenolic acid influences T helper 2 (Th2) cytokine induced expression of intercellular cell adhesion molecule-1 (ICAM-1) on human endothelial cells. pp. 253-257, Walter De Gruyter & Co.
140. Salomon, B., and Bluestone, J.A. (1998). Cutting edge: LFA-1 interaction with ICAM-1 and ICAM-2 regulates Th2 cytokine production. Journal of Immunology *161*, 5138-5142.
141. Suzuki, J., Isobe, M., Izawa, A., Takahashi, W., Yamazaki, S., Okubo, Y., Amano, J., and Sekiguchi, M. (1999). Differential Th1 and Th2 cell regulation of murine cardiac allograft acceptance by blocking cell adhesion of ICAM-1/LFA-1 and VCAM-1/VLA-4. Transplant Immunology *7*, 65-72.
142. Isobe, M., Suzuki, J., Yamazaki, S., Yazaki, Y., Horie, S., Okubo, Y., Maemura, K., Yazaki, Y., and Sekiguchi, M. (1997). Regulation by differential development

of Th1 and Th2 cells in peripheral tolerance to cardiac allograft induced by blocking ICAM-1/LFA-1 adhesion. Circulation *96*, 2247-2253.
143. Schaumann, F., Borm, P.J.A., Herbrich, A., Knoch, J., Pitz, M., Schins, R.P.F., Luettig, B., Hohlfeld, J.M., Heinrich, J., and Krug, N. (2004). Metal-rich ambient particles (Particulate Matter(2.5)) cause airway inflammation in healthy subjects. American Journal of Respiratory and Critical Care Medicine *170*, 898-903.
144. Adamson, I.Y.R., Prieditis, H., Hedgecock, C., and Vincent, R. (2000). Zinc is the toxic factor in the lung response to an atmospheric particulate sample. Toxicology and Applied Pharmacology *166*, 111-119.
145. Merolla, L., and Richards, R.J. (2005). In vitro effects of water-soluble metals present in uk particulate matter. Experimental Lung Research *31*, 671-683.
146. Amdur, M.O., Bayles, J., Ugro, V., and Underhill, D.W. (1978). Comparative Irritant Potency of Sulfate Salts. Environmental Research *16*, 1-8.
147. Gavett, S.H., Madison, S.L., Dreher, K.L., Winsett, D.W., McGee, J.K., and Costa, D.L. (1997). Metal and sulfate composition of residual oil fly ash determines airway hyperreactivity and lung injury in rats. Environmental Research *72*, 162-172.
148. Carter, J.D., Ghio, A.J., Samet, J.M., and Devlin, R.B. (1997). Cytokine production by human airway epithelial cells after exposure to an air pollution particle is metal-dependent. Toxicology and Applied Pharmacology *146*, 180-188.
149. Dreher, K.L., Jaskot, R.H., Lehmann, J.R., Richards, J.H., McGee, J.K., Ghio, A.J., and Costa, D.L. (1997). Soluble transition metals mediate residual oil fly ash induced acute lung injury. Journal of Toxicology and Environmental Health *50*, 285-305.
150. Vincent, R., Goegan, P., Johnson, G., Brook, J.R., Kumarathasan, P., Bouthillier, L., and Burnett, R.T. (1997). Regulation of promoter-CAT stress genes in HepG2 cells by suspensions of particles from ambient air. Fundamental and Applied Toxicology *39*, 18-32.
151. Steerenberg, P.A., Withagen, C.E.T., van Dalen, W.J., Dormans, J., Cassee, F.R., Heisterkamp, S.H., and van Loveren, H. (2004). Adjuvant activity of ambient particulate matter of different sites, sizes, and seasons in a respiratory allergy mouse model. Toxicology and Applied Pharmacology *200*, 186-200.
152. Vijay, H.M., Kumar, V., Abebe, M., Sevinc, S., and Vincent, R. (2006). Adjuvant activity of ambient particulate matter on allergic immune response to Alternaria alternata. pp. 109, Mosby, Inc.
153. Chou, C.H., Hsu, J.Y., Fu, L.S., Chu, J.J., and Chi, C.S. (2008). The air pollutant sodium sulfite enhances mite crude extract-stimulated detachment of A549 airway epithelium cells. Journal of Microbiology Immunology and Infection *41*, 26-31.
154. Ulanova, M., Tarkowski, A., Hahn-Zoric, M., and Hanson, L.A. (2001). The common vaccine adjuvant aluminum hydroxide up-regulates accessory properties of human monocytes via an interleukin-4-dependent mechanism. Infection and Immunity *69*, 1151-1159.
155. Gesser, B., Lund, M., Lohse, N., Vestergaard, C., Matsushima, K., SindetPedersen, S., Jensen, S.L., ThestrupPedersen, K., and Larsen, C.G. (1996). IL-8 induces T cell chemotaxis, suppresses IL-4, and up-regulates IL-8 production by CD4(+) T cells. Journal of Leukocyte Biology *59*, 407-411.

156. Liao, F., Rabin, R.L., Yannelli, J.R., Koniaris, L.G., Vanguri, P., and Farber, J.M. (1995). Human Mig Chemokine - Biochemical and Functional-Characterization. Journal of Experimental Medicine *182*, 1301-1314.
157. Banchereau, J., Briere, F., Caux, C., Davoust, J., Lebecque, S., Liu, Y.T., Pulendran, B., and Palucka, K. (2000). Immunobiology of dendritic cells. Annual Review of Immunology *18*, 767-+.
158. Schlesinger, R.B. (1984). Comparative Irritant Potency of Inhaled Sulfate Aerosols - Effects on Bronchial Mucociliary Clearance. Environmental Research *34*, 268-279.
159. Reiss, R., Anderson, E.L., Cross, C.E., Hidy, G., Hoel, D., McClellan, R., and Moolgavkar, S. (2007). Evidence of health impacts of sulfate- and nitrate-containing particles in ambient air. Inhalation Toxicology *19*, 419-449.
160. Schlesinger, R.B. (2007). The health impact of common inorganic components of fine particulate matter (PM2.5) in ambient air: A critical review. Inhalation Toxicology *19*, 811-832.
161. Rogge, W.F., Mazurek, M.A., Hildemann, L.M., Simoneit, B.R.T., and Cass, G.R. (14 July 1991). Determination of Organic Compounds Present in Airborne Particulate Matter, prepared for South Coast Air Quality Management District by Environmental Engineering Science Department and Environmental Quality Laboratory, California Institute of Technology, Pasadena, California.
162. Eleghasim, M.N. (2007). Effects of Inorganic Ambient Particle Type Mimics on the Differential Expression of a Pro-Inflammatory Mediator by A549 Cells In Vitro, Simon Fraser University, Burnaby.